Biomechanical Simulations of the Interfragmentary Movement

Dissertation

zur Erlangung des Grades
des Doktors der Ingenieurwissenschaften
der Naturwissenschaftlich – Technischen Fakultät
der Universität des Saarlandes

von

Annchristin Andres, M. Sc.

Saarbrücken
2025

Tag des Kolloquiums:	02.04.2026
Dekan:	Prof. Dr.-Ing. Dirk Bähre
Berichterstatter:	Prof. Dr.-Ing. Stefan Diebels
	Prof. Dr. med. Benedikt Johannes Braun
	Prof. Dr.-Ing. Tim Ricken
Vorsitz:	Prof. Dr.-Ing. Matthias Nienhaus
Akademischer Mitarbeiter:	Dr.-Ing. Oliver Maurer

Eidesstattliche Versicherung

Hiermit versichere ich an Eides statt, dass ich die vorliegende Arbeit selbständig und ohne Benutzung anderer als der angegebenen Hilfsmittel angefertigt habe. Die aus anderen Quellen oder indirekt übernommenen Daten und Konzepte sind unter Angabe der Quelle gekennzeichnet. Die Arbeit wurde bisher weder im In- noch im Ausland in gleicher oder ähnlicher Form in einem Verfahren zur Erlangung eines akademischen Grades vorgelegt.

Ich erkläre darüber hinaus mit meiner Unterschrift, dass ich

- keine im Merkblatt „Hinweise zur Vermeidung von Plagiaten“ der Naturwissenschaftlich-Technischen Fakultät beschriebene Form des Plagiats begangen habe,
- alle Methoden, Daten und Arbeitsabläufe wahrheitsgetreu dokumentiert und
- keine Daten manipuliert habe.

_____ _____

Ort, Datum Annchristin Andres

Preface

I received many valuable contributions and support while working on this dissertation. My special thanks go to:

Prof. Dr.-Ing. Stefan Diebels for the opportunity to work in the field of biomechanics and for his comprehensive support. His scientific knowledge, explanations, and patience made him the perfect doctoral supervisor for me.
Dr. Michael Roland, who is my supervisor in every way. Michael taught me everything I need to know about the academic world and how to navigate it. He was always willing to listen, and I could turn to him with any question. I have fond memories of every business trip, conference, and project meeting, and they have strengthened my confidence.
Prof. Dr. med. Benedikt Braun for his insights into the world of medicine. There was no question he couldn't answer, and our discussions always gave me new insights into his field.
Kerstin Wickert, who, as my office partner, noticed even the slightest change in my mood. She always cheered me up and celebrated every milestone with me. You can always rely on her. Our lunches, conversations, trips, and meetings together provided the important input for this work.
My parents and sister supported me in every decision and were always there for me during this phase of my life.
My greatest thanks go to my husband, *Matthias Andres*. He has been by my side with advice and support since my bachelor's degree. He encouraged me to follow my path and never lose sight of my goal. No matter how exhausting the day was, he was and always is my rock. Thank you for your endless love, encouragement, understanding, and trust in me.
Finally, I would like to thank my “bonus daughter”, *Lina Gratz*, for always looking at things from a different perspective and never losing sight of the fact that life is an adventure full of wonders.

“It is far more important to know what person the disease has

than what disease the person has.”

Hippocrates

The actual work was carried out between 2021 and 2025 at the Chair of Applied Mechanics at Saarland University. The research was funded by the BMFTR (Federal Ministry of Research, Technology, and Space) as part of the “VirtuS” funding program (FKZ: 13GW0572), by the Werner Siemens Foundation as part of the “Smart Implants 2.0” funding program, and the DFG (Deutsche Forschungsgemeinschaft) as part of the “SPP2311” (DI 430/43-1).

Abstract

Interfragmentary motion (IFM) is a key factor in healing and is stimulated by the patient's movements. To optimize the healing process of bone fractures, it is important to understand how loads from muscle forces and rehabilitation exercises influence the mechanical environment at the fracture site.

This paper presents a biomechanical simulation workflow designed to define patient-specific boundary conditions using musculoskeletal simulations based on motion capture and CT data. Our goal is to simulate patient-specific fracture mechanics across different healing phases by creating individualized digital twin models. We use finite element simulations to analyze local stress and strain distributions within the fracture gap and to evaluate the bone-implant interactions. We hypothesize that we can specify specific threshold values for fracture healing depending on the fracture type and phase, and that personalized mechanical conditions are required for optimal healing.

Our results show that different movement patterns significantly influence the micromechanical conditions within the fracture zone. The attached publications cover the individual development steps towards a digital twin. Starting with a detailed description of the creation of patient-specific simulations, through the possibilities of patient monitoring, to the digital twin, and application examples for different patient-specific use cases. The challenges include precisely defining the mechanical healing window and incorporating additional biological and patient-specific factors.

Zusammenfassung

Die interfragmentäre Bewegung (IFM) ist eine Schlüsselgröße für die Heilung und wird durch Bewegungen des Patienten stimuliert. Um den Heilungsprozess von Knochenbrüchen zu optimieren, ist es wichtig zu verstehen, wie Belastungen durch Muskelkräfte und Rehabilitationsübungen das mechanische Umfeld an der Frakturstelle beeinflussen.

In dieser Arbeit wird ein biomechanischer Simulationsworkflow vorgestellt, der darauf ausgelegt ist, patientenspezifische Randbedingungen mit Hilfe von muskuloskelettalen Simulationen zu definieren, die auf Bewegungserfassung und CT-Daten basieren. Unser Ziel ist es, die patientenspezifische Frakturmechanik über verschiedene Heilungsphasen hinweg zu simulieren, indem wir individualisierte digitale Zwillingsmodelle erstellen. Wir verwenden Finite-Elemente-Simulationen, um lokale Spannungs- und Dehnungsverteilungen innerhalb des Frakturspalts zu analysieren und die Knochen-Implantat-Wechselwirkungen zu untersuchen. Wir stellen die Hypothese auf, dass wir je nach Frakturtyp und -phase spezifische Grenzwerte für die Frakturheilung festlegen können und dass für eine optimale Heilung personalisierte mechanische Bedingungen erforderlich sind.

Unsere Ergebnisse zeigen, dass unterschiedliche Bewegungsmuster die mikromechanischen Bedingungen innerhalb der Frakturzone erheblich beeinflussen. Die beigefügten Veröffentlichungen behandeln die einzelnen Entwicklungsschritte hin zu einem digitalen Zwilling. Angefangen mit der detaillierten Beschreibung der Erstellung von patientenspezifischen Simulationen, über die Möglichkeiten des Patienten-Monitorings bis hin zum digitalen Zwilling und patientenspezifischen Anwendungsfällen. Zu den Herausforderungen gehört, das mechanische Heilungsfenster genau zu definieren und zusätzliche biologische und patientenspezifische Faktoren miteinzubeziehen.

List of Appended Papers

This thesis consists of a summary and five appended papers as an author:

Paper A Andres, A., Roland, M., Wickert, K., Ganse, B., Pohlemann, T., Orth, M. & Diebels, S. Individual Postoperative and Preoperative Workflow for Patients with Fractures of the Lower Extremities. *Clin. Biomech.* (2025). 106503. https://doi.org/10.1016/j.clinbiomech.2025.106503

Paper B Andres, A., Roland, M., Orth, M., & Diebels, S. (2025). From Injury to Full Recovery: Monitoring Patient Progress Through Advanced Sensor and Motion Capture Technology. *Sensors*, *25*(13), 3853. https://doi.org/10.3390/s25133853

Paper C Andres, A., Roland, M., Wickert, K., Diebels, S., Stöckl, J., Herrmann, S., Reinauer, F., Leibinger, R., Pavlov, A., Schuppener, L., Schäfer, D., Histing, T. & Braun, B. J. (2025). Advantages of digital twin technology in orthopedic trauma Surgery–Exploring different clinical use cases. *Scientific Reports*, *15*(1), 1-13. https://doi.org/10.1038/s41598-025-04792-w

Paper D Andres, A., Wickert, K., Gneiting, E., Binmoeller, F., Diebels, S. & Roland, M. (2025). Simulation of a Custom-Made Temporomandibular Joint – An Academic View on an Industrial Workflow. Bioengineering, 12(5), 545. https://doi.org/10.3390/bioengineering12050545

Journal contributions as a co-author

- Braun, B. J., Orth, M., Diebels, S., Wickert, K., **Andres, A.**, Gawlitza, J., ... & Roland, M. (2021). Individualized determination of the mechanical fracture environment after tibial exchange nailing—A simulation-based feasibility study. *Frontiers in Surgery*, *8*, 749209.
- Braun, B. J., Histing, T., Herath, S. C., Rollmann, M. F., Reumann, M., Menger, M. M., **Andres, A.**, Diebels, S. & Roland, M. (2022). Bewegungsanalyse und muskuloskeletale Simulation in der Pseudarthrosentherapie–Erfahrungen und erste klinische Ergebnisse. *Die Unfallchirurgie*, *125*(8), 619-627.
- Wickert, K., Roland, M., **Andres, A**., Diebels, S., Ganse, B., Kerner, D., ... & Orth, M. (2024). Experimental and virtual testing of bone-implant systems equipped with the AO Fracture Monitor with regard to interfragmentary movement. *Frontiers in Bioengineering and Biotechnology*, *12*, 1370837.
- Orth, M., Ganse, B., **Andres, A.**, Wickert, K., Warmerdam, E., Müller, M., ... & Pohlemann, T. (2023). Simulation-based prediction of bone healing and treatment recommendations for lower leg fractures: Effects of motion, weight-bearing and fibular mechanics. *Frontiers in Bioengineering and Biotechnology*, *11*, 1067845.
- Ganse, B., Orth, M., Roland, M., Diebels, S., Motzki, P., Seelecke, S., Kirsch, S., Welsch, F., **Andres, A**., Wickert, K., Braun, B.J. & Pohlemann, T. (2022). Concepts and clinical aspects of active implants for the treatment of bone fractures. *Acta Biomaterialia*, *146*, 1-9.

Under review:

- Under review: Andres, A. *et al.* Predicting the Effect of Individual Weight-Bearing on Tibial Load and Fracture Healing after Tibial Plateau Fractures – Introduction of a Biomechanical Simulation Model. *Front. Bioeng. Biotech..*

Table of Contents

1 Introduction

Fractures of bones are a global burden in any society, for any human, independent of age, social, or societal status. They incur very high costs for the health system. Surgical fracture care has improved the results dramatically over the last 60 years regarding anatomical healing and restoring function. Today, the gold standard of fracture care is surgical treatment, i.e., open or, in an increasing number of cases, minimally invasive reconstruction of the fractured bone and mechanical neutralization of forces and loads acting on the fractured bone by implants such that immediate functional and physiotherapeutic training of the injured extremity is possible. However, wide availability is still limited to an advanced health care system. Due to the progress made, the development of conventional implants has reached a plateau; therefore, current efforts focus on refining details. New technological concepts, such as implants with novel sensor technology or even technologically active components, still need to be expanded to basic research. They will not be brought into clinical practice any time soon. Even with all the progress in minimizing perioperative surgical trauma and precision in planning, designing active implants, and execution of surgical stabilization, complications like infection, delayed healing, and non-healing (non-unions) can compromise the expected result dramatically.
Therefore, primary fracture healing and fracture non-union are the opposing ends of a continuum, rather than precisely defined entities (1–3). Despite advances in operative fracture care, studies report complications in up to 20% of cases, and clinicians can expect non-healing bones (delayed unions and non-unions) in up to 10% of cases (4,5). This complication significantly amplifies the burden of disease by extending treatment duration and necessitating additional surgical procedures, while also placing a substantial strain on the healthcare system through dramatically increased treatment costs, estimated at US$25,500 for a tibial non-union in the USA (6) and between €8,000 and €91,000 in the UK (7,8).

Fracture healing is a complex, self-organizing, multi-scale process designed to completely restore the shape and function of a damaged anatomical structure. The impact of mechanical stimuli on bone physiology, remodeling, and repair was first described by Wolff's law, with Perren's strain theory and Frost's concept of the "mechanistic" providing the conceptual foundations for today's surgical fracture care. Two factors with arguably the greatest healing influence are vascularity and the mechanical fracture environment. Fracture pattern, the type and quality of surgical stabilization, muscle forces, and axial and bending forces from movement and mobilization influence the latter. Claes and colleagues (9) have demonstrated that the resulting interfragmentary movements (IFM) within the fracture have prognostic value for healing.

Consequently, mechanical and implant-related aspects of fracture care have dominated research and development. In 2007, Giannoudis and colleagues (1) conceptualized fracture healing as a multi-scale and multi-domain process, such that the biological aspects of fracture healing were the focus of clinical and laboratory research. Nonetheless, mechanical and implant-related aspects still dominate clinical strategies. The typical treatment today is to screw a standard-sized orthopaedic plate to the fractured bone. These fixation plates are purely passive components. Medical protocols usually monitor healing by taking intermittent X-rays at set intervals, which

limits real-time insights into healing dynamics. Typically, physicians or physiotherapists monitor rehabilitation through clinical assessments at fixed intervals. This approach provides limited possibilities to adjust rehabilitation based on healing progress in real time. However, every fracture is unique due to its origin, biological factors, and healing progress. Nevertheless, treatment approaches are largely standardized. Complications like non-union are relatively common, affecting about 14% of tibial fracture cases, with delayed intervention often extending recovery times and increasing healthcare costs (3,10).
While clinical experience cannot be substituted or augmented by any technical device or algorithm, understanding the mechanical performance, i.e., applying the general laws of mechanics in a given case, is amenable to modeling, simulation, and optimization. Recording movement during recovery provides valuable insights into how movement affects the healing process. An important step towards personalized simulation is the observation of movements using instrumented pressure sensors for kinetic analysis and a motion-capturing system for kinematic analysis. Sports medicine professionals already use these systems for injury prevention and rehabilitation. Analyzing movement patterns helps prevent injuries and enables professionals to closely monitor injured athletes, thereby accelerating their recovery. Experts widely recognize movement as essential for healing after a fracture, but still need to determine the exact amount and types of movement that best support recovery. Beyond the medical aspects, social and economic factors are also important. Longer treatment times increase healthcare costs, and revision treatments require additional resources. Advanced simulation tools, including finite element (FE) models and musculoskeletal simulations, allow biomechanical analysis of patient-specific cases. By actively integrating such tools into the treatment period from preliminary examination and surgery to follow-up care, patient-specific treatment plans can be created. This, in turn, can lead to shorter recovery times and improvements in socioeconomic outcomes. Combining personalized simulations with real-time movement data offers a more comprehensive understanding of the healing process.

The following work aims to develop and validate a novel digital workflow that integrates personalized biomechanical simulations with patient-specific motion capture in the form of digital twins — a technology widely adopted in industrial settings but underutilized in healthcare. Digital twins of patients could transform rehabilitation by enabling personalized treatment planning, virtual examinations, and real-time feedback systems.
This dissertation presents a novel biomechanical workflow that continuously records and analyzes patient-specific movement data during the healing process, as illustrated in Figure 1, to assess and simulate conditions for optimizing fracture healing. The process begins with acquiring kinematic data (e.g., joint angles, motion trajectories) and ground reaction forces, which, together with individual anthropometric parameters, are fed into an inverse dynamics analysis. The outcomes of the inverse dynamics from the musculoskeletal model (e.g., joint forces, muscle forces) are the boundary conditions for the modeling process. The integration of electromyography (EMG) data allows musculoskeletal simulations to be expanded and deepened. The evaluation of computer-assisted simulations provides information about the stability of bone implants and individual healing progress. The workflow is based on existing biomechanical and imaging principles, combining the following aspects:

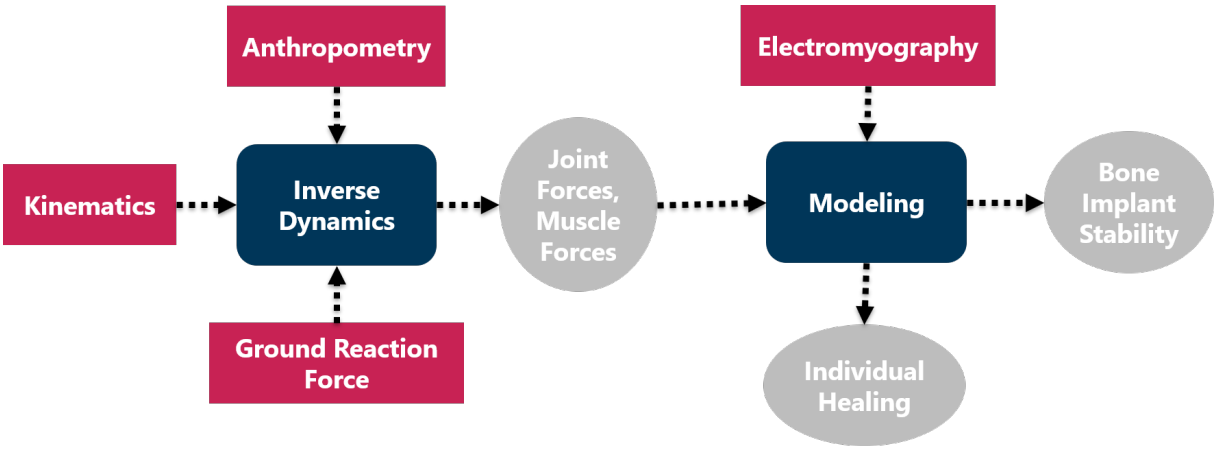

Figure 1: Biomechanical workflow with kinetic and kinematic measurement tools (red) to accurately measure parameters in healthy individuals and patients. Analysis of the collected data in computational methods (blue) to estimate outcomes (grey) related to fracture healing.

1. Systematic recording and analysis of healing processes over different time periods,
2. Implementation of clinical and biomechanical data in biomechanical models,
3. Integration of realistic boundary conditions, such as muscle and joint forces in finite element simulations,
4. Derivation of interfragmentary movements from real patient movement,
5. Feedback of this data into a digital patient twin model.

This process chain enables early detection of healing disorders and creates the basis for simulation-supported, adaptive therapy planning. It makes it possible for the first time to investigate the influence of different loading scenarios on interfragmentary movement and healing success. This approach represents a paradigmatic step towards adaptive, patient-centered fracture therapy. In contrast to previous "fire-and-forget" approaches, this approach provides a dynamic model of fracture healing with personalized prognostic power.

2 Motivation

This study aims to address key questions regarding fracture healing mechanics, particularly focusing on processes occurring within the fracture gap. Specifically, it seeks to answer the following questions: What happens in the fracture gap? What stresses and strains are present in this area? What individual factors influence these processes?

The primary objective is to investigate how patient-specific conditions affect IFM and bone-implant stability. IFM is a critical parameter for fracture healing (11), as both external and individual factors directly influence it. The thesis hypothesis proposes

testing different levels of partial loading virtually and individually quantifying their effects on the IFM. The initial step has been the implementation of a functional monitoring workflow for patients, with the analysis of musculoskeletal simulations. This approach helps to identify individual factors, determine and validate a biomechanical model, and help patients with early results by implementing patient-specific treatment plans and rehabilitation. The final step involves identifying key parameters and creating a functional digital process chain that combines personalized biomechanical simulations and patient-specific boundary conditions via digital twins. The term “Digital Twin” (DT) has widespread adoption in industrial sectors, such as aerospace and manufacturing (12). Their application in healthcare, however, remains underrepresented. Human Digital Twins (HDTs) are defined as ‘computer models of humans tailored to any patient to allow researchers and clinicians to monitor the patient's health, for providing and testing treatment protocols’ (13,14), but their adoption is still hindered by key challenges, including ethical concerns, trust, adaptability, and cognitive-behavioral modeling (14).

3 Clinical Relevance

Fracture healing can be a complex and lengthy process that significantly burdens patients and society. With a lifetime prevalence of 44% in adults aged 55 years or older, fractures remain a major public health problem. In 2019, 688.403 fractures were registered in Germany (15). With this knowledge, it is unsurprising that orthopedic and trauma surgeries represent a significant portion of hospital interventions in Germany, with fracture management playing a central role. Among the various procedures, the open reduction of multi-fragment fractures in the joint area of a long tubular bone is the 7th most common, performed 241.174 times annually. In contrast, closed reduction with osteosynthesis ranks 14th, with approximately 171.251 cases per year (16).

The economic burden is substantial, with statutory health insurance funds reporting expenditures of €98.1 million for femur fractures, €57.8 million for lower leg fractures, and €35 million for forearm fractures in January 2011 alone (17). Globally, tibial shaft fractures are among the most prevalent, with an incidence of 20 per 100,000 people annually (18) and 492,000 cases reported annually in the United States (19). An analysis of the national registers for the years 2004 to 2012 in the Netherlands revealed a significant increase in extremity fractures of 26.7% (20). Functional recovery after tibial shaft fractures is often associated with limitations in sports participation reported by 60% of patients, restrictions in quality of life experienced by 58%, and a higher incidence of persistent knee pain (18). Despite various treatment strategies, complications persist. One type of complication is the occurrence of healing delays, so-called non-unions or pseudarthrosis. In 5–10% of cases, impaired bone consolidation leads to pseudoarthrosis, which negatively affects physical and mental health (3,21); some sources even estimate rates as high as 20% (5). In most cases, this leads to a delayed reintegration into everyday life and the original activity (22). To better understand and address the biomechanical factors contributing to delayed healing, researchers have focused on the role of interfragmentary shear in the fracture repair process.

Experimental studies have investigated the in vivo effects of interfragmentary shear on bone healing (23–25), primarily in animal experiments. For example, Steiner et al. used numerical models in sheep to show that translational shear impairs healing more than torsional shear (26). Other experiments investigate rabbit tibia models (27) or rat fracture healing studies to improve the characterization of interfragmentary motion (28). The complexity of these experimental studies is evident in various reviews. For example, Betts et al. (29) describe the mechanical regulation of bone regeneration using theories, models, and experiments, and Barcik et al. (30) discuss the effects of optimizing the mechanical environment on fracture healing time. The studies also show that pure shear is not necessarily harmful to bone healing. This means that it is important to analyze the exact strength and direction of the movements between the fragments. This highlights the importance of precise mechanical boundary conditions for optimal fracture healing.

4 Thesis Structure

The introductory section already provides insight into the complex question of what influences the healing process of bone fractures and how these factors interact. This question cannot be answered adequately by any single discipline. However, an interdisciplinary view of the processes can provide partial solutions and explanations.

The following sections actively introduce the fundamentals of scientific research and clinical application, while examining fracture healing through various disciplinary lenses. We begin with biomechanics as a central interdisciplinary field that provides a unifying framework for the topics discussed throughout this work. Biomechanics applies the laws of mechanics to biological systems. It serves as a basis for further introduction to other relevant areas:

- **Biology:** Introduction to the physiological mechanisms of bone healing phases
- **Medicine:** Influence on fracture movement and the effects on fracture care
- **Biomechanics:** Analysis of the interfragmentary movement and mechanical stimulation
- **Life Science:** Consideration and influence of human movement during recovery and presentation of a clinical workflow for recording movement patterns.
- **Mechanics**: Therapeutic framework of computer-based modeling through numerical simulations

The end of the thesis describes the concept of the digital twin, detailing its core elements and development phases. The digital twin is explained theoretically and in the context of the interdisciplinary topics discussed above. The insights gained in the individual areas are systematically linked to the theoretical foundations and categorized in the attached scientific publications. A summary for each publication provides an overview of the most important findings. The thesis concludes with a

conclusion and an outlook that outlines potential future research questions and further developments of the digital twin.

5 Biomechanics

Figure 2 presents a detailed multi-scale-dimensionality in space of a bone-implant system. The macro level considers the entire bone implant system, where the mechanobiological concept of fracture healing comes into play. It is based on mechanical stimuli and interfragmentary movements (31,32), explained in more detail in Chapter 7. The multiscale structure consists of the mesoscale, which zooms in on the fracture gap. The micro level describes cellular structures via mesh modeling. And finally, the sub-micro level depicts molecular and sub-cellular interactions, using histological imagery.

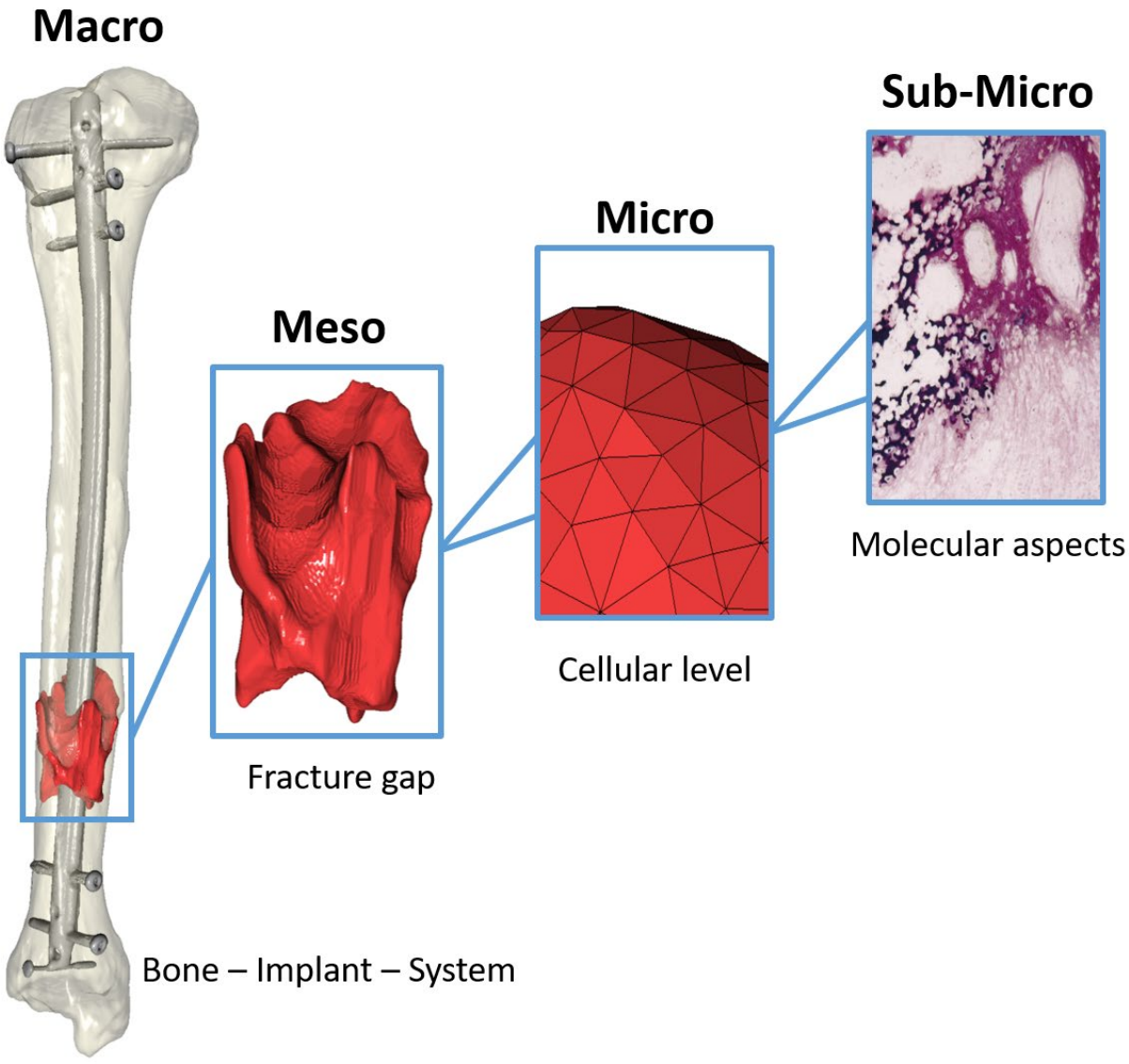

Figure 2: Multiscale structure of a bone-implant system, from the macro scale (whole bone) to meso (fracture gap), micro (cellular), and sub-micro (molecular aspects).

Biomechanics examines the movements of humans and animals from the point of view of the laws of mechanics. Since no non-mechanical movement exists in material systems, biomechanics examines human and animal movement through the lens of mechanical principles. Consequently, the subject of biomechanical investigations is the mechanical movement (change of position of mass parts) of humans and animals, taking into account the mechanical properties and prerequisites of the locomotor system, which are functionally dependent on the biological conditions of the organisms. Subject areas of our biomechanics research group are:

- Quantifying IFM
- Quantifying implant bone interactions
- Assessing implant stability
- Patient-specific individualization for in vitro and in silico models

Our group uses imaging techniques, movement analysis, and musculoskeletal modeling to individualize the estimation of joint and muscle forces. We emphasize a holistic approach, particularly concerning the validity of our results. Consequently, in vitro experiments using human cadaveric specimens to test forces and moments in bones and implants are essential to our research (33).

6 Bone Healing

Fracture healing is a dynamic, multifactorial, and multistructural process. Understanding the various influencing factors is crucial to the healing outcome. Starting with the patient's environment, their physical living conditions, and their socioeconomic status. On the patient side, factors such as the type and severity of the injury, age, the kind of movement, the level of stress, existing illnesses, infections, blood circulation, and material compatibility have a decisive effect on the healing process. Clinically, treatment type and the physician's experience influence the healing outcome. Treatment methods can promote healing (e.g., load-sharing implants, bioactive surfaces, integrated sensors and actuators) or impair it (e.g., mechanical failure, material fatigue, inadequate fixation). The interaction of all these factors ultimately determines the duration and quality of the healing process. Regarding the bone healing itself, five essential foundational theories provide insight into bone regeneration:

- Wolff's law (34): Bones strengthen in density with mechanical loading and weaken with disuse.
- Pauwels' causal histogenesis (35): Specific mechanical stimuli influence tissue differentiation during healing.
- Frost mechanistic (36): Mechanical usage thresholds regulate bone turnover, and stimulation is necessary to maintain bone mass.

- Perren's strain theory (37): The Magnitude of interfragmentary strain dictates the type of tissue formed.
- Claes fracture gap hypothesis (31): Micromotion at the fracture site and its role in stimulating tissue formation.

The mentioned theories describe how the mechanotransduction process transforms mechanical signals (mechanical stimuli) into cellular responses. The intensity, duration, and timing of mechanical stimulation are crucial in shaping bone structure.

Figure 3 outlines bone healing as a multiphase and multiscale process comprising various stages. At the beginning (seconds to days), a hematoma forms at the site of injury, triggering inflammation in the early healing phase. This phase is characterized by coagulation, proinflammatory reactions, and the organization of granulation tissue. Preserving the hematoma is important because it triggers the inflammatory response to create the biological environment necessary for healing. A balanced inflammatory response regulates cell recruitment and matrix formation. If the body produces too many inflammatory signals, healing can be delayed or disrupted. On the other hand, if there are not enough, the body may not send enough repair cells to the injury site (38). Subsequently, revascularization and cartilage formation occur during the soft callus phase (days to weeks), where new blood vessels invade the area, and the enchondral ossification process begins. Angiogenesis, the formation of new blood vessels, plays a vital role in ensuring adequate oxygen and nutrient delivery to regenerating tissue (39–41). The integrity of surrounding muscle tissue further contributes to vascular supply and limits mechanical shear at the fracture site. In the next stage, the hard callus phase (weeks), cartilage is mineralized, producing woven bone. This marks the beginning of structural regeneration. Resorption and remodeling of the callus complete the healing process (weeks to months). In this final phase, the cells rebuild the vascular structures, reopen the bone marrow cavity, and reduce excess callus tissue. This restores the original structure and strength of the bone. The biological potential for regeneration varies significantly between individuals and fracture sites. Below are some statements with references to literature on factors influencing bone fractures:

- Age: With increasing age, bone density decreases, and the elasticity of the tissue diminishes (42).
- Nutrition: A lack of nutrients such as calcium and vitamin D can impair bone regeneration (43,44).
- Gender: Women are at a higher fracture risk during menopause due to falling oestrogen levels (45).
- Lifestyle: Smoking, excessive alcohol consumption, and lack of exercise (46).
- Diseases: Diabetes impairs fracture healing due to reduced function of immune cells (47), and rheumatism delays fracture healing (48).

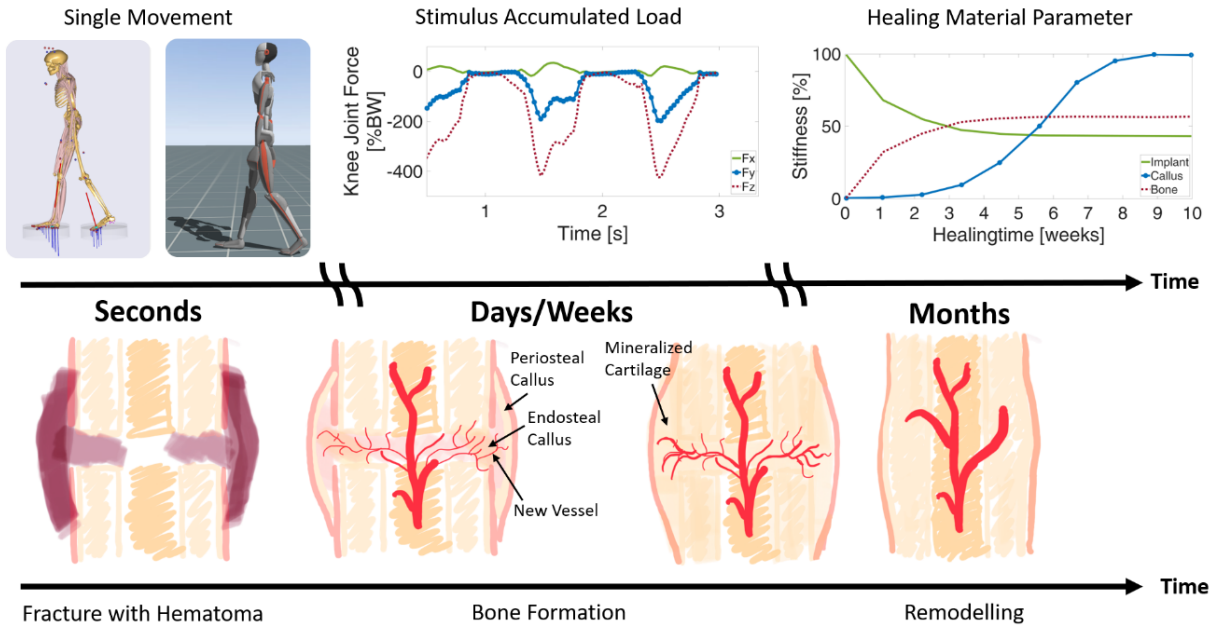

Figure 3: Illustration of different time scales of fracture healing.

Figure 3 also illustrates the influence of biomechanical stimuli and biological responses over time.

- Seconds — Individual movements that cause mechanical stimuli between the bone fragments (IFM, see Chapter 6.1).
- Days — Various movements and, therefore, various mechanical stimuli accumulate. Physiotherapy sessions during this phase apply mechanical stimuli without overloading or underloading to promote healing. The goal is to use an appropriate activity.
- Weeks — Material parameters change as local tissue stiffens and callus forms. Stimuli must be adapted accordingly.

In order to detect changes in movement patterns with increasing resilience in patients, the individual collection of movement data during the healing process is essential. In this context, Paper B examines the results of continuous motion recording, from the first steps after a distal tibial fracture to complete recovery. Key parameters are analyzed in terms of their development over time and related to the osteosynthetic used. The effectiveness of personalized approaches, such as the concept of the digital twin (Paper C), always depends on individual patient factors and biological processes that can influence both the risk of fracture and the healing process.

6.1 Interfragmentary Movement

IFM refers to the micro-movements between bone fragments of a fracture during the healing process. Controlled IFM plays an important role in stimulating callus formation and promoting bone regeneration. However, the influences of the extent and direction of IFM must be considered. Excessive movements can lead to non-healing or delayed healing. Insufficient movement, for example, due to overly rigid fixation, can inhibit the biological processes. Effective bone healing depends not only on the occurrence of IFM but also on appropriate IFM for the fracture type and geometry. Targeted loading of the fracture site is crucial for healing progress. During the healing process, the bone gradually regains the ability to bear increasing loads itself, meaning that the implant gradually has to contribute less to load transfer, as shown in Figure 3 by the progression of stiffness over the healing period. Several biomechanical and implant-related factors shape the extent of the IFM, including fracture gap size and geometry (49,50), applied load, and the stiffness of the fixation construct, which depends on the configuration of screws and plates (including their material, restraint, and position) (51,52).

Research, such as the studies by MacLeod et al. (53), highlights key factors affecting IFM. Patient-specific material properties and implant-bone interface modeling play a minor role. In contrast, the configuration of devices (placement, number, tension, and materials), geometry, and loading conditions have a major impact on the extent of IFM. Because of the complex interplay between geometry, load, and fixation, defining exact thresholds for IFM remains challenging. Quantitative studies on axial IFM analyzed by Rechter et al (54) show a high degree of variability in the interfragmentary movements measured. Small to moderate movements of 0.03 to 1.0 mm are indicative of successful healing, while larger movements of up to 2.4 mm can compromise the quality of the callus. In addition, the directional component of the movement also matters. Märdian et al (55) demonstrated experimentally that shear movement delays healing, while axial movement can be beneficial.

6.2 Fracture Repair and Treatment

From a biological perspective, the primary goal of surgical fracture reduction and stabilization is to create an optimal environment that supports the intricate process of fracture healing. Whether a patient benefits from surgical treatment depends on several patient-specific factors, such as existing comorbidities, the ability to adhere to the rehabilitation plan, and functional expectations and needs. In addition, each patient receives individual care throughout the entire treatment process. Another decisive factor influencing the outcome is the choice of a suitable treatment. These decisions are based on the clinical expertise and practical experience of the treating surgeon. Figure 4 shows four different ways of treating a tibial fracture. Each option offers advantages and disadvantages, but the treating physician ultimately chooses the type of treatment based primarily on their knowledge and training.

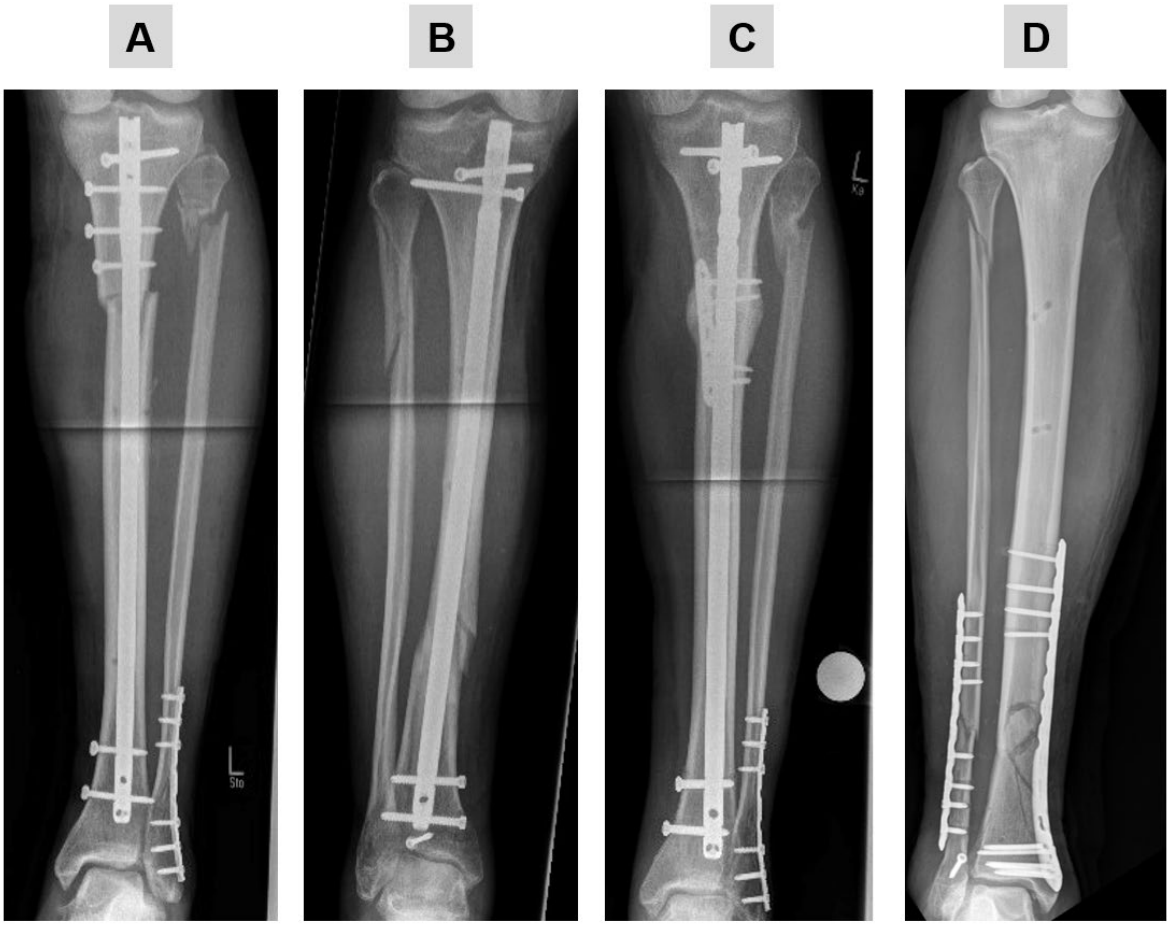

Figure 4: Different treatment variations for tibia fractures. (A) Intramedullary nail with six screws, (B) intramedullary nail with four screws, (C) intramedullary nail with adaptive plating, and (C) plate osteosynthesis.

Equally important is an understanding of mechanical principles to effectively control the microscopic processes of fracture healing. Biomechanical factors are often the primary reason for failure of fracture healing. Common complications in fracture treatment include malalignment, delayed healing, bone failure, hardware failure, and non-union (permanent failure of the healing process). The previous chapter discussed biological influences on fracture healing. However, this thesis focuses primarily on mechanical factors, as supported by the following quote.

“Fracture Repair – It is all mechanics”

(Rossiter Nigel (56))

The mechanical aspects play a critical role in successful fracture management. Key factors include bone-implant stability, fracture stability, stress shielding, load sharing,

implant stability, and implant fixation. Figure 5 illustrates the concept of plate screw density in 2D (A) and 3D (B). The example shows that the central section over the fracture is left without screws. The total plate screw density is therefore 50% (57). The overarching aim of osteosynthesis is to maintain implant stability while creating appropriate fracture stability to promote healing. However, technical errors, such as undersizing the plate, selecting an incorrect working length (too short or too long), or improperly applying screws, cause many plate failures. In addition, there is no universally accepted standard for fracture treatment. Several studies have examined how the working length of locking plates influences interfragmentary movement in distal femur fractures (58–60). Fracture repair and treatment paper C details the topic of fracture repair and treatment in more detail, and paper B investigates the healing process of the case shown in Figure 4 (D) and Figure 5.

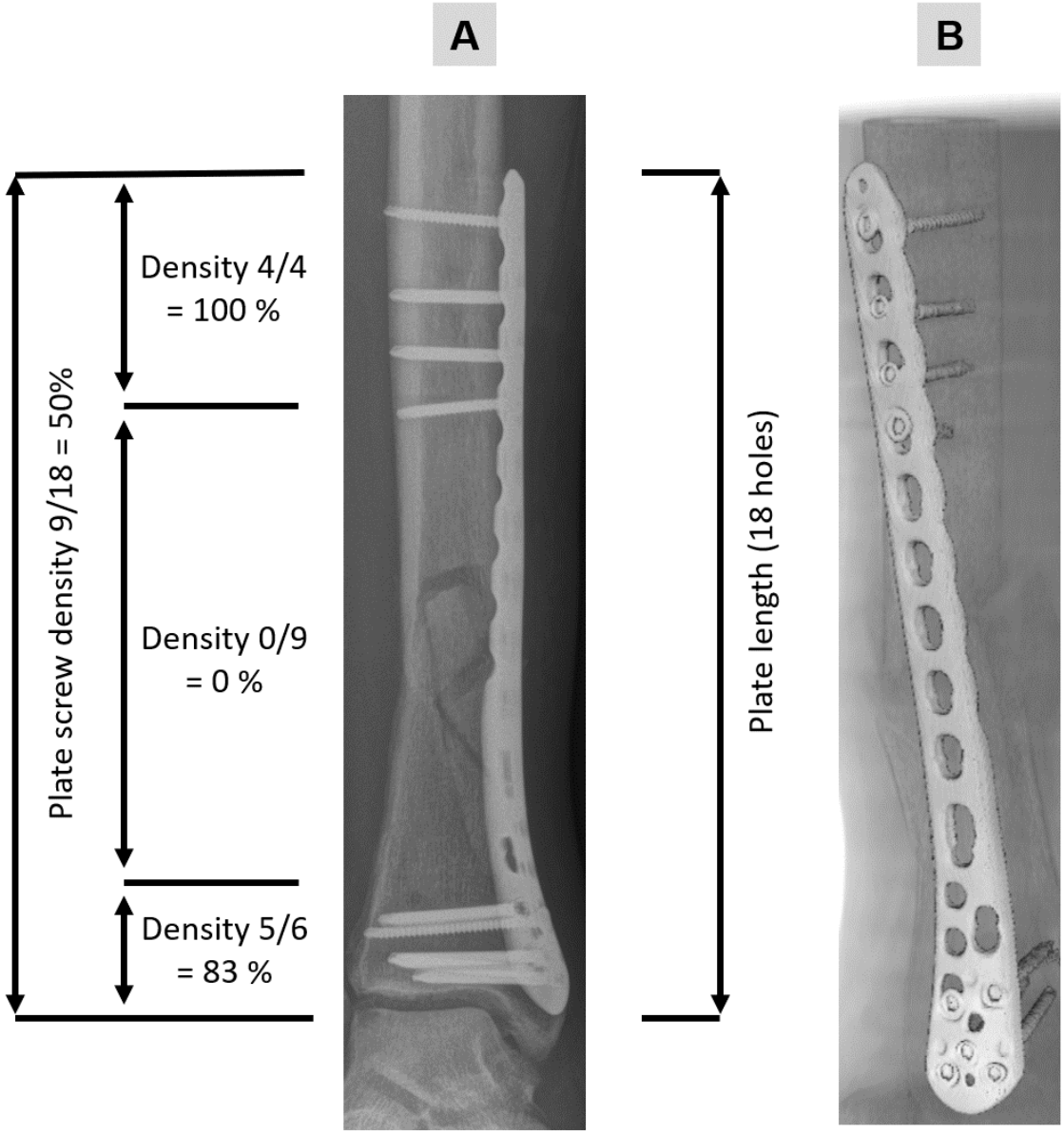

Figure 5: Definition of the plate screw density.

6.3 Stimulation

The following section explains the mechanical stimulation of fractures, specifically the effects of frequency, amplitude, and the controlled application of mechanical forces on bone healing. Ultimately, it refers to the laws defined by Wolff in section 2.2. Briefly summarized, Wolff´s law states that bone adapts to mechanical loads by strengthening in response to stress. One type of mechanical stimulation, dynamization, relates to fracture treatment by reducing fixation stiffness to allow controlled micromovements at the fracture site (11,61). A subtype of this is reverse dynamization, which alternates between rigid and flexible fixation phases (62). Clinically, early postoperative phases often use weight-bearing stimulation to prevent fixation failure, while actively supporting callus stimulation. Weight-bearing grades range from "non-weight bearing", where the leg must not touch the floor, and crutches are essential, to "touch-down weight bearing", allowing only toe contact for balance. "Partial weight bearing" permits a small, gradually increasing load with an ambulatory device (cane or crutch), while "weight bearing as tolerated" allows 50 to 100% weight depending on the patient's condition. "Full weight bearing" enables the leg to support the entire body. Current clinical practice often advises partial or no weight bearing in the early postoperative phase to prevent fixation failure, waiting for the callus to form.

Research on mechanical stimulation presents mixed findings (see Table 1). The major challenge in interpreting these results lies in the diversity of their methodological origins. Each publication uses different animal models and fixation methods, making a direct evidence comparison impossible. Furthermore, it is unclear what the optimal dosage of mechanical stimulus is and how individual patient-specific factors (fracture type, treatment method, bone quality, etc.) influence it.

Table 1: Different statements to timing and impact of mechanical stimulation.

Timing and impact of mechanical stimulation	
Statement: **“**Early is important.**”**	**Statement** “Later is preferred, while earlier is less desirable.”
“Frequent, early postoperative stimulation accelerates healing progression” (63)	“Early full weight bearing with flexible fixation delays fracture healing” (64)
“Early mechanical stimulation only promotes timely bone healing” (65)	“Early dynamization by reduced fixation stiffness does not improve fracture healing” (66)
“Reverse dynamization accelerates bone healing” (62)	“Late dynamization by reduced fixation stiffness enhances fracture healing” (67)

7 Clinical Workflow and Digital Process Chain

The clinical workflow described in this chapter complements the biomechanical workflow presented in Figure 1, offering additional clinical context and practical applications for each step outlined in the figure. Our established clinical workflow (see Paper A) consists of the following steps: (I) Monitoring of the patients during the planning and follow-up visits with a motion capturing system (Xsens^{TM}) and sensor insoles; (II) Transfer of the motion data into the musculoskeletal simulation system AnyBody^{TM} to achieve the corresponding individual muscle and joint forces, as well as moments; (III) Clinical imaging of the patients, if available, via postoperative computed tomography (CT) scans, ideally combined with a six-rod bone density calibration phantom; (IV) Segmentation of the CT images and generation of the corresponding adaptive finite element (FE) meshes of the bone implant systems, including the material parameters based on the Hounsfield units and the calibration phantom via the software Simpleware^{TM}; (V) Integration of all information from the musculoskeletal simulation as patient-specific boundary conditions into our biomechanical FE simulation process based on the patient-specific meshes. Figure 6 shows a typical setup of a patient measurement using the Awinda system from Xsens^{TM}.

Figure 6: Patient measurement with a motion-capturing system and sensor insoles. [Image: Werner Siemens Stiftung/Oliver Lang]

7.1 Monitoring

The monitoring strategy described in this section refers to the first part of the biomechanical workflow depicted in Figure 1. This first part includes the recording of kinematics, ground reaction force, and anthropometry as parameters for calculating joint and muscle forces. Monitoring generally refers to the continuous or regular observation and recording of data or conditions. Monitoring generally refers to continuous or regular observation and recording of data or conditions. The main objective of this work regarding monitoring was to create a movement database for healthy subjects and patients. The movements are dependent on the injury in question. Precise analysis of movement patterns in fractures of the lower and upper extremities led to the creation of parameters that identify deviations from the natural, healthy movement profile. Many studies primarily utilize camera-based motion analysis (68), while we used a more portable version of kinematic recording. The Xsens™ system is a room-independent system consisting of 17 inertial measurement units attached to strategically important body positions (69). The system proves particularly effective for measuring patients directly in their hospital room a few days after their operation, during their rehabilitation process, and even in their homes during daily living. Figure 7 presents knee joint angle data from a participant walking with crutches under two conditions: one with correctly adjusted crutches (Figure 7A) and one with too-low crutches (Figure 7B). It shows three types of knee motion: flexion/extension, abduction/adduction, and internal/external rotation over a 15-second interval. During flexion, the curve for crutches set too low shows an increase in the knee joint angle above 60 degrees. In a healthy gait, the knee joint angle typically does not exceed 60 degrees during the swing phase. These higher knee joint angles indicate an additional load, which further affects knee joint forces, as discussed in more detail in Figure 8.

A key step in the biomechanical workflow is the inverse dynamics to analyze muscle forces**,** joint reaction forces, and joint moments. The software AnyBody™ enables inverse dynamics analysis based on predefined kinematic data. For this purpose, the workflow uses the AnyBody™ Managed Model Repository (AMMR), an open-source database containing a wide range of anatomical and functional model components. This allows for the creation of individualized anatomical representations of the musculoskeletal system. The underlying muscle models are phenomenological and based on the classical work of A. V. Hill (70). Contractile elements represent muscles. Muscle activation is solved using optimization algorithms (71). The underlying models and computational implementation are described in the work of Damsgaard et al. (72). Various fields already use models developed with AnyBody™, including ergonomic optimization (73), clinical surgical planning (74), and orthopedics (75,76).

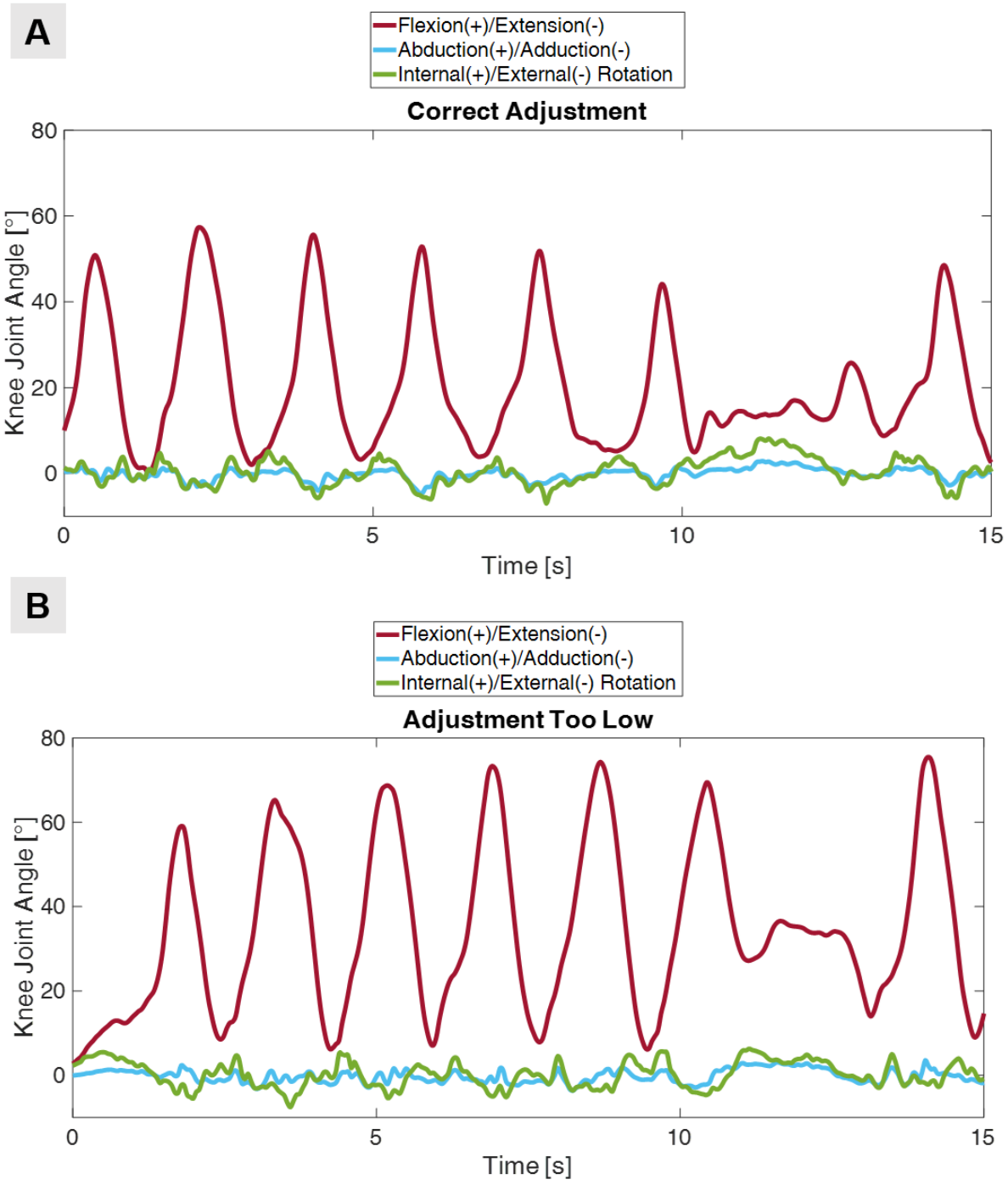

Figure 7: Visualization of knee joint angles during two crutch-assisted steps, illustrating the impact of incorrect crutch adjustment on gait.

Figure 8 shows the knee joint force data of the same participant under the same two conditions: correctly adjusted crutches (Figure 8A) and crutches set too low (Figure 8B). The graphs present forces in three anatomical directions (anterior/posterior (blue), proximal/distal (red), and medial/lateral (yellow)) normalized to body weight (%BW) over time. The proximal/distal direction shows the highest and most cyclical forces, reflecting the primary load-bearing role of the knee during walking. If the crutches are set too low, there is an increase in force values in both the proximal/distal and

anterior/posterior directions. The latter indicates inefficient or unstable gait mechanics. The test subject must exert more effort to maintain balance. The stooped posture caused by low crutch settings increases the axial knee load by approximately 20%. This crutch example demonstrates how even small adjustments, such as crutch height, can significantly influence kinematics. Papers B, C, and D describe the influence and effect of motion capturing in different use cases.

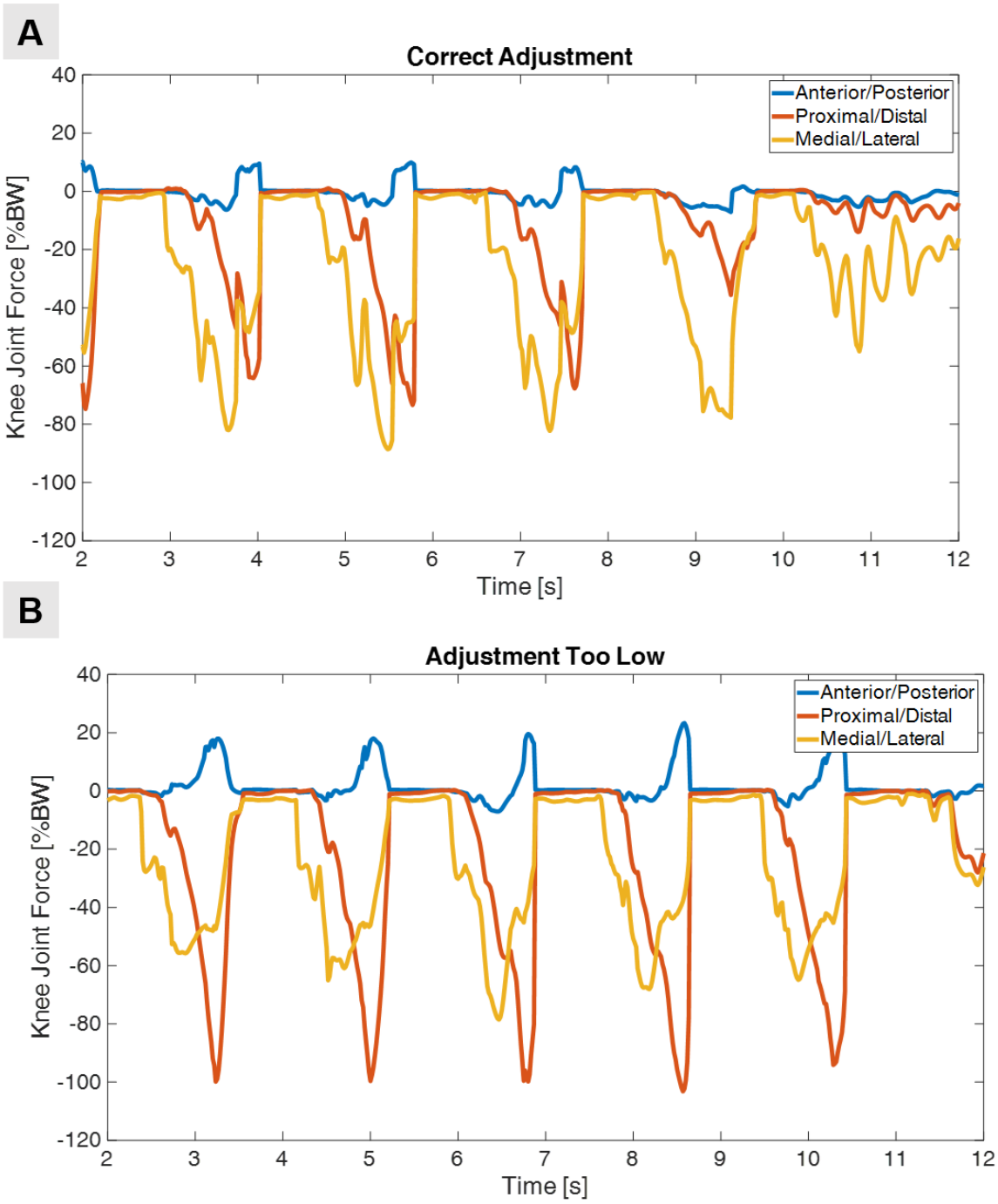

Figure 8: Visualization of knee joint forces during two crutch-assisted steps, illustrating the impact of incorrect crutch adjustment on gait.

A validation opportunity for joint forces is the free public database OrthoLoad™ (77). The data collection provides in vivo joint force data collected from instrumented implants in real patients. The database includes measurements for the hip, knee, shoulder, and spine during everyday activities. However, it is limited to the directly measured joint forces, without information on the involved muscular activity. Other software tools for musculoskeletal modelling are OpenSim™ (78) or 3R-BioMedicUS™ (79). All tools enable a more comprehensive analyses that include muscle forces.

In addition to kinematic motion capture, it is also possible to record kinetic data. This is particularly important in patients with lower limb fractures and their healing progress. As described in Chapter 5.6, partial weight bearing during the initial healing phase significantly influences the mechanical stimulation. Measuring insole sensors are essential to capture this partial weight bearing accurately (80). Paper C analyzes the development of kinetic parameters over a 12-week healing period. Figure 9 shows two systems used for force measurement: Figure 9A displays the values from the force-measuring insoles, while Figure 9B shows the contact forces recorded by the loadpads. During the monitoring, participants wore insoles that measured ground reaction forces inside their shoes. At the same time, capacitive sensors in the form of loadpads equipped the crutches. The loadpads measure contact forces between palms and crutches. Data collection occurred simultaneously, which explains the structure of Figure 9: 9A emphasizes the insole force data, while 9B focuses on the concurrently recorded contact forces from the loadpads. The insole data for the left foot (reference leg) shows a characteristic double-peaked curve corresponding to the stance phase of the gait cycle. An initial upward acceleration of the body's center of gravity is needed to move the trailing leg past the reference leg, leading to the first peak, where the ground reaction force exceeds body weight. A minimum follows as the body accelerates upward. A second upward force occurs to prevent further descent of the center of gravity, producing the second peak in the force curve.

In contrast, the force curve for the right leg differs significantly due to offloading with the crutches. Under normal, healthy conditions, the force curve of the right leg would resemble that of the left. Figure 9B focuses on the loadpad data as the primary signal (dotted lines), while the insole data appears in the background as a reference. The loadpad results for the left (dashed red) and right (dashed blue) contact range between 200 and 400 N. It is also clearly visible that the force values from both loadpads occur simultaneously, indicating a three-point gait with crutches, where both crutches are placed on the ground first, followed by the movement of the leg intended for relief. The loadpad measurements align with the stance phase of the right leg. The crutches actively support the portion of body weight that the injured leg cannot—or should not—bear during the stance phase, especially in cases where partial weight-bearing is prescribed.

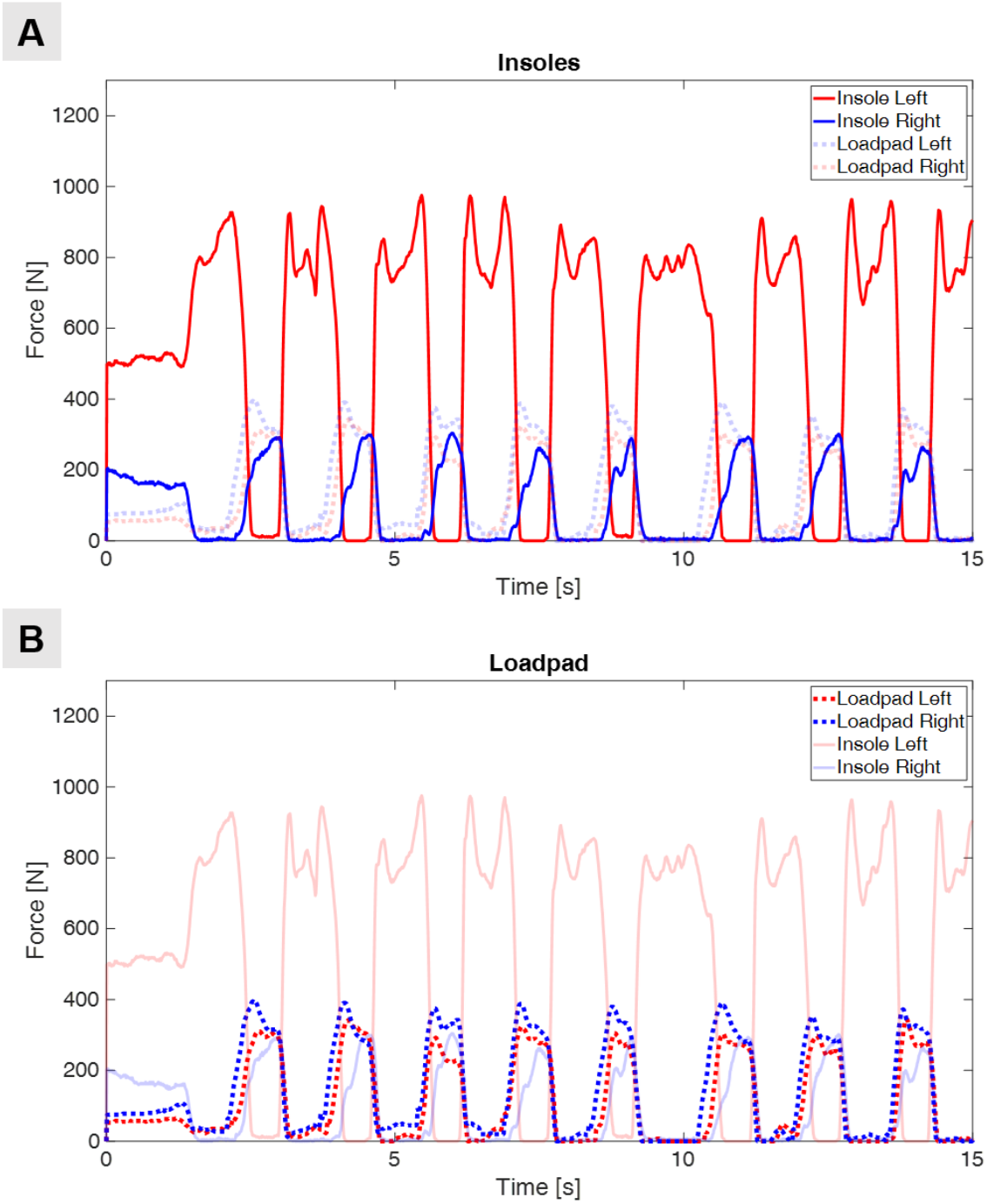

Figure 9: Force measurements over time using instrumented insoles and loadpad sensors.

7.2 Computational Models

The computational modeling processes correspond to the second part of Figure 1, which applies individualized boundary conditions and finite element simulations. The simulations use musculoskeletal outputs as boundary conditions to analyze the IFM and stress distributions of the osteosynthesis. The finite element method (FEM) is a numerical calculation method for the approximate solution of problems from different areas, for example, in mechanical applications, vibration, and stability analyses. Further evaluations address failure predictions and material fatigue (81). In a clinical context, researchers can use FEM to optimize implant designs, reconstruct fracture segments, or evaluate implant configurations. Furthermore, it is possible to analyze the effect of physiological boundary conditions on the bone-implant system. The process of a finite element calculation consists of the following parts:

- Definition of the task
- Creation of a mechanical model (idealization of the geometry, material properties, bearing, and load)
- Preprocessing: Discretization
- Calculation: Setting up a system of equations and solving for system variables
- Post-processing: Presentation of results and evaluation
- Control: plausibility check, experiments.

The discretization process utilizes finite elements. Possible shapes of these elements are triangles, squares, tetrahedra, hexahedra, and other geometries. Each element has a node at each corner, which acts as a connecting point for neighboring elements. Together they form a continuous mesh. However, higher-order elements may also include mid-side or internal nodes (82). The separation of a continuum into finite elements enables numerical approximations of desired results such as stress, strain, and deformation. FEM models must take control points into account to ensure reliable results. The greatest source of error originates from inadequate model creation and incorrect operation of the FEM software. For this reason, error checking imposes various requirements on an FEM model. The following criteria are especially relevant when assessing model design:

- **Appropriate**: Does the model address the question/problem? From a biomechanical point of view, for example, is the simulation tailored to the specific issue, such as evaluating interfragmentary movement or optimizing implant placement?
- **Reliable**: Are the results reproducible under identical conditions to ensure consistency and dependability?
- **Valid**: Does the simulation quantify the intended mechanical properties and behaviors?

- **Relevant**: Can your target audience (engineers, researchers, or surgeons) recognize and interpret the result?

Figure 10 presents the process diagram of a simulation framework in a biomechanical context. It outlines the key steps for setting up a FEM simulation with individualized adaptations. The flowchart illustrates a model credibility assessment framework that begins with the question of interest, which in turn leads to the initial model proposal. After defining the application of the model, its influence, and how validation and verification should be conducted, it proceeds to the credibility activities. The model risk in the initial model proposal depends on the model influence, the importance of the simulation factor for later decisions, and the decision consequence, which is the significance of a statement with wrong predictions. Two parallel frameworks are presented in this section, interacting through calibration and adjustment using realistic patient-specific data and input sharing, which enables model modification based on experimental results. Following that is the verification, validation, and applicability section:

- Verification confirms the correct implementation of the computation model, ensures adherence to its mathematical formulation, and verifies that the numerical algorithms converge to the proper solution.
- Validation involves comparing the model's predictions with in vitro (e.g., human cadaveric specimens or animal experiments) or in vivo (e.g., clinical trials) findings to establish its accuracy and reliability in representing the actual physical systems.
- Applicability ensures that the context of use is in context with the evaluated validation points.

The possible outcomes are shown at the end of the flowchart in Figure 10. If the evaluation is positive, the model under investigation can be used in the intended application. If, on the other hand, the results are unsatisfactory, the test steps performed must be adjusted. This may include, for example, refining the model or optimizing the test setup. The procedure is based on the ASME V6V 40-2018 standard (83), as there is no comparable guideline in Europe to date.

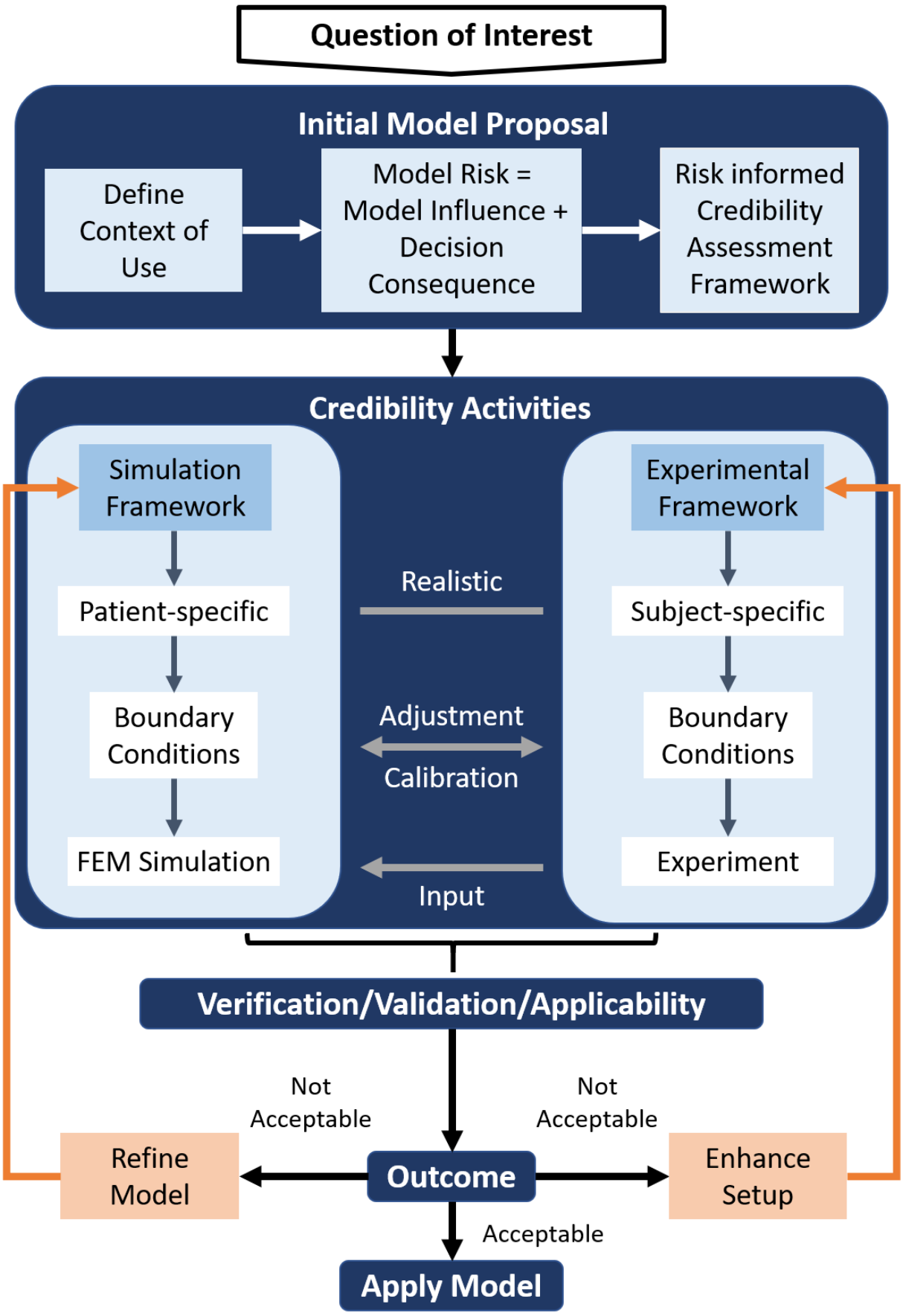

Figure 10: Model credibility assessment framework.

7.3 Segmentation Process and Material Parameters

The segmentation and material mapping in this chapter refer to the second part of Figure 1, which involves integrating clinical imaging into biomechanical models. By deriving patient-specific geometries and bone properties from CT data, this stage provides the structural foundation for accurate simulation outcomes. Our working group uses Simpleware™ version V-2024.06 to process patient CT data.

The underlying geometric models of the patients form the basis of all simulations, i.e., the virtual representation of the virtual twin. Here, the quality of the clinical image data directly determines the degree of individualization. In the best-case scenario, a postoperative CT scan is available that shows the entire fractured and surgically treated bone, allowing a fully personalized three-dimensional (3D) model of the patient using a semi-automatic segmentation process. However, data of this quality and scope are rarely available. The image data available for a patient range from preoperative X-ray images or CT scan data, which provide a partial or complete view of the fracture, to various types of image data captured intraoperatively during surgery, and to postoperative X-ray images at different time points (patient follow-up) or CT scans when clinically necessary.

To achieve the goal of a model as individualized as possible for a patient, the existing two-dimensional (2D) and/or 3D image data are segmented, and the corresponding anatomical landmarks are identified. A common model then registers the segmented data. During segmentation, the system creates masks from the volumetric 3D data. These masks act as segmentation labels, applied to the voxel-based representation of the 3D data. Each voxel (= 3D pixel) in the dataset is assigned a label indicating whether it belongs to a particular structure, material, or region of interest. The multi-mask system enables the simultaneous creation and management of multiple masks, which is useful for differentiating between different anatomical areas and materials.

Figure 11 illustrates the comprehensive process for generating a finite element mesh with a personalized bone mineral density distribution derived from medical imaging. The example CT scan shows a tibia with an intramedullary nail, a fibula with plate osteotomy, and a calibration phantom. The semi-automatic segmentation process assigns masks to individual materials, represented in gray for metallic artifacts, light yellow for bone, red for fractures, and brownish for calluses. The transparent 3D representation illustrates the individual areas in detail. The segmentation process requires the following steps:

1. Start a new project from DICOM images.
2. Image processing
    - **Threshold**: Perform segmentation based solely on lower and upper grayscale boundaries.
    - **Morphological close filter**: Merge fine structures and add connectivity to the mask.
    - **Cavity filter**: Removes small holes while preserving the marrow as a cavity within the segmented bone.

- **Smoothing and removing artifacts from the data:** The mask keeps the grayscale background information to generate more accurate and faithful surfaces.

These steps are necessary for all masks. Additional image processing options, such as painting or erasing an active mask, are available, utilizing smart grayscale selection algorithms or Boolean operations.

The next step involves mesh generation and materials assignment. The output includes volume meshes of various sizes and their respective material properties. The system incorporates all masks required for the subsequent finite element model. Figure 11 also shows a cross-section through the distal part of the tibia depicting the tetrahedral high-resolution adaptive volumetric mesh. The model configuration area defines settings for the following points:

- **Volume meshing:** Settings to define the desired element type (tetrahedra, linear, or quadratic) and the mesh density.
- **Materials:** Settings for the material type are placeholder, homogeneous, or grayscale-based.
    - **Bone**: Material type: grayscale based
    - Material properties based on the image intensity: Higher grayscale values correspond to a greater material modulus. Material properties are created by setting up mapping functions from greyscale to mass density, then the mass density to Young's modulus and Poisson´s ratio.
- **Define node sets:** Create custom node sets using the region of interest to set up boundary conditions in the finite element simulation tool.

The color coding then ranges from material with a lower modulus of elasticity (blue) to material with a higher modulus of elasticity (red), as is visible, for example, in the cortical bone.

In summary, segmentation and material assignment are important preprocessing steps to ensure anatomical accuracy. Currently, this step is very time-consuming, as only semi-automatic segmentation is possible. Automatic segmentation currently only works on healthy bones, and even then, only in certain areas. Another major factor is subjectivity: our models are always created in consultation with the treating physician. Nevertheless, there may be slight deviations between the generated model and the actual anatomical situation. Accurate reconstruction of the fracture pattern is particularly difficult when image quality is poor and image spacing is large.

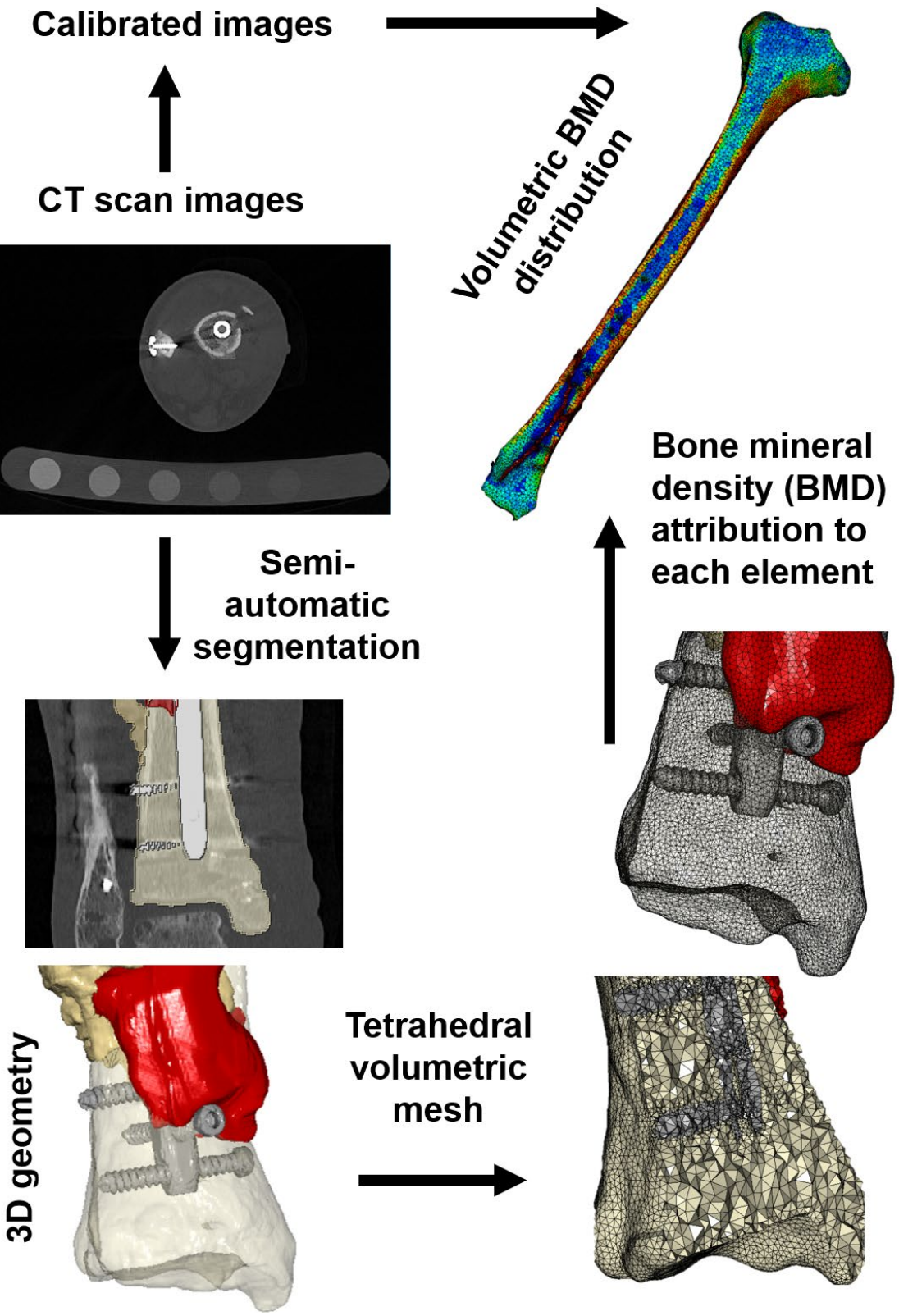

Figure 11: Segmentation process and high-resolution adaptive FE mesh.

7.4 Boundary Conditions

The boundary conditions have already been mentioned several times in the previous chapters. The more precisely the boundary conditions are specified, the more accurate the result will be. The quality of boundary conditions determines the precise presentation of reality. Studies on this topic demonstrate the impact of boundary conditions on in vitro (84,85) and in silico results (53,86). We utilize patient-specific joint and muscle forces derived from musculoskeletal simulations based on motion data. Figure 12 illustrates an example application of biomechanical boundary conditions for a tibia, with load settings from musculoskeletal simulations.

The modeling process starts with the anatomical geometry and customized node sets defined at the distal and proximal ends of the tibia using the segmentation software Simpleware™. To replicate physiological loading conditions, joint reaction forces calculated during the gait cycle act in the x, y, and z directions (F_x, F_y, F_z) at the proximal end of the bone. The selected forces are distributed to the proximal nodes and scaled relative to body weight. The distal node set restricts all directions of translation ($U_1 = U_2 = U_3 = 0$). Mesh and boundary conditions are implemented and visualized in Abaqus™. This example refers to a tibia. Depending on the bone and the specific problem, the boundary conditions are applied differently (see Paper C). The configuration allows it to simulate both static forces and full load cycles as motion sequences, making it possible to analyze effects such as the impact of a step or every other relevant movement on the fracture gap. Paper C discusses the application of boundary conditions to different fracture types on the lower and upper extremities.

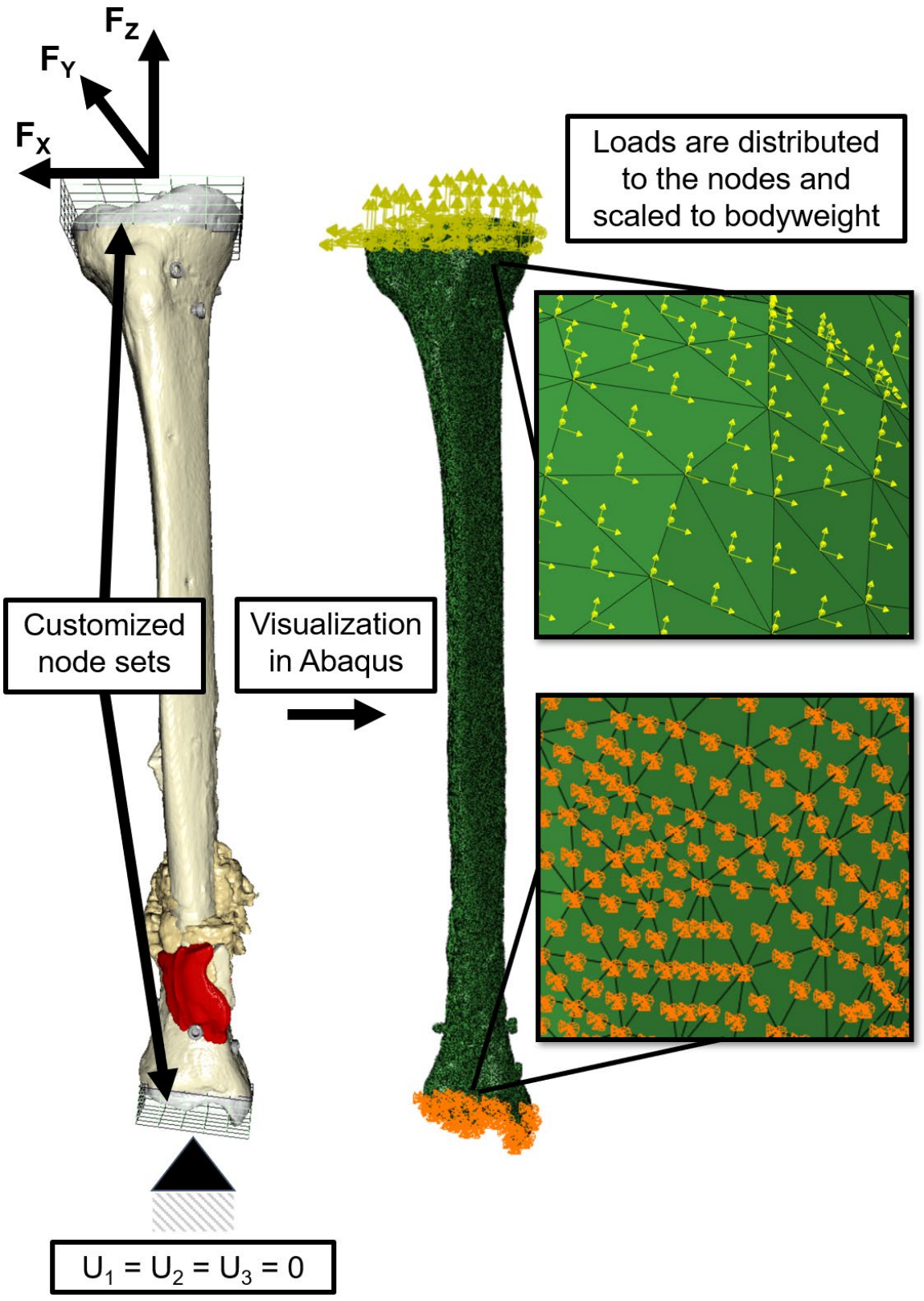

Figure 12: Application of boundary conditions using the example of a tibia with node sets defined in Simpleware™. The load is applied proximally, and the rotation is fixed distally.

Further developments on boundary conditions focused on incorporating muscle attachments. The idea is to recreate physiological conditions where muscle tension and the joint forces together form the boundary conditions. Figure 13 illustrates the workflow setup for this purpose.

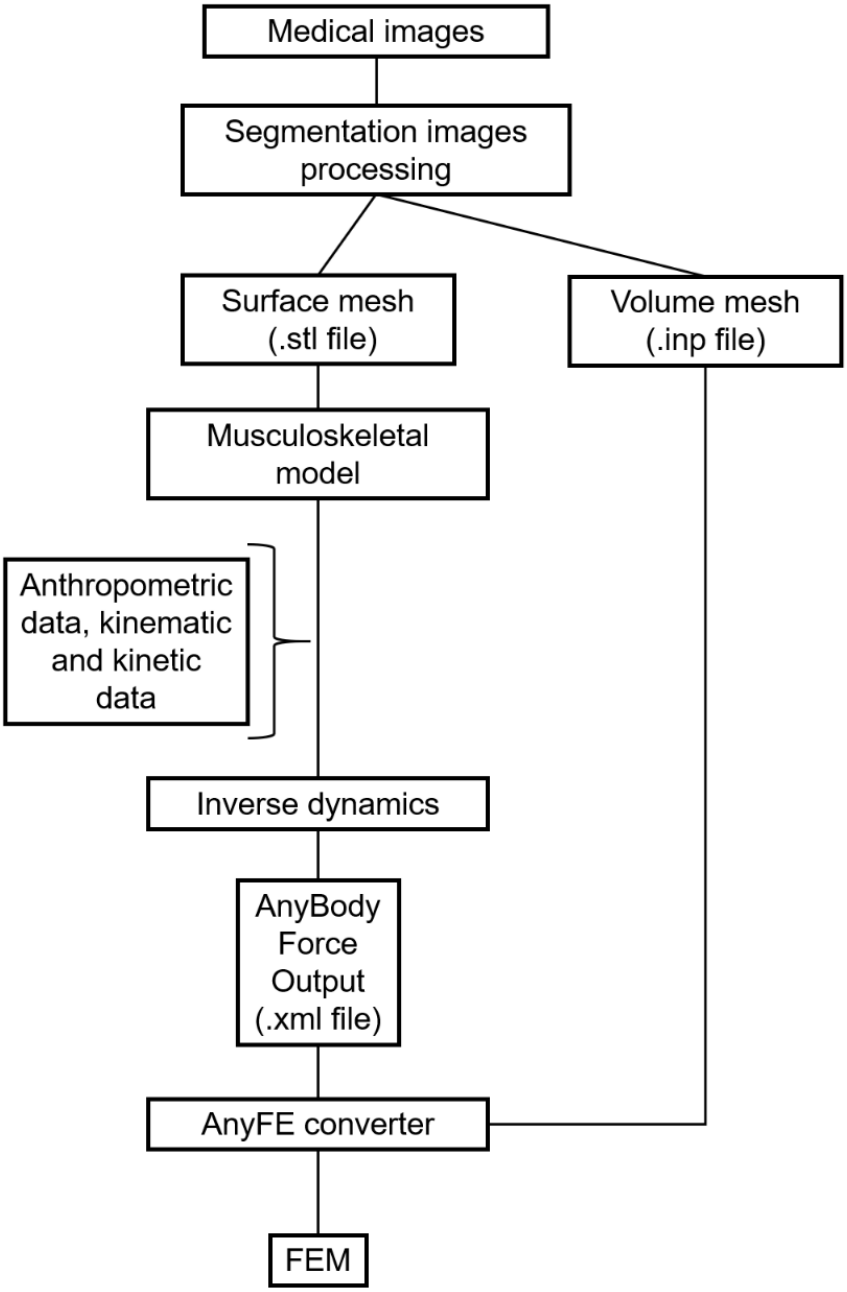

Figure 13: Workflow to implement muscle origin and insertion points as boundary conditions.

The greatest challenge is to harmonize the muscle attachments with the patient-specific geometries and incorporate variations related to fractures and implants. The results of an applied workflow, as shown in Figure 13, are presented in Figure 14. Panel A shows the tibial bone geometry with 180 coupling constraints applied via

Coupling Continuum Distribution (CCD) elements. The model connects these constraints to anatomical landmarks that correspond to muscle groups and joint reactions (labeled A–V). Each force is applied as a concentrated load with a defined direction and time-dependent amplitude. Inset views magnify the distal tibia region, showing detailed placement of muscle and joint force vectors, including the ankle reaction and flexor/extensor muscles of the foot and toes.

Panel B displays the von Mises stress distribution within the tibia, as calculated by the FE analysis. The stress values are in Pascals, consistent with using meters as the unit of length in Abaqus™. The color scale visualizes the von Mises stress, with warmer colors (e.g., red and orange) indicating higher von Mises stress. This representation visualizes areas where the attacking forces exert different influences.

The presented modeling approach, which includes muscle-driven boundary conditions via CCD elements, is published in Paper D, which applies the principles in simulating a custom-made temporomandibular joint.

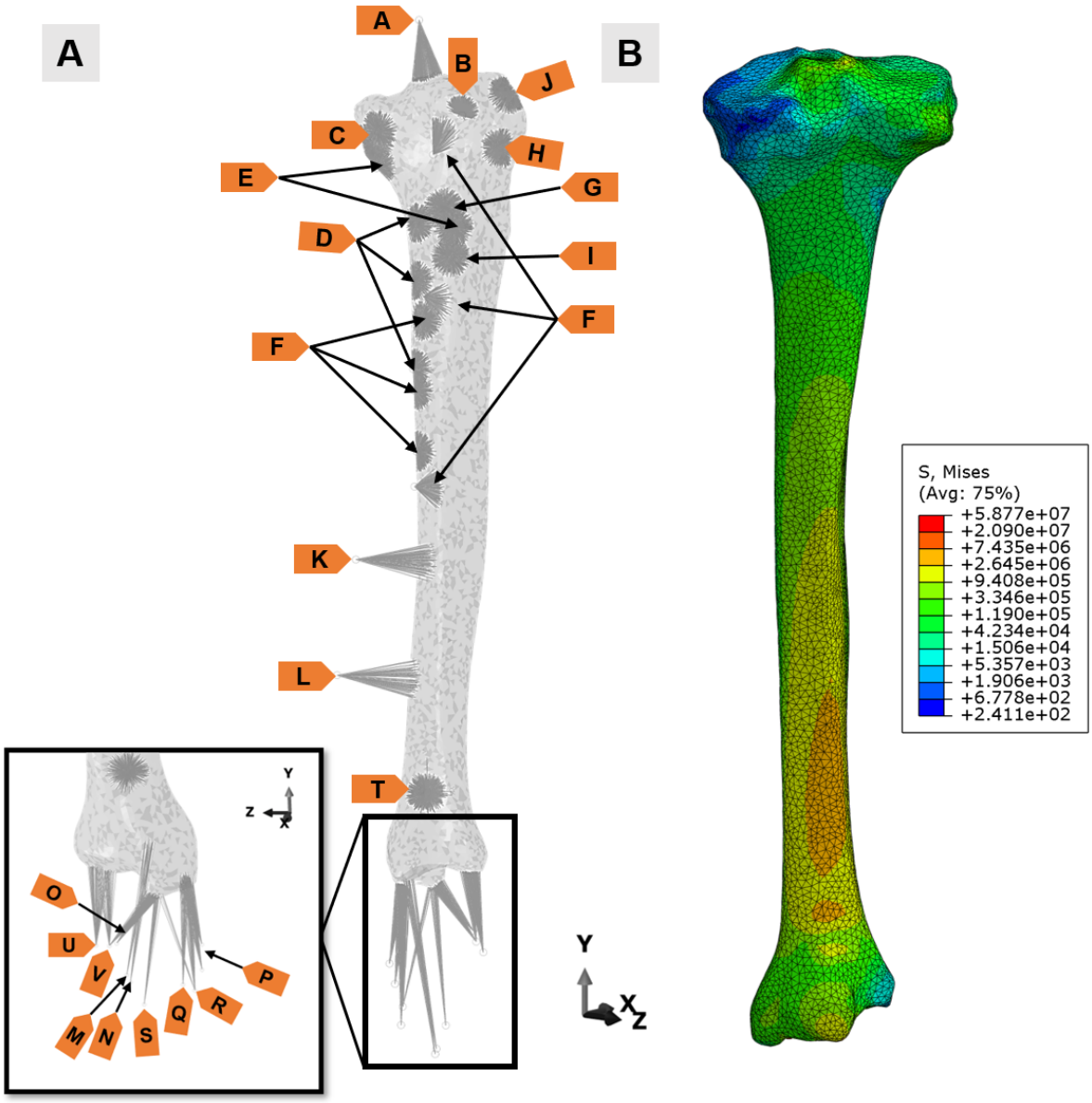

A	Knee reaction	L	Gastrocnemius medial head
B	Biceps femoris muscle	M	Fibularis brevis muscle
C	Semimembranosus muscle	N	Fibularis longus muscle
D	Popliteus muscle	O	Tibialis anterior muscle
E	Gracilis muscle	P	Tibialis posterior muscle
F	Soleus muscle	Q	Flexor hallucis longus muscle
G	Sartorius muscle	R	Flexor digitorum longus muscle
H	Patella movement	S	Ankle reaction
I	Semitendinosus muscle	T	Center of mass
J	Tensor fasciae latae muscle	U	Extensor digitorum longus muscle
K	Gastrocnemius lateral head	V	Extensor hallucis longus muscle

Figure 14: Muscle attachments with muscle groups and joint reactions labeled A – V (A) and the corresponding von Mises stress result (B).

8 Digital Twin

The term "Digital Twin" is based on Dr. Michael Grieves's idea and subsequent concept (87). The National Aeronautics and Space Administration (NASA) later popularized the term by using the concept of spacecraft maintenance and analysis in space. A digital twin is a virtual representation of a physical object, system, or process. This digital copy can be useful to analyze, simulate, and predict outcomes without the need of in vivo testing. The main aspect of "Digital Twins" is real-world data as input. The digital twin is widely utilized in manufacturing, aerospace, and smart cities, and it also holds significant potential for the healthcare sector. The creation of a digital twin follows various development stages that build on each other and require the fulfillment of key foundational definitions.

1. **Virtual Twin:**
    a. Patient-specific anatomy
    b. Fracture modelling
    c. Implant visualization
    d. Surgical planning
2. **Connected Twin:**
    a. Real-time monitoring
    b. Sensor-integrated implants
    c. Patient compliance tracking
    d. Healing rate evaluation
3. **Predictive Twin:**
    a. Predictive analytics
    b. Healing trajectory modeling
    c. Risk stratification
    d. Delayed healing forecasting
4. **Prescriptive Twin:**
    a. Machine learning
    b. Rehabilitation optimization
    c. What-if simulation
5. **Autonomous Twin:**
    a. AI-driven intervention
    b. Autonomous adaptation
    c. Continuous improvement

Our research group has made considerable progress in creating a digital twin. Paper C focused in detail on implementing the first two stages of development. Paper A connects these initial stages 1 and 2 by thoroughly describing the creation of patient-specific geometry, the integration of real-time monitoring, and potential applications in surgical planning. Paper B emphasizes patient compliance tracking options. Paper C summarizes experiences across five use cases and explores the possible applications in various treatments.

9 Summaries of Appended Papers

Paper A:

Paper A presents the development of an individual postoperative and preoperative workflow for patients with fractures of the lower extremities. The workflow combines clinical imaging, patient monitoring, finite element modeling, and musculoskeletal simulations to analyze fracture healing. The integration of patient-specific data supports early detection of delayed healing and tailor-made postoperative treatment plans. The results show how personalized movement influences interfragmentary movement, implant stability, and fracture healing.

Paper B:

Paper B demonstrates how sensor insoles and motion capture can effectively monitor recovery in patients with distal tibial fractures. After revision surgery, the patient was monitored for 12 weeks, from his first attempts at walking to full recovery. The results show that easily evaluable parameters such as cadence, imbalance, and ground reaction force can be used to track healing progress. The results make it possible to detect deviations at an early stage, support individualized rehabilitation, and improve clinical outcomes.

Paper C:

Paper C examines the use of clinically informed digital twins to manage fracture non-unions and plan revision surgeries in orthopedic trauma care. By integrating imaging, motion capture, and patient-specific data, digital twins allow virtual testing of treatment strategies, such as implant variations, to optimize mechanical conditions for healing. The approach supports both pre-surgical decision-making and post-operative assessment, offering a promising tool for personalized surgical planning.

Paper D:

Paper D compares academic and industrial simulation processes for customized temporomandibular joint prostheses. Finite element analyses were performed for both methods based on a real patient case. In addition, physiological boundary conditions were applied through the use of muscle attachments. This work shows that academic simulations can effectively support research and design of temporomandibular joint prostheses.

10 Conclusion and Outlook

Future efforts must explore how to further integrate biomechanics into the surgical fracture care process. Anticipating the interaction between an implant and the dynamic fracture healing process remains a significant challenge. The main reason for this challenge is that, on the one hand, mechanical and biological processes at the micro level promote fracture healing. On the other hand, however, factors at the macro level, such as the choice of treatment method or the load, also have a significant influence on the process. Several factors make it difficult to identify precise parameters and set limits for optimal fracture healing. As a result, personalized, software-based biomechanical analysis and simulation represent a meaningful advancement toward bridging this gap. However, further development is necessary to bring such an approach into clinical practice. Specifically, the optimization of algorithms to deliver patient-specific simulations and insights quickly enough to fit into routine surgical workflows, enabling real-time or near-real-time decision support at the point of care.

This thesis, titled “Biomechanical Simulations of Fracture Gap Movement”, investigates the impact of boundary conditions on the mechanical behavior of the fracture gap. A central question of this work concerns the necessary degree of individualization. How patient-specific should the simulation be, and where can standardized assumptions be used without compromising accuracy? The different publications of this dissertation are the first attempt to answer these questions. But there is still a need for comprehensive sensitivity studies to provide a final answer. Regarding the development of the digital twin and standardizing assumptions, the motion capture systems enable the analysis of a broader range of real-world boundary conditions.

Despite promising developments, accurately modeling IFM remains the primary challenge. Mechanically, a fracture disrupts the bone's structural integrity. The main treatment goal is the restoration of load-bearing capacity. Critical mechanical factors in this process include micro-movements determined by the stability of the fixation, mechanical stimulation due to stress, and the influence of stress shielding. Finite element simulations can provide information about the stress and strain distribution at the fracture site. Finite element simulations can provide insights into stress and strain distribution at the fracture site. However, there are still gaps in our knowledge regarding biological responses at the cellular level, specifically, which mechanical stimuli are beneficial or harmful to healing. Currently, only animal studies provide information on these processes, such as those by Perren (88) and Claes (89). The transferability of the conclusions to clinical scenarios in humans is limited. Although the potential of biomechanical simulations is promising, it is difficult to gain trust and acceptance in an interdisciplinary environment. In surgical practice in particular, simulations are perceived by many as opaque “black boxes” – complex, inaccessible tools whose functioning is difficult to understand. Several factors cause this skepticism. One factor is whether the results are realistic enough. Others regarding the validations. Both points are fundamental challenges in researching living subjects. In cases such as fracture movement during healing, validation may not be feasible, as no definitive solution exists for verifying the internal processes involved.

Transparency, experimental validation, a clear explanation, and a comparison with real clinical data are essential to overcome this barrier. Building trust also requires a continuous dialogue between engineers and clinicians to ensure that the simulations meet scientific standards and have clinical applicability.

11 Ethical Statement

The study was conducted under the Declaration of Helsinki and approved by the Ethics Committees of the University of Tuebingen (Protocol codes 317 and 318/2022BO2). Informed consent was obtained from all subjects involved in the study. The studies involving human participants were reviewed and approved by Ethical Approval was obtained from the IRB of Saarland Medical Board (Aerztekammer des Saarlandes, Germany, application number 30/21). Informed consent was conducted according to the Declaration of Helsinki. The study is part of the project Smart Implants 2.0 – Weight-bearing and Gait Observation for Early Monitoring of Fracture Healing and Individualized Therapy after Trauma, funded by the Werner Siemens Foundation. It is registered in the German Clinical Trials Register (DRKS-ID: DRKS00025108). The patients/participants provided their written informed consent to participate in this study. Written informed consent was obtained from the individual(s) for the publication of any potentially identifiable images or data included in this article.

12 Scientific Publications

The published journal papers are attached:

Paper A Andres, A., Roland, M., Wickert, K., Ganse, B., Pohlemann, T., Orth, M. & Diebels, S. Individual Postoperative and Preoperative Workflow for Patients with Fractures of the Lower Extremities. *Clin. Biomech.* (2025). 106503. https://doi.org/10.1016/j.clinbiomech.2025.106503

Paper B Andres, A., Roland, M., Orth, M., & Diebels, S. (2025). From Injury to Full Recovery: Monitoring Patient Progress Through Advanced Sensor and Motion Capture Technology. *Sensors*, *25*(13), 3853. https://doi.org/10.3390/s25133853

Paper C Andres, A., Roland, M., Wickert, K., Diebels, S., Stöckl, J., Herrmann, S., Reinauer, F., Leibinger, R., Pavlov, A., Schuppener, L., Schäfer, D., Histing, T. & Braun, B. J. (2025). Advantages of digital twin technology in orthopedic trauma Surgery–Exploring different clinical use cases. *Scientific Reports*, *15*(1), 1-13. https://doi.org/10.1038/s41598-025-04792-w

Paper D Andres, A., Wickert, K., Gneiting, E., Binmoeller, F., Diebels, S. & Roland, M. (2025). Simulation of a Custom-Made Temporomandibular Joint – An Academic View on an Industrial Workflow. Bioengineering, 12(5), 545. https://doi.org/10.3390/bioengineering12050545

13 References

1. Tzioupis C, Giannoudis P V. Prevalence of long-bone non-unions. Injury. 2007;38(SUPPL. 2):S3. Available from: https://doi.org/10.1016/S0020-1383(07)80003-9

2. Calori GM, Giannoudis P V. Enhancement of fracture healing with the diamond concept: The role of the biological chamber. Injury. 2011;42(11):1191–3. Available from: https://doi.org/10.1016/j.injury.2011.04.016

3. Zura R, Xiong Z, Einhorn T, Watson JT, Ostrum RF, Prayson MJ, et al. Epidemiology of fracture nonunion in 18 human bones. JAMA Surg. 2016;151(11):1–12. Available from: doi:10.1001/jamasurg.2016.2775

4. Augat P, Simon U, Liedert A, Claes L. Mechanics and mechano-biology of fracture healing in normal and osteoporotic bone. Osteoporos Int. 2005;16(SUPPL. 2):36–43. Available from: https://doi.org/10.1007/s00198-004-1728-9

5. Fong K, Truong V, Foote CJ, Petrisor B, Williams D, Ristevski B, et al. Predictors of nonunion and reoperation in patients with fractures of the tibia: An observational study. BMC Musculoskelet Disord. 2013;14. Available from: https://doi.org/10.1186/1471-2474-14-103

6. Antonova E, Le TK, Burge R, Mershon J. Tibia shaft fractures: Costly burden of nonunions. BMC Musculoskelet Disord. 2013;14. Available from: https://doi.org/10.1186/1471-2474-14-42

7. Dahabreh Z, Dimitriou R, Giannoudis P V. Health economics: A cost analysis of treatment of persistent fracture non-unions using bone morphogenetic protein-7. Injury. 2007;38(3):371–7. Available from: https://doi.org/10.1016/j.injury.2006.08.055

8. Kanakaris NK, Giannoudis P V. The health economics of the treatment of long-bone non-unions. Injury. 2007;38(SUPPL. 2). Available from: https://doi.org/10.1016/S0020-1383(07)80012-X

9. Claes LE. Mechanobiology of Fracture Healing. From Basic Science to Clinical Application. 2017. Available from: https://link.springer.com/bookseries/10280

10. Dunlop S, McCormack M, Zigler J, Neher R. Pit23 the Cost Burden of Nonunion Following Long Bone Fracture in a Commercially Insured Population in the United States. Value Heal. 2019;22(May):S215. Available from: https://doi.org/10.1016/j.jval.2019.04.995

11. Kenwright J, Goodship A. Effect of controlled axial micromovement on healing of tibial fractures. Lancet. 1986;1185–7. Available from: https://doi.org/10.1016/S0140-6736(86)92196-3

12. Barricelli BR, Casiraghi E, Fogli D. A survey on digital twin: Definitions, characteristics, applications, and design implications. IEEE Access. 2019;7(MI):167653–71. Available from: 10.1109/ACCESS.2019.2953499

13. Barricelli BR, Casiraghi E, Gliozzo J, Petrini A, Valtolina S. Human Digital Twin for Fitness Management. IEEE Access. 2020;8:26637–64. Available from:

10.1109/ACCESS.2020.2971576

14. Lauer-Schmaltz MW, Cash P, Hansen JP, Maier A. Designing Human Digital Twins for Behaviour-Changing Therapy and Rehabilitation: A Systematic Review. Proc Des Soc. 2022;2:1303–12. Available from: doi:10.1017/pds.2022.132

15. Rupp M, Walter N, Pfeifer C, Land S, Kerschbaum M, Krutsch W, et al. Inzidenz von Frakturen in der Erwachsenenpopulation in Deutschland - Eine Analyse von 2009 bis 2019. Dtsch Arztebl. 2021;118(665–9). Available from:

16. International Osteoporosis Foundation. 2025. Available from: https://www.osteoporosis.foundation/facts-statistics/epidemiology-of-osteoporosis-and-fragility-fractures?utm_source=chatgpt.com

17. www.destatis.de. 2025. Available from: https://www.destatis.de/DE/Themen/Gesellschaft-Umwelt/Gesundheit/Krankenhaeuser/Tabellen/drg-operationen-insgesamt.html

18. Larsen P, Elsoe R, Hansen SH, Graven-Nielsen T, Laessoe U, Rasmussen S. Incidence and epidemiology of tibial shaft fractures. Injury. 2015;46(4):746–50. Available from: http://dx.doi.org/10.1016/j.injury.2014.12.027

19. Wennergren D, Bergdahl C, Ekelund J, Juto H, Sundfeldt M, Möller M. Epidemiology and incidence of tibia fractures in the Swedish Fracture Register. Injury. 2018;49(11):2068–74. Available from: https://doi.org/10.1016/j.injury.2018.09.008

20. Beerekamp MSH, de Muinck Keizer RJO, Schep NWL, Ubbink DT, Panneman MJM, Goslings JC. Epidemiology of extremity fractures in the Netherlands. Injury. 2017;48(7):1355–62. Available from: http://dx.doi.org/10.1016/j.injury.2017.04.047

21. Johnson L, Igoe E, Kleftouris G, Papachristos I V., Papakostidis C, Giannoudis P V. Physical health and psychological outcomes in adult patients with long-bone fracture non-unions: Evidence today. J Clin Med. 2019;8(11). Available from: https://doi.org/10.3390/jcm8111998

22. Houben IB, Raaben M, Van Basten Batenburg M, Blokhuis TJ. Delay in weight bearing in surgically treated tibial shaft fractures is associated with impaired healing: a cohort analysis of 166 tibial fractures. Eur J Orthop Surg Traumatol. 2018;28(7):1429–36. Available from: https://doi.org/10.1007/s00590-018-2190-2

23. Bishop NE, Tami I, Schneider E IK. In vivo comparison of early fracture healing under deviatoric and volumetric deformations. Acta Bioeng Biomech. 2003;4:754–5.

24. Bishop NE, van Rhijn M, Tami I, Corveleijn R, Schneider E, Ito K. Shear Does Not Necessarily Inhibit Bone Healing. Clin Orthop Relat Res. 2006;443(443):307–14. Available from: 10.1097/01.blo.0000191272.34786.09

25. Feng JN, Zhang CG, Li BH, Zhan SY, Wang SF SC. Global burden of hip fracture: The Global Burden of Disease Study. Osteoporos Int. 2024;(Jan;35(1):41-52). Available from: https://doi.org/10.1007/s00198-023-06907-3

26. Steiner M, Claes L, Ignatius A, Simon U, Wehner T. Numerical simulation of callus healing for optimization of fracture fixation stiffness. PLoS One. 2014;9(7):1–11. Available from: https://doi.org/10.1371/journal.pone.0101370

27. Park SH, O'Connor K, Mckellop H, Sarmiento A. The influence of active shear or compressive motion on fracture-healing. J Bone Jt Surg. 1998;80(6):868–78.

28. Meyers N, Sukopp M, Jäger R, Steiner M, Matthys R, Lapatki B, et al. Characterization of interfragmentary motion associated with common osteosynthesis devices for rat fracture healing studies. PLoS One. 2017;12(4). Available from: https://doi.org/10.1371/journal.pone.0176735

29. Betts DC, Müller R. Mechanical regulation of bone regeneration: Theories, models, and experiments. Front Endocrinol (Lausanne). 2014;5(DEC):1–14. Available from: https://doi.org/10.3389/fendo.2014.00211

30. Barcik J, Epari DR. Can optimizing the mechanical environment deliver a clinically significant reduction in fracture healing time? Biomedicines. 2021;9(6):1–10. Available from: https://doi.org/10.3390/biomedicines9060691

31. Claes LE, Heigele CA. Magnitudes of local stress and strain along bony surfaces predict the course and type of fracture healing. J Biomech. 1999;32(3):255–66. Available from: https://doi.org/10.1016/S0021-9290(98)00153-5

32. Carter D. Mechanobiology of skeletal regeneration. Clin Orthop Rel Res. Available from: 1998;355:41–55. 10.1097/00003086-199810001-00006

33. Wickert K, Roland M, Andres A, Diebels S, Ganse B, Kerner D, et al. Experimental and virtual testing of bone-implant systems equipped with the AO Fracture Monitor with regard to interfragmentary movement. Front Bioeng Biotechnol. 2024 Mar 8;12. Available from: https://doi.org/10.3389/fbioe.2024.1370837

34. Wolff J. Das Gesetz der Transformation der Knochen. Hirschwald Verlag; 1892.

35. Pauwels F. Gesammelte Abhandlungen zur funktionellen Anatomie des Bewegungsapparates. Springer Berlin Heidelberg; 1965. Available from: https://doi.org/10.1007/978-3-642-86841-2

36. Frost H. Bone "mass" and the "mechanostat". A proposal. Anat Rec. 1987;(9):1–9. Available from: https://doi.org/10.1002/ar.1092190104

37. Perren SM. Cellular differentiation and bone biomechanics during the consolidation of a fracture. Anat Clin. 1978;28:13–28. Available from: 10.1007/BF01654345

38. Mountziaris PM, Mikos AG. Modulation of the inflammatory response for enhanced bone tissue regeneration. Tissue Eng - Part B Rev. 2008;14(2):179–86. Available from: https://doi.org/10.1089/ten.teb.2008.0038

39. Claes L, Eckert-Hübner K, Augat P. The effect of mechanical stability on local vascularization and tissue differentiation in callus healing. J Orthop Res. 2002;20(5):1099–105. Available from: https://doi.org/10.1016/S0736-0266(02)00044-X

40. Lienau J, Schell H, Duda GN, Seebeck P, Muchow S, Bail HJ. Initial vascularization and tissue differentiation are influenced by fixation stability. J Orthop Res. 2005;23(3):639–45. Available from: https://doi.org/10.1016/j.orthres.2004.09.006

41. Boerckel JD, Uhrig BA, Willett NJ, Huebsch N, Guldberg RE. Mechanical regulation of vascular growth and tissue regeneration in vivo. Proc Natl Acad Sci U S A. 2011;108(37). Available from: https://doi.org/10.1073/pnas.1107019108

42. Dimai HP, Muschitz C, Amrein K, Bauer R, Cejka D, Gasser RW, et al. Osteoporose – Definition, Risikoerfassung, Diagnose, Prävention und Therapie (Update 2024) : Leitlinie der Österreichischen Gesellschaft für Knochen- und Mineralstoffwechsel. Vol. 136, Wiener klinische Wochenschrift. 2024. 599–668 p. Available from: https://doi.org/10.1007/s00508-024-02441-2

43. Niedermair T. Der Einfluss des sensiblen Neurotransmitters SP und des sympathischen Nervensystems auf die enchondrale Ossifikation im Verlauf der Frakturheilung und auf die allgemeine Knochenstruktur in vivo und in vitro. 2015;18–23. Available from: 10.5283/epub.32210

44. Méndez-Sánchez L, Clark P, Winzenberg TM, Tugwell P, Correa-Burrows P, Costello R. Calcium and vitamin D for increasing bone mineral density in premenopausal women. Cochrane Database of Systematic Reviews, 2023, Issue 1. Art. No.: CD012664. DOI: 10.1002/14651858.CD012664.pub2.

45. Ziller V. Bone health in the postmenopause. Gynakologische Endokrinol. 2022;20(3):170–7. Available from: https://doi.org/10.1007/s10304-022-00459-1

46. Kanis JA, Johnell O, Oden A, Johansson H, De Laet C, Eisman JA, et al. Smoking and fracture risk: A meta-analysis. Osteoporos Int. 2005;16(2):155–62. Available from: https://doi.org/10.1007/s00198-004-1640-3

47. Biermann S. Einfluss monozytärer Zellen auf die diabetische Frakturheilung der Eberhard Karls Universität vorgelegt von. 2020;

48. Stief M. Einfluss von Diclofenac auf die Frakturheilung bei alten Mäusen. 2021; Available from: http://dx.doi.org/10.22028/D291-36121

49. Ganse B. Methods to accelerate fracture healing - a narrative review from a clinical perspective. Front Immunol. 2024;15(June):1–13. Available from: https://doi.org/10.3389/fimmu.2024.1384783

50. Glatt V, Evans CH, Tetsworth K. A concert between biology and biomechanics: The influence of the mechanical environment on bone healing. Front Physiol. 2017;7(JAN):1–18. Available from: https://doi.org/10.3389/fphys.2016.00678

51. Miramini S, Zhang L, Richardson M, Mendis P, Oloyede A, Ebeling P. The relationship between interfragmentary movement and cell differentiation in early fracture healing under locking plate fixation. Australas Phys Eng Sci Med. 2016;39(1):123–33. Available from: https://doi.org/10.1007/s13246-015-0407-9

52. Mori Y, Kamimura M, Ito K, Koguchi M, Tanaka H, Kurishima H. applied sciences. 2024; Available from: https://doi.org/10.3390/app14062259

53. MacLeod AR, Pankaj P. Pre-operative planning for fracture fixation using locking plates: device configuration and other considerations. Injury.

2018;49(June):S12–8. Available from: https://doi.org/10.1016/S0020-1383(18)30296-1

54. Rechter GR, Anthony RT, Rennard J, Kellam JF, Warner SJ. The Impact of Early Axial Interfragmentary Motion on the Fracture Healing Environment: A Scoping Review. Injury. 2024;55(12):111917. Available from: https://doi.org/10.1016/j.injury.2024.111917

55. Märdian S, Schmölz W, Schaser KD, Duda GN, Heyland M. Locking plate constructs benefit from interfragmentary lag screw fixation with decreased shear movements and more predictable fracture gap motion in simple fracture patterns. Clin Biomech. 2019;70(May):89–96. Available from: https://doi.org/10.1016/j.clinbiomech.2019.08.008

56. Rossiter N, Trompeter A. Personal theories on non-union: it's all mechanics! Orthop Trauma. 2021;35(2):68–75. Available from: https://doi.org/10.1016/j.mporth.2021.01.001

57. Bavonratanavech, Suthorn, Reto Babst, and Chang-Wug Oh E. Minimally Invasive Plate Osteosynthesis. Georg Thieme Verlag; 2023. Available from: ISBN 9783132454255

58. Märdian S, Schaser KD, Duda GN, Heyland M. Working length of locking plates determines interfragmentary movement in distal femur fractures under physiological loading. Clin Biomech. 2015;30(4):391–6. Available from: http://dx.doi.org/10.1016/j.clinbiomech.2015.02.006

59. Heyland M, Duda GN, Haas NP, Trepczynski A, Döbele S, Höntzsch D, et al. Semi-rigid screws provide an auxiliary option to plate working length to control interfragmentary movement in locking plate fixation at the distal femur. Injury. 2015;46:S24–32. Available from: http://dx.doi.org/10.1016/S0020-1383(15)30015-2

60. Kanakaris NK, Obakponovwe O, Krkovic M, Costa ML, Shaw D, Mohanty KR, et al. Fixation of periprosthetic or osteoporotic distal femoral fractures with locking plates: a pilot randomised controlled trial. Int Orthop. 2019;43(5):1193–204. Available from: https://doi.org/10.1007/s00264-018-4061-1

61. Kershaw C. Tibial External Fixation, Weight Bearing, and Fracture Movement. Clin Orthop Relat Res. 1993;293:28–36. PMID: 8339493.

62. Glatt V, Evans CH, Tetsworth K. Reverse dynamisation: A modern perspective on stephan perren's strain theory. Eur Cells Mater. 2021;41:668–79. Available from: doi: 10.22203/eCM.v041a43

63. Windolf M, Ernst M, Schwyn R, Arens D, Zeiter S. The relation between fracture activity and bone healing with special reference to the early healing phase – A preclinical study. Injury. 2021;52(1):71–7. Available from: https://doi.org/10.1016/j.injury.2020.10.050

64. Augat P, Merk J, Ignatius A, Margevicius K, Bauer G, Rosenbaum D, et al. Early, full weightbearing with flexible fixation delays fracture healing. Clin Orthop Relat Res. 1996;328(328):194–202. Available from: 10.1097/00003086-199607000-00031

65. Tufekci P, Tavakoli A, Dlaska C, Neumann M, Shanker M, Saifzadeh S, et al.

Early mechanical stimulation only permits timely bone healing in sheep. J Orthop Res. 2018;36(6):1790–6. Available from: https://doi.org/10.1002/jor.23812

66. Claes L, Blakytny R, Melanie Göckelmann, Schoen M, Ignatius A, Willie B. Early dynamization by reduced fixation stiffness does not improve fracture healing in a rat femoral osteotomy model. J Orthop Res. 2009;27(1):22–7. Available from: https://doi.org/10.1002/jor.20712

67. Claes L, Blakytny R, Besse J, Bausewein C, Ignatius A, Willie B. Late Dynamization by Reduced Fixation Stiffness Enhances Fracture Healing in a Rat Femoral Osteotomy Model. J Orthop Trauma. 2011;25(3):169–74. Available from: 10.1097/BOT.0b013e3181e3d994

68. Baker R. Gait analysis methods in rehabilitation. J Neuroeng Rehabil. 2006;3:1–10. Available from: 10.1186/1743-0003-3-4

69. Movella. Xsens Awinda. Available from: https://www.movella.com/products/motion-capture/xsens-mvn-awinda

70. Hill AV. The heat of shortening and the dynamic constants of muscle. Proc R Soc London Ser B - Biol Sci. 1938;126(843):136–95. Available from: 10.1098/rspb.1938.0050

71. Rasmussen J, Damsgaard M, Voigt M. Muscle recruitment by the min/max criterion - A comparative numerical study. J Biomech. 2001;34(3):409–15. Available from: https://doi.org/10.1016/S0021-9290(00)00191-3

72. Damsgaard M, Rasmussen J, Christensen ST, Surma E, de Zee M. Analysis of musculoskeletal systems in the AnyBody Modeling System. Simul Model Pract Theory. 2006;14(8):1100–11. Available from:

73. Rasmussen J, Rasmussen J. From Knowledge to Leverage : How to Use Musculoskeletal Simulation to Design Exoskeleton Concepts From Knowledge to Leverage : How to Use Musculoskeletal Simulation to Design Exoskeleton Concepts. 2025;0–10. Available from: https://doi.org/10.1016/j.simpat.2006.09.001

74. Ehreiser S, Asseln M, Radermacher K. Personalized Prediction of Total Knee Arthroplasty Mechanics Based on Sparse Input Data—Model Validation Using In Vivo Force Data. Biomech. 2025;5(1):1–11. Available from: https://doi.org/10.3390/biomechanics5010008

75. Guo X, Xu XS, Geng X, Zhang Z, Ma X, Chen WM. Strain energy in human tibia during different exercises with adjustable leg weights: a subject-specific computational model analysis. Med Biol Eng Comput. 2025;(0123456789). Available from: https://doi.org/10.1007/s11517-025-03335-9

76. Mitani T, Inoue K, Takahashi S. Relationship between joint angle and contact force at the knee during normal gait. J Adv Mech Des Syst Manuf. 2025;19(2):1–9. Available from: https://doi.org/10.1299/jamdsm.2025jamdsm0015

77. Orthoload - Loading of Orthopaedic Implants. 2024. Available from: https://orthoload.com/

78. University S. OpenSim. 2025. Available from:

https://simtk.org/projects/opensim

79. Röhrle R group of PO. 3R-BioMedicUS, Biomechanical modeling & simulation. 2025. Available from: https://www.verbund.uni-stuttgart.de/3r-biomedicus/3r-research/roehrle/

80. North K, Maass SD, Hitchcock RW. An insole sensor for recording weight bearing behavior during tibial fracture rehabilitation. 2010 Annu Int Conf IEEE Eng Med Biol Soc EMBC'10. 2010;1856–9. Available from: 10.1109/IEMBS.2010.5626006

81. Zienkiewicz OC, Taylor RL, Fox D. The finite element method for solid and structural mechanics (7th ed.). Elsevier; 2014. Available from: ISBN-13: 978-0-7506-6321-2

82. Cook RD, Malkus DS, Plesha ME, Witt RJ. Concepts and Applications of Finite Element Analysis (4th Edition). Wiley; 2001. Available from: ISBN: 978-0-471-35605-9

83. V&V40, A. S. M. E. TAS of ME. Assessing credibility of computational modeling through verification and validation: application to medical devices. 2018. Available from: ISBN: 9780791872048

84. Hoffmeier KL, Hofmann GO, Mückley T. Choosing a proper working length can improve the lifespan of locked plates: A biomechanical study. Clin Biomech. 2011;26(4):405–9. Available from: http://dx.doi.org/10.1016/j.clinbiomech.2010.11.020

85. Bottlang M, Doornink J, Lujan TJ, Fitzpatrick DC, Marsh JL, Augat P, et al. Effects of construct stiffness on healing of fractures stabilized with locking plates. J Bone Jt Surg. 2010;92(SUPPL. 2):12–22. Available from: 10.2106/JBJS.J.00780

86. MacLeod, Alisdair and PP. Computer simulation of fracture fixation using extramedullary devices: an appraisal. New York, NY: Springer New York; 2014. Available from: https://doi.org/10.1007/978-1-4939-0745-8_7

87. Grieves M. Digital twin: manufacturing excellence through virtual factory replication. White Pap. 2014;1:1–7.

88. Perren S. Physical and biological aspects of fracture healing with special reference to internal fixation. Clin Orthop Relat Res. 1979;138:175–96. Available from: PMID: 376198

89. Claes L, Augat P, Suger G, Wilke HJ. Influence of size and stability of the osteotomy gap on the success of fracture healing. J Orthop Res. 1997;15(4):577–84. Available from: https://doi.org/10.1002/jor.1100150414

14 Paper A

Title:

Individual Postoperative and Preoperative Workflow for Patients with Fractures of the Lower Extremities

Authors:

Annchristin Andres, Michael Roland, Kerstin Wickert, Bergita Ganse, Tim Pohlemann, Marcel Orth & Stefan Diebels

Original Publication:

Andres, A., Roland, M., Wickert, K., Ganse, B., Pohlemann, T., Orth, M. & Diebels, S. Individual Postoperative and Preoperative Workflow for Patients with Fractures of the Lower Extremities. *Clin. Biomech.* (2025). 106503. https://doi.org/10.1016/j.clinbiomech.2025.106503

Clinical Biomechanics xxx (xxxx) xxx

Contents lists available at ScienceDirect

Clinical Biomechanics

journal homepage: www.elsevier.com/locate/clinbiomech

Individual postoperative and preoperative workflow for patients with fractures of the lower extremities☆

Annchristin Andres [a,*], Michael Roland [a], Kerstin Wickert [a], Bergita Ganse [b], Tim Pohlemann [c], Marcel Orth [c], Stefan Diebels [a]

[a] Applied Mechanics, Saarland University, Saarbrücken, Germany
[b] Werner Siemens Endowed Chair of Innovative Implant Development (Fracture Healing), Saarland University, Homburg, Germany
[c] Department of Trauma, Hand and Reconstruction Surgery, Saarland University Hospital, Homburg, Germany

ARTICLE INFO

Keywords:
Motion capturing
Gait analysis
Interfragmentary movement
Finite element simulation
Musculoskeletal simulation
Patient-specific

ABSTRACT

Background: The individual assessment of the postoperative healing situation contributes significantly to detecting healing disorders, ensuring the mechanical stability of implants, and planning revision surgeries.
Methods: Our established workflow consists of the following steps: (1) Monitoring of the patients during their treatment course with a motion capturing system as kinematic and sensor insoles for the kinetic gait analysis, (2) transfer of the motion data into the musculoskeletal simulation system AnyBody™ to achieve the corresponding individual muscle and joint forces. (3) Clinical imaging of the patients via postoperative computed tomography scans, ideally combined with a six-rod bone density calibration phantom. (4) Segmentation of the CT images and generation of the corresponding adaptive finite element meshes of the bone-implant systems, including the material parameters based on Hounsfield units and calibration phantom via the software ScanIP™. (5) Based on the patient-specific model, all information from the musculoskeletal simulation and gait analysis is transferred to our biomechanical simulation process as patient-specific constraints.
Findings: This workflow allows us to simulate individual patient models based on their respective actual motion data over their treatment course. Thus, pathological processes that may lead to non-healing fractures can be detected early after surgery and prevented by adapting the postoperative treatment protocol. Furthermore, it is possible to understand the forces that affect the fracture and its healing process permanently in more detail.
Interpretation: The findings demonstrate that the individual motion parameters and fracture morphology influence the local healing parameters and create individual weight-bearing recommendations.

1. Introduction

Certain areas of the skeleton are prone to fracture healing problems for anatomical reasons, i.e., the tibia or the femur. Tibia fractures are a common orthopedic trauma entity (Court-Brown and Caesar, 2006). Bone healing disturbances are a challenge for the physician, a considerable economic burden for society, and highly irksome for the patient. Impaired fracture healing significantly affects a patient's life, causing pain, reduced mobility, repeated hospitalization, and additional surgeries (Pountos et al., 2013). In addition to the significant impact on the health of affected individuals, they result in substantial direct treatment costs, estimated at about 12,000 Euros per patient, and additional indirect treatment costs that are ten times that amount (Hak et al., 2014). The development of delayed healing depends on many factors that often cannot be adequately influenced once the fracture has occurred (Bishop et al., 2012). Multiple factors influence the healing process, including individual characteristics, gender-specific aspects, and various parameters associated with the fracture pattern, fixation methods, mechanical loading, and activity levels (Peter Augat et al., 2005; Claes and Heigele, 1999; Dijkman et al., 2010; Warmerdam et al., 2024). Even modern surgical stabilization and aftercare concepts are based on traditional, highly standardized protocols. These include fixed follow-up intervals, outpatient visits, and radiographic examinations, although these techniques already showed low sensitivity and specificity

☆ This article is part of a Special issue entitled: 'Methods in Orthopaedic Biomechanics' published in Clinical Biomechanics.

* Corresponding author at: Applied Mechanics, Saarland University, Campus A4 2, 1. OG, D-66123 Saarbrücken, Germany.
E-mail addresses: annchristin.andres@uni-saarland.de (A. Andres), michael.roland@uni-saarland.de (M. Roland), kerstin.wickert@uni-saarland.de (K. Wickert), Bergita.Ganse@uks.eu (B. Ganse), Tim.Pohlemann@uks.eu (T. Pohlemann), Marcel.Orth@uks.eu (M. Orth), stefan.diebels@uni-saarland.de (S. Diebels).

https://doi.org/10.1016/j.clinbiomech.2025.106503
Received 12 September 2024; Received in revised form 20 February 2025; Accepted 21 March 2025
Available online 22 March 2025

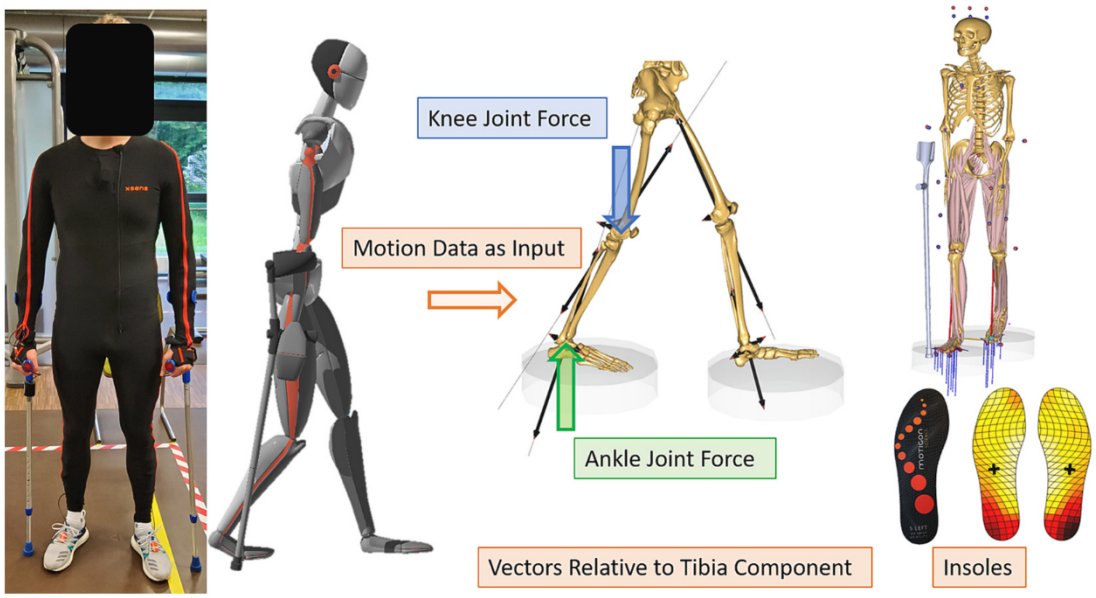

Fig. 1. Illustration of the workflow for the kinematic and kinetic gait analysis.

regarding biological fracture healing (P. Augat et al., 2014; Ganse, 2024; Ganse et al., 2022). Understanding that the mechanical stimulus is a crucial quantity in fracture healing, two main variables influence it: the surgical stabilization and the rehabilitation protocol, both in combination with the patient's activity level in daily life. Numerical modeling and computer simulations have become increasingly important in analyzing the mechanical factors influencing fracture healing (Dahmen et al., 2015; Ghiasi et al., 2017; M. Roland et al., 2015; Michael Roland et al., 2024; Tjardes et al., 2014; Wickert et al., 2024; Wriggers and Zavarise, 2011). The decisions regarding follow-up management heavily rely on clinical imaging conducted at specific intervals during the weeks and months following the fracture. Equally significant is the personal experience of the trauma surgeons, resulting in a knowledge gap concerning the patient's ongoing healing process. Despite the potential and advantages of integrating (musculoskeletal) modeling and simulations into clinical applications, their utilization in standard clinical practice still needs to be improved. The lack of integration stems from multiple factors, including challenges related to seamless integration at the point of care, expertise in usage and interpretation, resource-intensive frameworks, and, in some cases, limited awareness of the additional value they can provide (Killen et al., 2020).

Our workflow can determine the mechanical environment of fracture fixation calculate implant stresses, interfragmentary movement, and the resulting fracture strain. Critical mechanical boundary conditions for fracture healing can be determined concerning individual loading parameters. Based on this, individualized treatment recommendations during the early postoperative phase in lower leg fractures can prevent implant failure and non-union development. With this study, the mobility of the adjacent joints of our patients can be mapped in all cases, and the joint analysis with the patient, an individual follow-up treatment procedure can be determined with special consideration of the patient's functional deficits and individual needs. Efforts to increase "patient involvement" can also be mapped with this system via a direct feedback option within the measurement framework. We then define patient-specific boundary conditions via musculoskeletal simulations based on motion-capturing data to realize a high degree of individualization in the virtualization process. The software is already established on the upper and lower extremities and validates different purposes and movements (Bassani et al., 2017). Several recent studies emphasize the role of simulation-based approaches in fracture treatment, demonstrating the effectiveness of personalized treatment strategies (Maisenbacher et al., 2024; Saravi et al., 2021). Although personalization and individualization of therapy and care through virtual or digital workflows are promising trends in the digitalization of healthcare (Lauer-Schmaltz et al., 2022), and a growing number of articles are being published on this topic, to date, no specific framework for the design of a digital process chain, particularly in the field of rehabilitation (Barricelli et al., 2019). Despite these advancements, challenges remain in integrating these technologies into routine clinical workflows and the clinical data of real patients (Aubert et al., 2021; Schwarzenberg et al., 2019).

We aimed to establish a patient-specific treatment workflow to determine the mechanical fracture environment and allow for an estimation of its healing potential from the clinical data of real patients. The findings of this analysis demonstrate that it is possible to collect data for individually adapted implants and to create individual loading recommendations.

2. Ethical statement

The studies involving human participants were reviewed and approved by ethical approval obtained from the IRB of Saarland Medical Board (Ärztekammer des Saarlandes, Germany, application number 30/21). Informed consent was conducted according to the Declaration of Helsinki. The study is part of the project Smart Implants 2.0 – Weight-bearing and Gait Observation for Early Monitoring of Fracture Healing and Individualized Therapy after Trauma, funded by the Werner Siemens Foundation. It is registered in the German Clinical Trials Register (DRKS-ID: DRKS00025108). The patients/participants provided their written informed consent to participate in this study. Written informed consent was obtained from the individual(s) for the publication of any potentially identifiable images or data included in this article.

3. Methods

Individual post-operative treatment is a combination of five different methods. The first point is patient measurement. The analysis of the recorded data then follows, distinguishing between kinematic, kinetic, and physiological gait parameters. The third section deals with musculoskeletal simulation. The segmentation and simulation work packages complete the workflow. The construction of a three-dimensional model of the treatment situation uses post-operative CT scans in an image processing and computer-aided design system. Resulting forces,

computed in a simulation-driven workflow based on patient monitoring and motion capturing, were used to simulate the mechanical fracture environment.

3.1. Patient monitoring

The inquiry of the method uses Xsens™ (Movella Technology B.V., Enschede, Nederland) for motion capturing as kinematic analysis and sensor insoles (Moticon™, ReGo AG, Munich, Germany) for the kinetic gait analysis. Besides that, the physiological gait parameters, such as gait line and center of pressure, are analyzed. The patient measurement is repeated after 6 and 12 weeks after the surgery to monitor the complete healing process. The measurement proceeds as follows: First, the surgeon decides whether a patient may be considered for the study by analyzing the pattern of injury using initial X-rays and CT images. If patients sign the informed consent form, the gait analysis with the two systems starts shortly after the surgical intervention, depending on the patient's mobility level. The two systems are used simultaneously during the measurement taken during physiotherapy. By this means, the patient learns to walk and take stairs in consideration of the prescribed limited gait load by using crutches. Representation of all measurement systems and their interrelationships (Fig. 1). On the left, a subject is shown wearing the Xsens™ Link suit, followed by the associated avatar. AnyBody™ (AnyBody™ Technology A/S Aalborg, Denmark) then uses the motion data as input to analyze the forces acting on the tibia, which here would be the knee and ankle joint forces. The upper right corner shows the musculoskeletal avatar of the whole body. The Moticon™ insoles can be seen at the bottom right. With the built-in pressure sensors, the load during walking can be recorded and evaluated.

With the Motion Capture System from Xsens™, tracking movements and creating a full-body movement image is possible. In addition, joint angle data, center of gravity, and other sensor data can be determined. One advantage of this system is that cameras are not necessary, as is the case with marker-based gait analysis. Another advantage of Xsens™ is that it is a portable system that allows measurements to be made outside a laboratory and in the patient's everyday life. The system consists of 18 trackers, 17 attached to the body, and one serves as an additional prop. The trackers are placed strategically on the body by straps to measure the motion of every segment. These trackers are called MTw for short, which stands for wireless motion trackers. These miniature inertial measurement units include:

- a 3D magnetometer to measure the 3D earth magnetic field,
- a 3D velocity gyroscope to measure 3D angular velocity,
- a linear accelerometer to measure the 3D acceleration, and
- a barometer for measuring atmospheric pressure.

The output is the kinematics of each segment, i.e., the position, velocity, acceleration, orientation, angular velocity, and angular acceleration. Each tracker transmits its raw data to the software, which is passed through a data filter. This raw data is then projected onto a biomechanical model. The biomechanical model leads to a digital person, an individualized avatar whose movements correspond to the test person. The final tracker serves as a prop. This additional tracker can be used, for example, to bring a walking aid or other object into the system. MATLAB™ uses the direct export from Xsens™ to evaluate the motion data, for example, extension/flexion, rotation, and external rotation angles of the hip, knee, and ankle joints. The data is also used as motion data for musculoskeletal simulation.

Another tool for analyzing stress scenarios is the Moticon™ measuring sole for gait analysis. They are self-sufficient measuring insoles with the following features:

- sixteen pressure sensors,
- an acceleration sensor and
- and a temperature sensor.

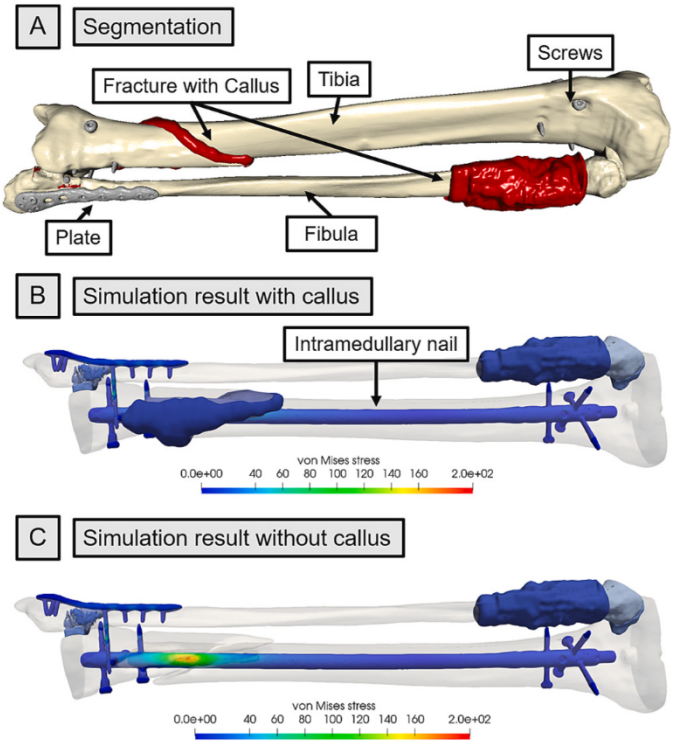

Fig. 2. Segmentation with ScanIP™ (A) and simulation of the von Mises stress (B and C).

The protruding instrumentation allows the ground reaction force to be measured. It also measures the pressure distribution in the contact zone between foot and ground, and the 6-axis inertial measurement unit allows the analysis of velocity, position, pressure distribution, center of pressure, and various other parameters. The soles allow the analysis of stride length, gait speed, distance covered, pressure distribution, and other gait cycle parameters. The evaluation of the sole data produces a gait analysis. The visual analysis of the pressure distribution in both 2D and 3D is of interest. This makes it possible to visualize the pressure loads in different foot areas. Other gait parameters, such as the gait line and the center of pressure, can also be evaluated graphically.

3.2. Musculoskeletal model

After the data acquisition, values are implemented into the software AnyBody™ to analyze the joint and muscle forces by creating a digital avatar of the subject. It is a musculoskeletal model system for the biomechanical simulation of reactions within the human body and between the body and the environment. Again, the primary body data is essential for accurate simulation, as it allows the user to adjust the height, weight, and segment lengths to suit the subject. The motion data previously recorded by Xsens™ is used to create the model.

3.3. Computer tomographic images and segmentation

The simulation process consists of three main stages:

1. The generation of a geometric model using clinical imaging
2. The calculation of individual biomechanical parameters derived from patient monitoring
3. The execution of the final finite element simulations and subsequent analysis of the mechanical data

The segmentation of the CT Images to generate a geometric model based on clinical imaging takes place with the model generation software ScanIP™ (Synopsys, Mountain View, CA, United States). The

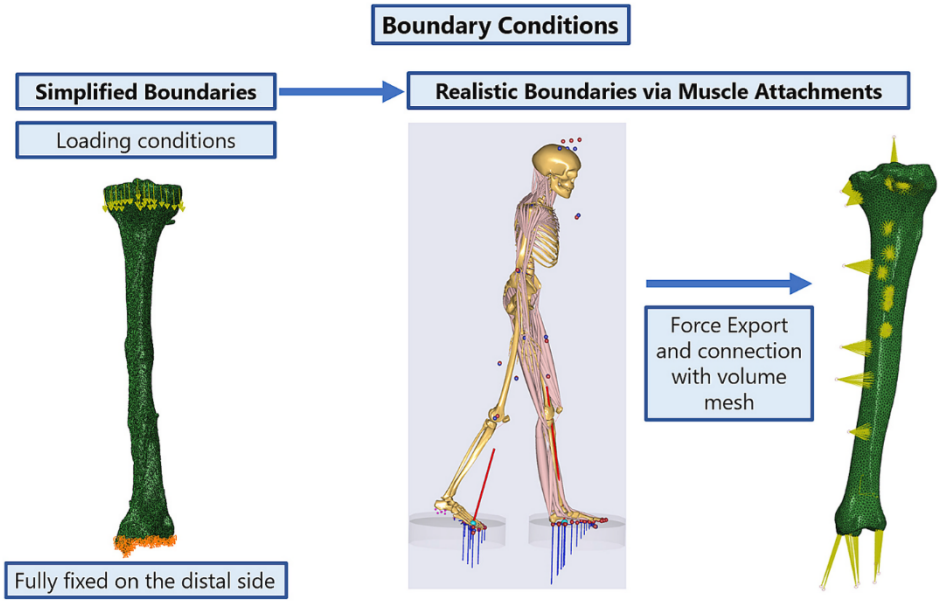

Fig. 3. Simplified and realistic boundary conditions.

image-processing chain uses a sequence of algorithmic steps semi-automated to create a geometric model. It begins with a DICOM image stack from the patient's post-operative CT scan and a six-rod bone density calibration phantom (QRM-BDC/6, QRM GmbH, Moehrendorf, Germany). The images are segmented into different masks for the implant, fracture gap, and bone using an adaptive thresholding technique based on the calibration phantom. Applying a morphological closing filter with isotropic values and smoothing the mask using a recursive Gaussian filter with anisotropic values enhance this process. Subsequently, the segmentation process includes island removal, cavity filling, and gap filling, executed in a prioritized order for each segmented mask. The process results in high segmentation quality with no detectable issues. Additionally, orthopedic trauma surgeons manually reviewed the segmentation results for the fracture gap and made corrections as necessary.

This process results in patient-specific bone Geometry (Fig. 2) and distribution of the different threshold values, which a further step maps to the material parameters. Computed tomography data sets are subjected to a segmentation procedure. After finishing the segmentation and reconstruction process, the next step involves generating a high-resolution adaptive mesh from the individual masks.

The team assigned homogeneous materials with standard properties from the literature to the masks of the treatment, the corresponding screws, and the fracture gap. The treatment, such as implants or interdental nails, uses the existing material parameters. The fracture gap has values of 3 MPa for Young's modulus and 0.4 for the Poisson ratio (initial connective tissue) based on (Claes and Heigele, 1999). Material properties concerning the calibration phantom defined the bone mask to derive an empirical elasticity-bone density relationship. For this purpose, the process first involved analyzing the histogram of the individual segmented rods. Then, linear regression mapped the Hounsfield units (HU) to the hydroxyapatite values from the calibration phantom. This mapping provides the basis for the gray-scale-dependent definition of the material parameters representing local bone properties (Rho et al., 1995; Zannoni et al., 1998). Here, an isotropic heterogeneous material was assumed, having a different value for Young's modulus and a fixed value for the Poisson ratio.

The resulting finite mesh represents the individual patient's fracture, including the implants initially used to fix the fracture. Geometric modeling is based on an image processing chain of various algorithmic steps in a semi-automated sequence. The starting point is the DICOM image stack of the patient's pre- or post-operative CT scan. The images are segmented into different masks for the treatment, the fracture gap, and the bone. A side product of this workflow is the ability to manufacture models of the fracture by 3D printing that might be used by the surgeon during preparation for surgery or for educational purposes, thereby resulting in faster and less invasive surgery.

3.4. Simulation

Abaqus™ (Dassault Systemes, Velizy-Villacoublay, France), a computer-aided engineering and FE analysis software suite, performs the simulation. For this purpose, 10-node quadratic tetrahedral elements of type C3D10 with straight lines were selected in a standard linear elasticity model. The data collected from the patient measurement can now be used to analyze the limited gait load factor by simulating the forces from the measurements with the patient-specific bone.

In addition to evaluating joint and muscle forces for the finite element simulation, the origin and insertion points of the muscles can also be used to apply boundary conditions. The simplified boundary conditions derived from the musculoskeletal simulations based on the patient's motion-capturing data apply to the knee joint in the computational model. Here, the loading conditions are a homogenized distribution of the knee forces in the tibial plateau and a fully fixed distal side. This type of boundary condition was also used in the present study and explained in the previous steps. The realistic boundaries use the origin and insertion points of the muscles attached to the required bone. The yellow points are the attachments on the volume mesh in Abaqus™. For this purpose, the available CT images of the patient are segmented, and a volume mesh is generated in ScanIP™, as described above. The resulting input file with the mesh information forms the model's basic structure. In AnyBody™, after the inverse analysis based on the patient's gait and anthropometry data, the acting forces are output as an XML file. In contrast to the simplified boundaries, the exported forces are now a combination of muscle and tendon forces in addition to the knee and ankle joint forces attacking in the present case of a tibia (Fig. 3). Finally, the input file of ScanIP™ is linked to the XML file of AnyBody™ to form a standard input file for Abaqus™. The simulation only considers the muscle tensile force acting on the bone and fracture and is free of externally imposed constraints.

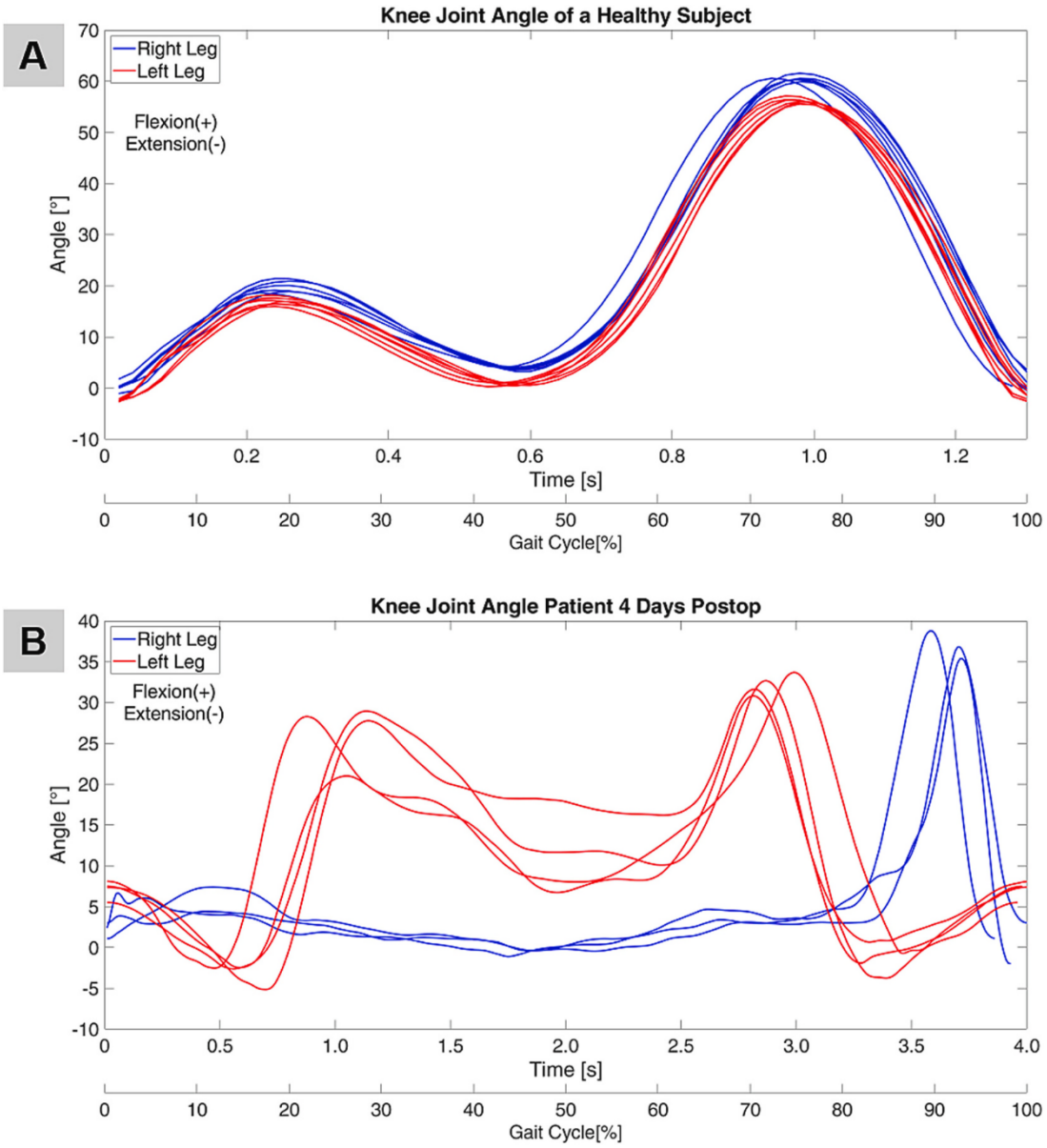

Fig. 4. Knee joint angle over gait cycle for (A) a healthy subject and (B) a patient four days after the operation of a distal tibia fracture.

4. Results

4.1. Patient measurements

The following graphs show an example of the kinematic gait cycle for a healthy subject (Fig. 4A) and a patient (Fig. 4B) with a tibia fracture. The patient's body weight is 105 kg. Both curves show the knee joint angle on the abscissa and the time or gait cycle on the ordinate. A gait cycle describes the period that begins with the first contact of one foot with the ground and ends with the following contact of the same foot with the ground. The corresponding leg is called the reference leg. The other leg is called the contralateral leg. It goes through the same movement cycle but is shifted by half a gait cycle. The gait cycle defines the time between two ground contacts of the same foot (Saur, 2016). The curve shown is the norm in healthy individuals (Fig. 4A) (Goetz-Neumann, 2003). In patients, however, it is very individual. The difference in the left fractured leg is particularly striking. No general statements can be made about the course of the curve in patients. It is, therefore, essential to record individual movements for later simulation.

The kinetic gait parameters (Fig. 5) show, in this case, the ground reaction force over time or the gait cycle, a very similar behavior to the motion capture curve (Fig. 4). Not only does the movement of the fractured leg change, but the load also decreases. Both measurement systems clearly show that the patient's entire gait behavior changes. Due to the relief of the fractured leg, the healthy leg must also adapt to the load's angle, force, gait speed, and duration. It becomes clear that the collection of postoperative gait data is crucial for accurately assessing the interfragmentary movement.

4.2. Joint forces

The recorded forces on the lower extremities of the patients are boundary conditions for the simulation (Fig. 6) of a fractured bone to calculate the effects on fracture healing. The analyzed knee forces and moments over the gait cycle are shown for the used patient data (Fig. 4 and Fig. 5). The forces F_x, F_y, and F_z act in lateral, anterior, and superior directions on the tibial plateau. In the sagittal plane of the tibial component, the moment M_x operates, rotating clockwise about the +x-axis. In the frontal plane, the moment M_y operates, it turns clockwise around the +y-axis, while M_z turns clockwise around the +z-axis within the transverse plane. They are normalized to the patient's body weight. These measurement points are then used as input variables for the force

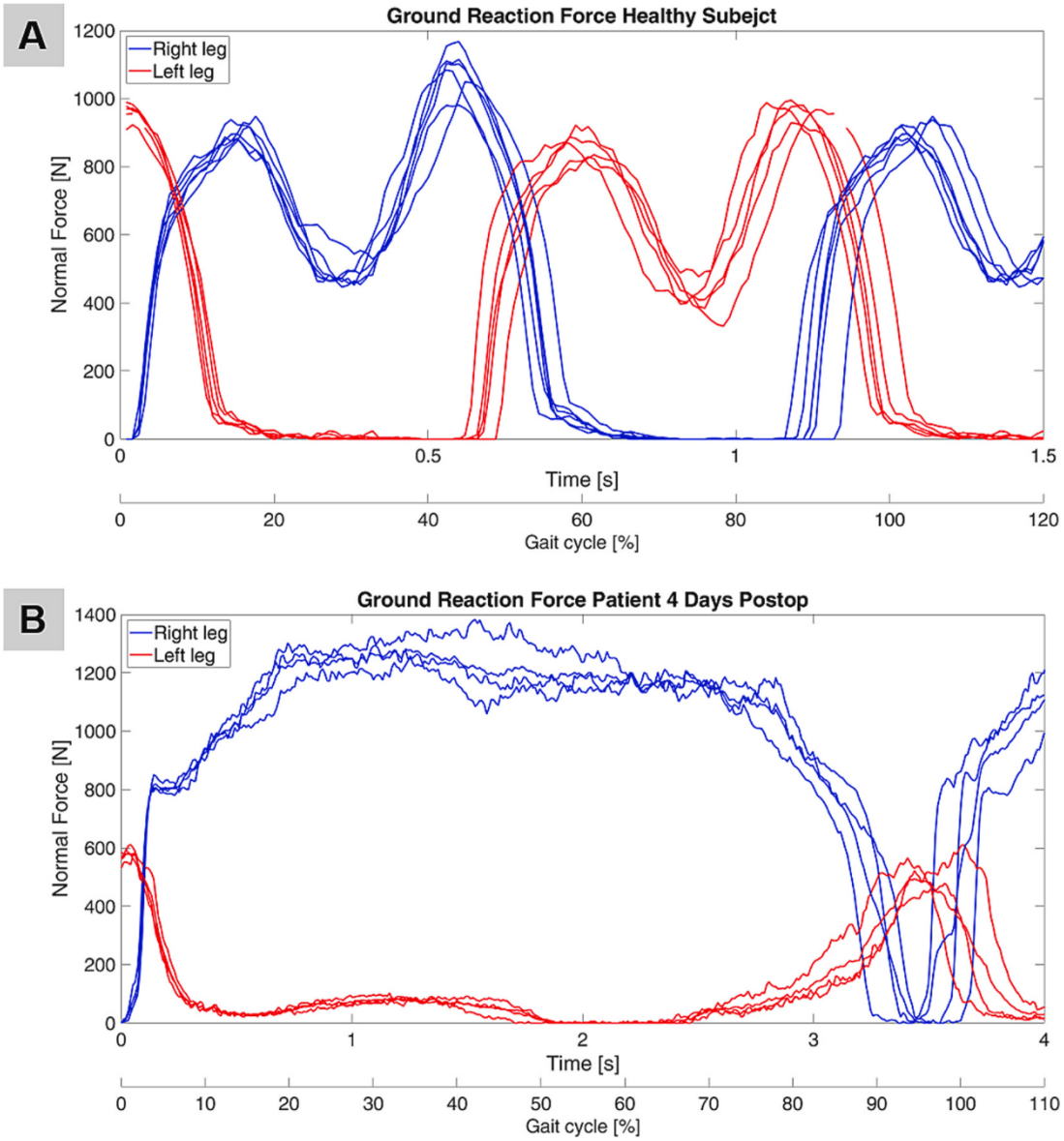

Fig. 5. Ground reaction force over gait cycle for (A) a healthy subject and (B) a patient four days after the operation of a distal tibia fracture.

amplitudes in the simulation.

4.3. Evaluation of the von Mises stress

The von Mises stress quantifies the local load and helps to evaluate the mechanical response of the implant or intramedullary nail, particularly with regard to compliance and the risk of failure. Its value and distribution can identify weaknesses in a treatment (Fig. 2), for example, the von Mises stress distribution at the moment of maximum force application during the patient's forward step. The region with the highest von Mises stress values is almost congruent with the fracture area above the most proximal-distal screws.

4.4. Simulation of the interfragmentary movement

This study simulates the movement between fragments and how different treatments influence it. We adopt a mechanobiological approach that is rooted in the mechanical stimulus, as explored by Claes and Heigele (Claes and Heigele, 1999) as well as Shefelbine et al. (Shefelbine et al., 2005). Essentially, we investigate the interaction between octahedral shear strain, which derives from the deviatoric part of the strain tensor, and volumetric strain, which is associated with changes in volume arising due to hydrostatic pressure (Ghiasi et al., 2017). This approach is closely connected to the idea that the extent of mechanical deviatoric strains plays a crucial role in cell differentiation and tissue formation. Moreover, it aligns well with the experimental findings of Bishop et al. (Bishop et al., 2003), Garcia et al. (Garcia et al., 2003), and Doblaré et al. (Doblaré et al., 2004). To ensure an accurate analysis of the mechanical behavior within the fracture gap, we investigate the strain tensor for each tetrahedral element individually. We then calculate and evaluate both the octahedral shear strain and the volumetric strain within the given limits, following the guidelines of Claes and Heigele (Claes and Heigele, 1999) and Shefelbine et al. (Shefelbine et al., 2005). This results in five areas of the healing window with the corresponding coloring in the legend for the interfragmentary movement (Fig. 7). Green corresponds to the perfect area for bone healing, while red assigns a too-large and blue to a too-small stimulus of the fracture. The patient was measured on a treadmill with the Xsens™ and Moticon™ soles, and the speed was increased from 1 km/h to 1.5 km/h and then to 2 km/h. The ground reaction force, knee joint angle, and knee joint force were evaluated over a gait cycle at each speed. The force values were then used as input to simulate the interfragmentary movement, always applying a complete step in Abaqus™ as the force amplitude. The results show a correlation between the knee joint force

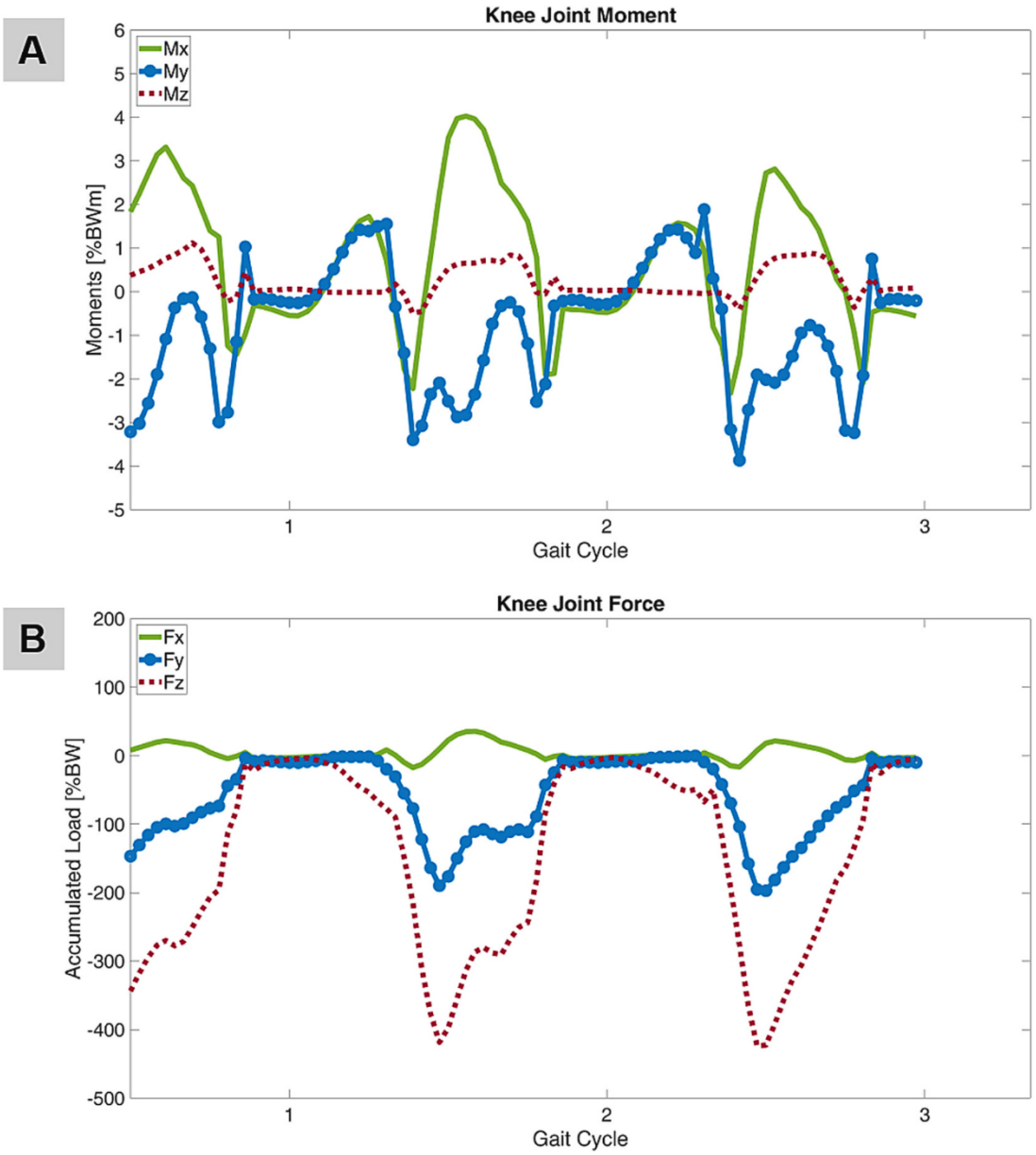

Fig. 6. Knee joint moment and force standardized to the patient's bodyweight.

and the portion of elements in a too-much-motion window. The greater the load due to increased velocity, the more significant the proportion of elements experiencing too much stimulus. On the other hand, the regions of the elements with too little motion decrease more and more. It is important to note that the interfragmentary movement is a snapshot. During a gait cycle, individual elements move back and forth between the individual healing windows.

5. Discussion

The kinematic gait analysis data are essential for the analysis of the healing process. They are also an important supplement to the data from the kinetic gait analysis. Kinetic gait analysis does not capture the swing phase because the foot is not in contact with the ground. Only the combination of joint angle trajectories by motion capture and ground reaction forces allows an accurate statement about the current gait condition of the patient. The motion of the avatar of the Xsens™ system also allows a precise analysis of the individual movement sequences. The advantage of motion capture lies primarily in location-independent data acquisition. As a result, many patients can be monitored by a physiotherapist during their first steps after surgery. This way, data can be tracked from the earliest possible loading in the healing process to full recovery. In addition, the wide range of rehabilitation and sports science applications can provide new insights into loading during recovery, for example, defining the exact influence of partial weight bearing on lower leg injuries. Individual observation of gait development during the healing process provides crucial information for patient-specific simulation. In particular, using motion data as input to musculoskeletal simulation provides significant individual constraints for evaluating interfragmentary movement. The biggest challenge is the need for CT scans to create a three-dimensional model. Most patients do not require a computed tomographic view of their fracture situation. Therefore, new capabilities need to be developed. However, it is currently impossible to create models from radiographs alone because the 3D course of the fracture through the bone is difficult to reconstruct in the two-dimensional plane. Virtual reconstructions of future treatment situations can be created if a CT scan is available, either preoperatively or postoperatively. In addition, the segmentation process is only partially automated. Each patient requires a precise analysis of the segmentation steps, which ultimately must be confirmed by the treating physician.

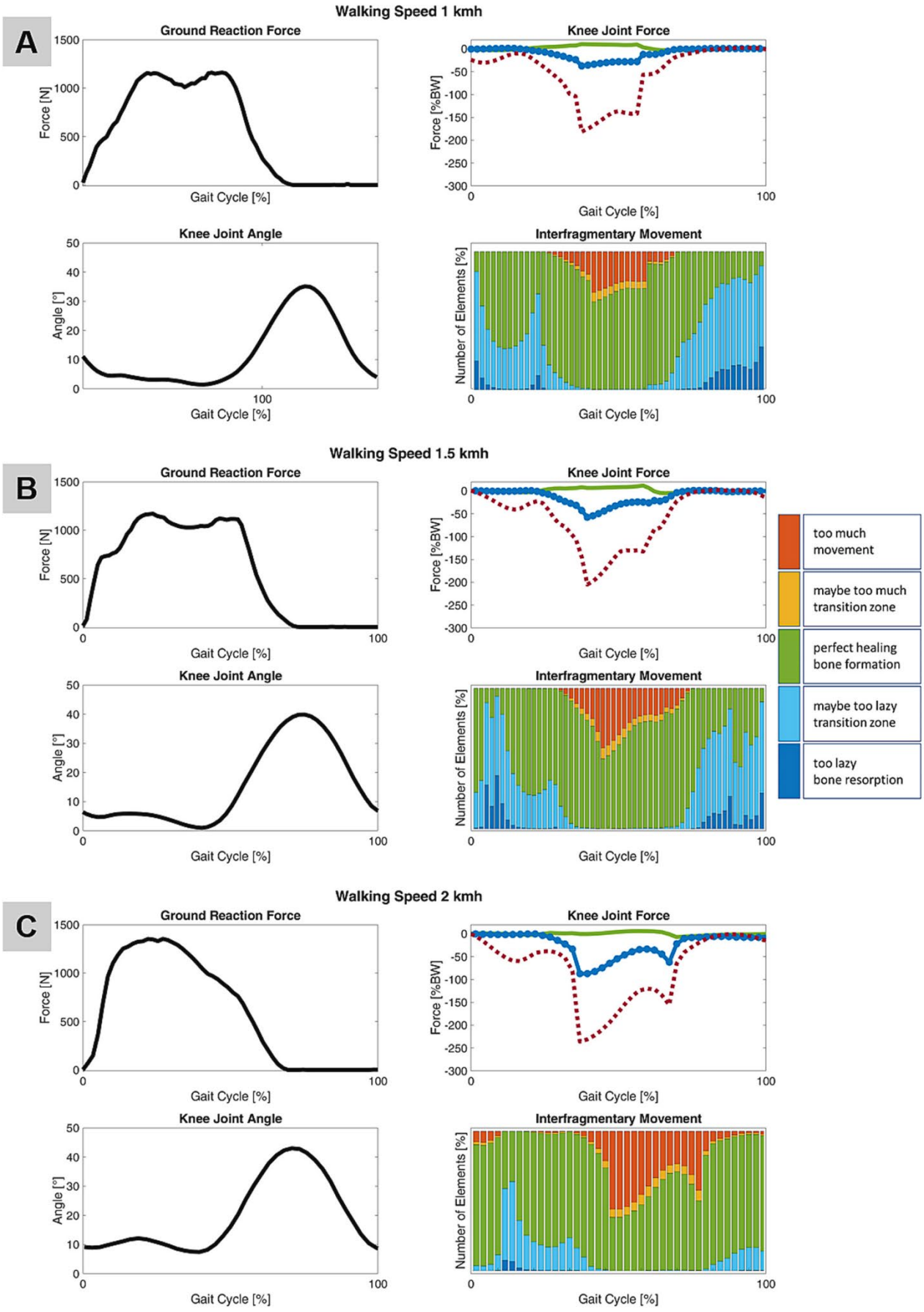

Fig. 7. Comparison between different walking speeds and the impact on the interfragmentary movement.

Another challenge is the highly variable quality of CT images. Metallic artifacts often obscure the fracture situation and make segmentation and restoration difficult. Often, the slice thicknesses between the CT slices are too coarse and prevent the construction of an appropriate 3D model. This study has several limitations. First, the mechanical conditions identified cannot be verified through experimental means due to the lack of commercially available implants to validate the simulated parameters. However, previous research has demonstrated the ability to validate fracture condition simulations through clinical validation, particularly in healed fractures (Ghiasi et al., 2017). In the paper from our working group (Wickert et al., 2024), we deal extensively with validating and verifying our simulations. We follow the procedures described by different publications to this topic (Augat et al., 2021a; Augat et al., 2021b; Lund et al., 2012), which is what makes a good simulation. Nevertheless, we try further to substantiate our results with additional experiments on human specimens. Our simulations only focus on the interaction of partial loads on the implant and the fracture gap. Up to now, there is no consideration of biological factors. In addition, the parameters of the bone material can only be accurately mapped with the help of a calibration phantom, as presented in Braun (Braun et al., 2021). In the present case, a calibration phantom was not available. Another limitation is a gait cycle with crutches in the musculoskeletal model. It is possible to consider partial weight bearings but not active walking with crutches. This requires a self-measuring crutch, which was not available.

6. Conclusion

The results presented here are only exemplary. A closer look give the articles by Orth (Orth et al., 2023) and Braun (Braun et al., 2019) on the presented patient and another case. The workflow has been successfully implemented several times and applied to various patient cases. The individual steps are well coordinated, as the systems were selected according to how well they are compatible with each other. However, the workflow can also be extended at any time, for example, by considering more explicit healing simulations. The automation of all steps is progressing steadily, and, in terms of time, the patient data can now be evaluated quickly. New therapeutic approaches for revision surgery will develop based on the finite element simulation results.

CRediT authorship contribution statement

Annchristin Andres: Writing – original draft, Methodology, Data curation, Conceptualization. **Michael Roland:** Writing – review & editing, Supervision, Software, Funding acquisition, Formal analysis. **Kerstin Wickert:** Validation, Data curation. **Bergita Ganse:** Writing – review & editing, Project administration. **Tim Pohlemann:** Funding acquisition. **Marcel Orth:** Resources, Investigation. **Stefan Diebels:** Writing – review & editing, Supervision.

Declaration of competing interest

The authors declare that they have no known competing financial interests or personal relationships that could have appeared to influence the work reported in this paper.

References

Aubert, K., Germaneau, A., Rochette, M., Ye, W., Severyns, M., Billot, M., Rigoard, P., Vendeuvre, T., 2021. Development of digital twins to optimize trauma surgery and postoperative management. A case study focusing on Tibial plateau fracture. Front. Bioeng. Biotechnol. 9, 1–11. https://doi.org/10.3389/fbioe.2021.722275.

Augat, Peter, Simon, U., Liedert, A., Claes, L., 2005. Mechanics and mechano-biology of fracture healing in normal and osteoporotic bone. Osteoporos. Int. 16 (Suppl. 2), 36–43. https://doi.org/10.1007/s00198-004-1728-9.

Augat, P., Faschingbauer, M., Seide, K., Tobita, K., Callary, S.A., Solomon, L.B., Holstein, J.H., 2014. Biomechanical methods for the assessment of fracture repair. Injury 45 (Suppl. 2), S32–S38. https://doi.org/10.1016/j.injury.2014.04.006.

Augat, Peter, Hast, M.W., Schemitsch, G., Heyland, M., Trepczynski, A., Borgiani, E., Russow, G., Märdian, S., Duda, G.N., Hollensteiner, M., Bottlang, M., Schemitsch, E. H., 2021a. Biomechanical models: key considerations in study design. OTA Int. 4 (2), E099. https://doi.org/10.1097/OI9.0000000000000099.

Augat, Peter, Hollensteiner, M., von Rüden, C., 2021b. The role of mechanical stimulation in the enhancement of bone healing. Injury 52, S78–S83. https://doi.org/10.1016/j.injury.2020.10.009.

Barricelli, B.R., Casiraghi, E., Fogli, D., 2019. A survey on digital twin: definitions, characteristics, applications, and design implications. IEEE Access 7 (MI), 167653–167671. https://doi.org/10.1109/ACCESS.2019.2953499.

Bassani, T., Stucovitz, E., Qian, Z., Briguglio, M., Galbusera, F., 2017. Validation of the AnyBody full body musculoskeletal model in computing lumbar spine loads at L4L5 level. J. Biomech. 58, 89–96. https://doi.org/10.1016/j.jbiomech.2017.04.025.

Bishop, N.E., Tami, I., Schneider, E., I. K., 2003. In vivo comparison of early fracture healing under deviatoric and volumetric deformationsitle. Acta Bioeng. Biomech. 4, 754–755.

Bishop, J.A., Palanca, A.A., Bellino, M.J., Lowenberg, D.W., 2012. Assessment of compromised fracture healing. J. Am. Acad. Orthop. Surg. 20 (5), 273–282. https://doi.org/10.5435/JAAOS-20-05-273.

Braun, B.J., Pohlemann, T., Herath, S.C., Klein, M., Rollmann, M.F., Derr, R., Diebels, S., Roland, M., 2019. An individualized simulation model based on continuous, independent, ground force measurements after intramedullary stabilization of a tibia fracture. Arch. Appl. Mech. 89 (11), 2351–2360. https://doi.org/10.1007/s00419-019-01582-5.

Braun, B.J., Orth, M., Diebels, S., Wickert, K., Andres, A., Gawlitza, J., Bücker, A., Pohlemann, T., Roland, M., 2021. Individualized determination of the mechanical fracture environment after Tibial exchange nailing—a simulation-based feasibility study. Front. Surg. 8, 1–9. https://doi.org/10.3389/fsurg.2021.749209.

Claes, L.E., Heigele, C.A., 1999. Magnitudes of local stress and strain along bony surfaces predict the course and type of fracture healing. J. Biomech. 32 (3), 255–266. https://doi.org/10.1016/S0021-9290(98)00153-5.

Court-Brown, C.M., Caesar, B., 2006. Epidemiology of adult fractures: a review. Injury 37 (8), 691–697. https://doi.org/10.1016/j.injury.2006.04.130.

Dahmen, T., Roland, M., Tjardes, T., Bouillon, B., Slusallek, P., Diebels, S., 2015. An automated workflow for the biomechanical simulation of a tibia with implant using computed tomography and the finite element method. Comput. Math. Appl. 70 (5), 903–916. https://doi.org/10.1016/j.camwa.2015.06.009.

Dijkman, B.G., Sprague, S., Schemitsch, E.H., Bhandari, M., 2010. When is a fracture healed? Radiographic and clinical criteria revisited. J. Orthop. Trauma 24 (Suppl. 1), 76–80. https://doi.org/10.1097/BOT.0b013e3181ca3f97.

Doblaré, M., García, J.M., Gómez, M.J., 2004. Modelling bone tissue fracture and healing: a review. Eng. Fract. Mech. 71 (13–14), 1809–1840. https://doi.org/10.1016/j.engfracmech.2003.08.003.

Ganse, B., 2024. Methods to accelerate fracture healing - a narrative review from a clinical perspective. Front. Immunol. 15, 1–13. https://doi.org/10.3389/fimmu.2024.1384783.

Ganse, B., Orth, M., Roland, M., Diebels, S., Motzki, P., Seelecke, S., Kirsch, S.M., Welsch, F., Andres, A., Wickert, K., Braun, B.J., Pohlemann, T., 2022. Concepts and clinical aspects of active implants for the treatment of bone fractures. Acta Biomater. 146, 1–9. https://doi.org/10.1016/j.actbio.2022.05.001.

Garcia, J.M., Kuiper, J.H., Doblare, M., R. J., 2003. A numerical model to study the mechanical influences on bone fracture healing. Acta Bioeng. Biomech. 4, 394–395.

Ghiasi, M.S., Chen, J., Vaziri, A., Rodriguez, E.K., Nazarian, A., 2017. Bone fracture healing in mechanobiological modeling: a review of principles and methods. Bone Rep. 6, 87–100. https://doi.org/10.1016/j.bonr.2017.03.002.

Goetz-Neumann, K., 2003. Gehen verstehen. Ganganal. Physiother. 195.

Hak, D.J., Fitzpatrick, D., Bishop, J.A., Marsh, J.L., Tilp, S., Schnettler, R., Simpson, H., Alt, V., 2014. Delayed union and nonunions: epidemiology, clinical issues, and financial aspects. Injury 45 (Suppl. 2), S3–S7. https://doi.org/10.1016/j.injury.2014.04.002.

Killen, B.A., Falisse, A., De Groote, F., Jonkers, I., 2020. In silico-enhanced treatment and rehabilitation planning for patients with musculoskeletal disorders: can musculoskeletal modelling and dynamic simulations really impact current clinical practice? Appl. Sci. 10 (20), 1–22. https://doi.org/10.3390/app10207255.

Lauer-Schmaltz, M.W., Cash, P., Hansen, J.P., Maier, A., 2022. Designing human digital twins for behaviour-changing therapy and rehabilitation: a systematic review. Proc. Des. Soc. 2, 1303–1312. https://doi.org/10.1017/pds.2022.132.

Lund, M.E., De Zee, M., Andersen, M.S., Rasmussen, J., 2012. On validation of multibody musculoskeletal models. Proc. Inst. Mech. Eng. H J. Eng. Med. 226 (2), 82–94. https://doi.org/10.1177/0954411911431516.

Maisenbacher, T.C., Libicher, S., Erne, F., Menger, M.M., Reumann, M.K., Schindler, Y., Niemeyer, F., Engelhardt, L., Histing, T., Braun, B.J., 2024. Case studies of a simulation workflow to improve bone healing assessment in impending non-unions. J. Clin. Med. 13 (13). https://doi.org/10.3390/jcm13133922.

Orth, M., Ganse, B., Andres, A., Wickert, K., Warmerdam, E., Müller, M., Diebels, S., Roland, M., Pohlemann, T., 2023. Simulation-based prediction of bone healing and treatment recommendations for lower leg fractures: effects of motion, weight-bearing and fibular mechanics. Front. Bioeng. Biotechnol. 11, 1–13. https://doi.org/10.3389/fbioe.2023.1067845.

Pountos, I., Georgouli, T., Pneumaticos, S., Giannoudis, P.V., 2013. Fracture non-union: can biomarkers predict outcome? Injury 44 (12), 1725–1732. https://doi.org/10.1016/j.injury.2013.09.009.

Roland, M., Tjardes, T., Otchwemah, R., Bouillon, B., Diebels, S., 2015. An optimization algorithm for individualized biomechanical analysis and simulation of tibia fractures. J. Biomech. 48 (6), 1119–1124. https://doi.org/10.1016/j.jbiomech.2015.01.015.

Rho, J.Y., Hobatho, M.C., Ashman, R.B., 1995. Relations of mechanical properties to density and CT numbers in human bone. Med. Eng. Phys. 17 (5), 347–355. https://doi.org/10.1016/1350-4533(95)97314-F.

Roland, Michael, Diebels, S., Wickert, K., Pohlemann, T., Ganse, B., 2024. Finite element simulations of smart fracture plates capable of cyclic shortening and lengthening: which stroke for which fracture? Front. Bioeng. Biotechnol. 12, 1–14. https://doi.org/10.3389/fbioe.2024.1420047.

Saravi, B., Lang, G., Steger, R., Vollmer, A., Zwingmann, J., 2021. Corrective osteotomy of upper extremity Malunions using three-dimensional planning and patient-specific surgical guides: recent advances and perspectives. Front. Surg. 8, 1–7. https://doi.org/10.3389/fsurg.2021.615026.

Saur, U., 2016. Funktionelle, Klinische, Sowie Ganganalytische Ergebnisse nach Resektion der proximalen Tibia und Strecksehnenrekonstruktion im Rahmen der Tumorendoprothetik.

Schwarzenberg, P., Maher, M.M., Harty, J.A., Dailey, H.L., 2019. Virtual structural analysis of tibial fracture healing from low-dose clinical CT scans. J. Biomech. 83, 49–56. https://doi.org/10.1016/j.jbiomech.2018.11.020.

Shefelbine, S.J., Augat, P., Claes, L., Simon, U., 2005. Trabecular bone fracture healing simulation with finite element analysis and fuzzy logic. J. Biomech. 38 (12), 2440–2450. https://doi.org/10.1016/j.jbiomech.2004.10.019.

Tjardes, T., Roland, M., Otchwemah, R., Dahmen, T., Diebels, S., Bouillon, B., 2014. Less than full circumferential fusion of a tibial nonunion is sufficient to achieve mechanically valid fusion - proof of concept using a finite element modeling approach. BMC Musculoskelet. Disord. 15 (1), 1–7. https://doi.org/10.1186/1471-2474-15-434.

Warmerdam, E., Wolff, C., Orth, M., Pohlemann, T., Ganse, B., 2024. Long-term continuous instrumented insole-based gait analyses in daily life have advantages over longitudinal gait analyses in the lab to monitor healing of tibial fractures. Front. Bioeng. Biotechnol. 12, 1–10. https://doi.org/10.3389/fbioe.2024.1355254.

Wickert, K., Roland, M., Andres, A., Diebels, S., Ganse, B., Kerner, D., Frenzel, F., Tschernig, T., Ernst, M., Windolf, M., Müller, M., Pohlemann, T., Orth, M., 2024. Experimental and virtual testing of bone-implant systems equipped with the AO fracture monitor with regard to interfragmentary movement. Front. Bioeng. Biotechnol. 12, 1–20. https://doi.org/10.3389/fbioe.2024.1370837.

Wriggers, P., Zavarise, G., 2011. Lecture notes in applied and computational mechanics: preface. In: Lecture Notes in Applied and Computational Mechanics: Vol. 58 LNACM. https://doi.org/10.1007/978-3-642-22167-5.

Zannoni, C., Mantovani, R., Viceconti, M., 1998. Material properties assignment to finite element models of bone structures: a new method. Med. Eng. Phys. 20, 735–740. https://doi.org/10.1016/S1350-4533(98)00081-2.

15 Paper B

Title:

From Injury to Full Recovery: Monitoring Patient Progress Through Advanced Sensor and Motion Capture Technology

Authors:

Annchristin Andres, Michael Roland, Marcel Orth & Stefan Diebels

Original Publication:

Andres, A., Roland, M., Orth, M., & Diebels, S. (2025). From Injury to Full Recovery: Monitoring Patient Progress Through Advanced Sensor and Motion Capture Technology. *Sensors*, *25*(13), 3853. https://doi.org/10.3390/s25133853

sensors

MDPI

Article

From Injury to Full Recovery: Monitoring Patient Progress Through Advanced Sensor and Motion Capture Technology

Annchristin Andres [1,*], Michael Roland [1], Marcel Orth [2] and Stefan Diebels [1]

[1] Applied Mechanics, Saarland University, 66123 Saarbrücken, Germany
[2] Department of Trauma, Hand and Reconstruction Surgery, Saarland University Hospital, 66424 Homburg, Germany
* Correspondence: annchristin.andres@uni-saarland.de; Tel.: +49-681-302-2168; Fax: +49-681-302-3992

Abstract

Background: Advanced sensor insoles and motion capture technology can significantly enhance the monitoring of rehabilitation progress for patients with distal tibial fractures. This study leverages the potential of these innovative tools to provide a more comprehensive assessment of a patient's gait and weight-bearing capacity following surgical intervention, thereby offering the possibility of improved patient outcomes. Methods: A patient who underwent distal medial tibial plating surgery in August 2023 and subsequently required revision surgery due to implant failure, involving plate removal and the insertion of an intramedullary nail in December 2023, was meticulously monitored over a 12-week period. Initial assessments in November 2023 revealed pain upon full weight-bearing without crutches. Following the revision, precise weekly measurements were taken, starting two days after surgery, which instilled confidence in accurately tracking the patient's progress from initial crutch-assisted walking to full recovery. The monitoring tools included insoles, hand pads for force absorption of the crutches, and a motion capture system. The patient was accompanied throughout all steps of his daily life. Objectives: The study aimed to evaluate the hypothesis that the approximation and formation of a healthy gait curve are decisive tools for monitoring healing. Specifically, it investigated whether cadence, imbalance factors, and ground reaction forces could be significant indicators of healing status and potential disorders. Results: The gait parameters, cadence, factor of imbalance ground reaction forces, and the temporal progression of kinematic parameters significantly correlate with the patient's recovery trajectory. These metrics enable the early identification of deviations from expected healing patterns, facilitating timely interventions and underscoring the transformative potential of these technologies in patient care. Conclusions: Integrating sensor insoles and motion capture technology offers a promising approach for monitoring the recovery process in patients with distal tibial fractures. This method provides valuable insights into the patient's healing status, potentially predicting and addressing healing disorders more effectively. Future studies are recommended to validate these findings in a larger cohort and explore the potential integration of these technologies into clinical practice.

Keywords: digital mobility outcome; wearables; patient monitoring; rehabilitation; fracture healing

Academic Editor: Tao Liu

Received: 20 March 2025
Revised: 9 May 2025
Accepted: 18 June 2025
Published: 20 June 2025

Citation: Andres, A.; Roland, M.; Orth, M.; Diebels, S. From Injury to Full Recovery: Monitoring Patient Progress Through Advanced Sensor and Motion Capture Technology. *Sensors* **2025**, *25*, 3853. https://doi.org/10.3390/s25133853

1. Introduction

Gait analysis has become an important parameter for monitoring the healing process of injuries and various medical conditions [1]. It has also been useful for monitoring

improvements in spatiotemporal gait parameters, kinematics, kinetics, and pedography throughout the healing process in lower leg fractures [2].

Wearable sensors, such as gait monitoring insoles, have been used to monitor patient behavior during rehabilitation [3]. These sensors track metrics like step count, walking time, cadence, and body weight per step, offering insights that influence rehabilitation outcomes [4]. Additionally, insole-force sensors measure loading on the lower extremities in patients with pelvic fragility fractures [4]. This study found differences in loading between the affected and unaffected limbs, suggesting that using insole-force sensors may improve treatment choices and timing [5]. Telemetric gait analysis insoles track postoperative fracture rehabilitation by analyzing ground reaction forces [6]. Combined with a mobile application and a convolutional neural network, these insoles can automate the monitoring of patient progress and identify bone healing disorders such as non-unions.

Recent advancements in sensor technology and motion capture systems have significantly transformed the rehabilitation landscape, particularly in the monitoring and management of partial weight-bearing (PWB) in individuals recovering from lower limb surgeries, injuries, or other medical conditions [7]. The critical role of PWB in rehabilitation involves limiting the amount of weight placed on the affected limb to prevent stress and pain, promote healing, and ensure a successful recovery by reducing the risk of re-injury and facilitating a smooth transition to full weight-bearing throughout the healing course. Integrating sensor insoles and motion-capturing systems has emerged as a breakthrough in enhancing the monitoring and guidance of PWB [8,9].

Sensor insoles (Moticon^{TM}, ReGo AG, Munich, Germany), designed to provide real-time feedback on foot pressure distribution, enable precise monitoring of how much weight a patient places on different aspects of the affected limb [9,10]. Likewise, the motion-capturing system from Xsens^{TM} (Movella Technology B.V., Enschede, The Netherlands) delivers an in-depth analysis of the patient's movement patterns, capturing a wide array of data points that facilitate monitoring progress and adjusting rehabilitation strategies. Xsens^{TM} technology allows for accurate assessments of gait, balance, and other functional movements, providing invaluable insights into a patient's recovery trajectory. Recent studies' contributions underscore the advancements and applications of these technologies in rehabilitation. For instance, Horenstein and colleagues [11,12] validated wireless inertial sensors for hip joint motion, demonstrating that most angles measured with the sensor-based system were within 6° of those measured with a traditional camera motion capture system.

By combining the capabilities of advanced sensor insoles and motion-capturing systems, healthcare professionals can comprehensively understand a patient's prescribed PWB adherence and overall movement health. This integrated approach enables a more tailored and effective rehabilitation process, leveraging the power of technology to facilitate better outcomes for patients navigating the complexities of PWB. These technological advancements, supported by a growing body of research, underscore the potential of sensor and motion capture technologies in revolutionizing rehabilitation practices and improving patient care. However, it remains unclear to what extent a thoroughly analyzed patient's gait curve over an entire healing cycle can be a critical indicator of successful bone healing. The study hypothesizes that approximating and stabilizing a patient's gait curve toward a normative healthy gait pattern are essential indicators of successful healing. We used metrics such as cadence, imbalance factor, and GRFs over time to assess the healing process and identify potential complications or delayed recovery.

2. Methods

Different activities that reflect the patient's daily life are part of a measurement workflow [13]. These include walking twice with crutches, climbing stairs, performing a sit-to-stand-to-sit cycle, and dorsiflexion and plantarflexion of his injured foot. The various exercises were measured simultaneously using sensor insoles and a motion-capturing system for activities such as climbing stairs, sitting down, and standing up, as well as navigating stairs in the hallway and using couches or dining room chairs in the patient's apartment. The supplementary material provides an example for the knee joint angle (see Figure S3) and the ground reaction force (see Figure S4) during walking. The purpose of the whole exercise is to represent his everyday situation as accurately as possible and the effect of these stresses. For example, stair climbing was essential in his daily living routine as his apartment is on the second floor, and he had to walk up and down several times a day from the outset. Table 1 details any deviations from this workflow.

Table 1. Summary of conducted measurements and prescribed partial weight-bearing.

	Date	Location	Measured Activity	Recommended Partial Weight-Bearing	Further Information
M00	22 November 2023	Fitness Studio	Walking	Full Bodyweight	Preoperative
M01	22 December 2023	Hospital	Gait school/Rehabilitation exercise	0 kg	2 days postoperative
M02	29 December 2023	Hospital	Walking	20 kg	
M03	5 January 2024	At home	Measurement workflow	20 kg	
M04	12 January 2024	At home	Measurement Workflow	20 kg	
M05	19 January 2024	At home	Measurement workflow	20 kg	
M06	26 January 2024	At home	Measurement workflow	20 kg	
M07	31 January 2024	Hospital	Measurement workflow	45 kg	Follow-up appointment
M08	9 February 2024	At Home	Measurement workflow Walking without crutches Walking with one crutch Indoor cycling	45 kg	First-time full weight-bearing
M09	16 February 2024	At Home	Measurement workflow without crutches	Full Bodyweight	
M10	23 February 2024	At Home	Measurement workflow without crutches		
M11	12 March 2024	Hospital			Follow-up appointment

2.1. Kinetic Gait Analysis

Measuring soles dynamically measure the ground reaction force and pressure distribution in the foot, making them essential for analyzing load scenarios and gait patterns. These self-sufficient measuring soles record with a sampling rate of 100 Hz. Each sole comprises sixteen pressure sensors, an acceleration sensor, and a temperature sensor. Figure S1 in the supplementary material provides a detailed image of the insoles. In kinetic gait analysis, particularly in observing the healing process by increasing the load-bearing capacity of the fractured leg, the ground reaction force plays a crucial yet straightforward interpretative role as per Newton's third law, which states that action equals reaction. The force that the ground exerts on a body in contact with it is a vector quantity representing the reaction force exerted by the ground on a person or object while standing, walking, or running. For the evaluation, the cadence (1), that is, the number of steps taken per minute, is considered on the one hand. The imbalance factor (2) more accurately represents the ground reaction force ratio between the healthy left leg and the fractured right leg. It quantifies asymmetry

in percent between the left (healthy) leg (GRF_left) and right (injured) leg (GRF_right) ground reaction force.

$$Cadence = \frac{Number\ of\ Steps}{Time\ [minute]} \quad (1)$$

$$Factor\ of\ Imbalance = \frac{|(GRF\_left - GRF\_right)|}{GRF\_left} * 100 \quad (2)$$

2.2. Kinematic Gait Analysis

The Xsens™ motion capture system "Awinda" tracks movements to create a full-body motion image, enabling immediate graphical output. Additionally, the system can determine joint angle data, center of gravity, and other sensor information. It comprises 17 inertial measurement units (IMUs) strategically attached to important body parts using straps. The sensor placement is bilateral on the thighs, shanks, feet, shoulders, hands, and lower and upper arms, as well as on the pelvis, trunk, and head. The 17 wireless inertial measurement units contain a 3D magnetometer to measure the 3D geomagnetic field, a 3D velocity gyroscope to measure the 3D angular velocity, a linear accelerometer to measure the 3D acceleration, and a barometer to measure the atmospheric pressure. The system recorded full-body kinematics at 60 Hz. Figure S2 in the supplementary material shows the complete setup of the system. The measured values from the lower body motion trackers—specifically those on the right and left thighs, lower legs, and feet—played a crucial role in analyzing this patient's gait. Due to the existing tibia fracture, examining the knee joint angle in greater detail was essential. The study examined the angle of the knee joint during both the stance and swing phases of walking. While extensive research has already been conducted on healthy individuals as evidenced in various literature sources [14–17], our studies, presented in the supplementary material, offer additional validation. The knee joint angle is a three-dimensional Euler angle derived from the transformation between the thigh and shank coordinate frames. In Xsens™, it is calculated based on positional data from the motion tracker on the thigh and the tracker on the lower leg. Our analysis focuses specifically on knee flexion and extension as these movements exhibit the most significant variations in response to the injury [18,19]. For the subsequent evaluations, the premise was also to take simple values with a relatively high significance, which do not require much prior knowledge for analysis. Acceleration is the first value taken directly from the measurement data. The acceleration variation between the right and left legs is a percentage for better visualization. The recorded measurement data allows easy retrieval of these values. The knee joint angle is subdivided into stance and swing phases as it reaches two maxima during a healthy stride. The first has up to 15 degrees of flexion in the loading response and thus falls in the middle of the stance phase, while the second has up to 60 degrees of flexion in the initial swing phase. Therefore, the deviations and approximations during the recovery phase are of interest. The analysis also includes the stride length, which is the distance between the position of a heel at the foot strike and that of the same heel at its next foot strike from the start to the end of a gait cycle.

3. Patient

A 12-week longitudinal monitoring study followed a patient who sustained a distal tibial fracture in August 2023 and received fixation with a distal medial tibial locking compression plate (LCP) (Figure 1). In November 2023, the patient returned for biomechanical assessment and underwent initial gait measurements using instrumented insoles and Xsens™ motion capture technology. At that time, the patient reported pain with every step but was walking independently with full weight-bearing and without crutches. In December 2023, surgeons performed a revision surgery, replacing the LCP with an intramedullary

nail. Gait measurements began two days after the operation. Over the following 12 weeks, the system recorded the patient's gait parameters weekly using Xsens™ and instrumented insoles, tracking progress through to full recovery.

Figure 1. A 29-year-old male patient suffering from a lower leg fracture after a previous and healed ankle fracture in the past (**A**). The patient was initially treated by plating osteosynthesis of the tibia and fibula (**B**). At 4 months after surgery, the patient showed an implant failure ((**C**); arrows) and signs of a hypertrophic non-union as a disturbed bone healing course. After revision surgery (**D**), the patient underwent a clinically uneventful course and demonstrated full bone healing 6 months post-revision surgery (**E**).

4. Results

The monitoring focused on key parameters, including cadence, ground reaction forces (GRFs), and imbalance factors, to assess changes in the patient's gait pattern and its approximation to a healthy gait curve (Figure 2). The factor of imbalance initially spikes (near 100%) due to severe asymmetry in gait caused by the fracture and surgery. Over time, there is a gradual reduction, approaching near-normal levels (~10%) by week 12, indicating improved symmetry in weight distribution between the legs. Cadence (steps per minute) begins relatively low, around 30 steps per minute, and steadily increases throughout the recovery period, plateauing at approximately 60–65 steps per minute after week 8. This trend reflects an improved gait rhythm and increased confidence in walking. The ground reaction force on the right leg starts near zero, indicating minimal weight-bearing capacity. After initiating full-body weight-bearing at week 6, the ground reaction force significantly increases, exceeding 1000 N by week 12.

This trend suggests strengthening of the right leg and the restoration of load-bearing functionality. Over time, this imbalance gradually decreases, approaching near-normal levels of approximately 10% by week 12, indicating an improvement in weight distribution between the legs.

The shading of the curves in Figure 3 represents the magnitude of the ground reaction force, with darker shades indicating higher forces. The gradual darkening from earlier to later weeks highlights the progressive increase in weight-bearing capacity. In the first three weeks, the ground reaction force remains low and demonstrates a flattened curve, indicating a reduced ability to generate force during the stance phase of gait. In week 5, a more defined force curve emerges for the first time. This corresponds with increased

limb stability and improved muscle engagement during the stance. The distinct peak indicates the restoration of better load transfer through the leg during the stance phase. After week 5, development of the two required maxima during the stance phase becomes visible, indicating a typical sign of an increasing physiological gait pattern.

Figure 4 shows the difference in acceleration between the right and left sides during walking. On day 2 after revision surgery, this difference peaks at nearly 70 percent. The patient's initial attempts at walking led to this significant discrepancy. A fluid gait pattern with crutches is not yet achievable at this early stage. However, it is encouraging to note that the ratio between the two sides becomes increasingly similar as the healing progresses over time. By week nine, there was obvious further improvement. The patient walked without crutches for the first time, making him more cautious and slower when using the fractured leg than the uninjured leg. Notably, gait performance was worse before the revision operation than 12 weeks after the surgery. This suggests that at the time of the measurement taken four months after the first operation, the patient still experienced significant gait disturbances and dragging of the fractured leg, which in turn corresponded to the pain described by the patient before revision surgery. Treatment with an intramedullary nail considerably reduced these issues. The swing time of the right leg directly reflects this observation. The analysis of acceleration differences supports this finding. When examining the knee joint angle, flexion during the stance phase begins at 0 degrees and reaches only 10 degrees by the end of the fourth week. Pain-adapted walking during the first week eliminated the stance phase, preventing the initial maximum of the knee joint curve from appearing during each gait cycle.

A

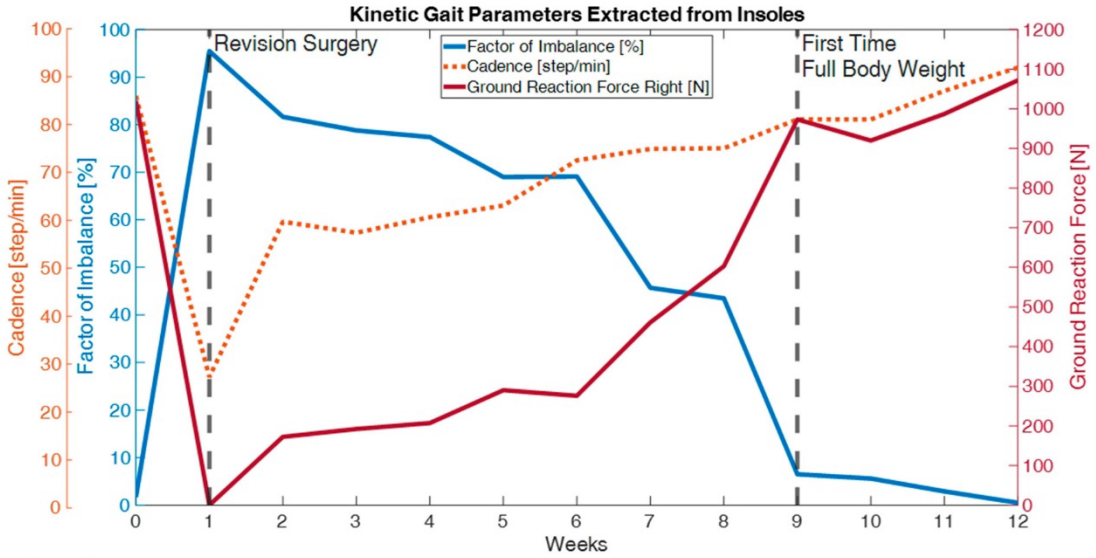

B

Week	Factor of Imbalance [%]	Cadence [step/min]	GRF right
0	1.7	86.1	1020
12	0.5	91.8	1072

Figure 2. Temporal evolution of kinetic parameters, including a factor of imbalance in percentage, cadence in steps per minute, and ground reaction force of the fractured right leg in Newtons, over a 12-week recovery period following revision surgery (**A**), and exact values for week 0 in grey and week 12 in white (**B**).

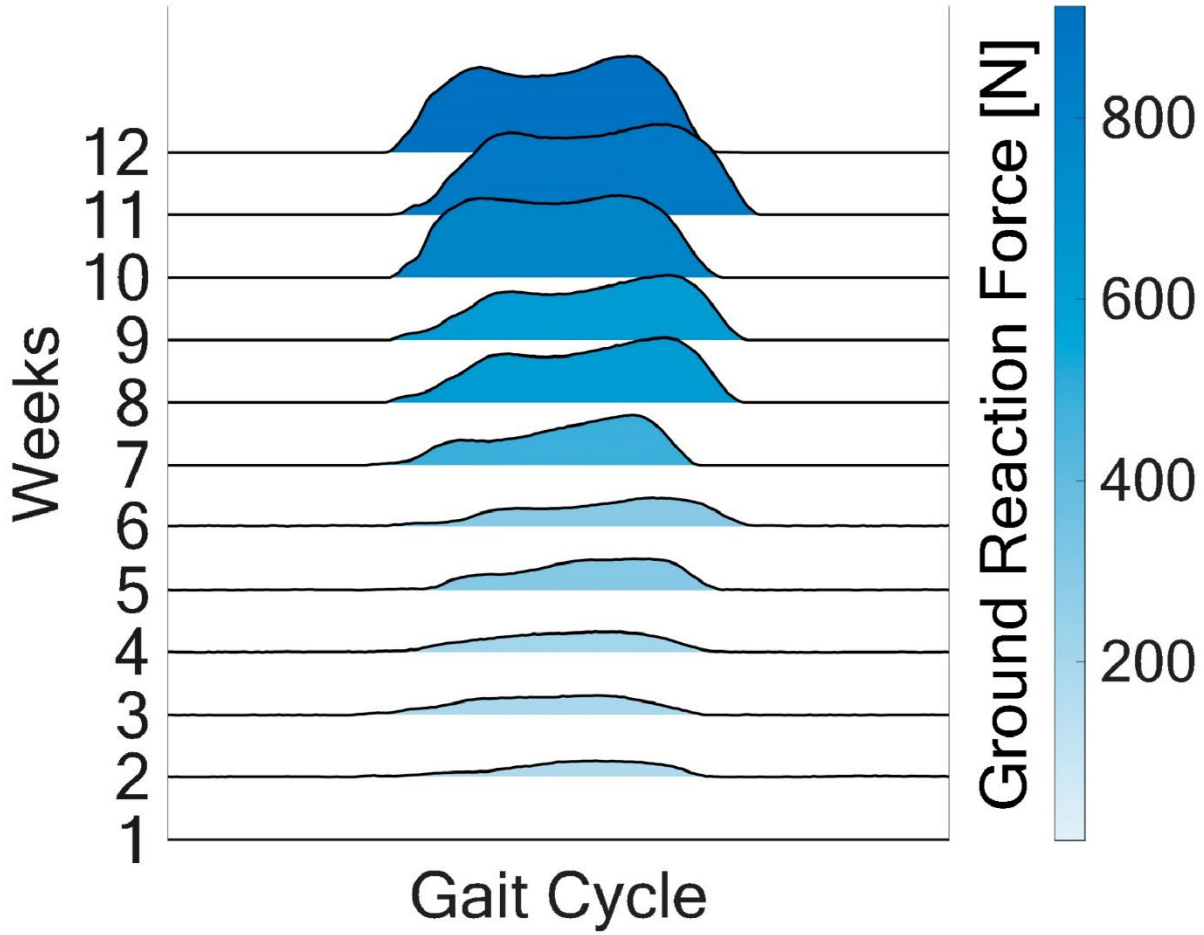

Figure 3. Illustration of the evolution of the ground reaction force in the right leg during a single gait cycle for the first seven weeks.

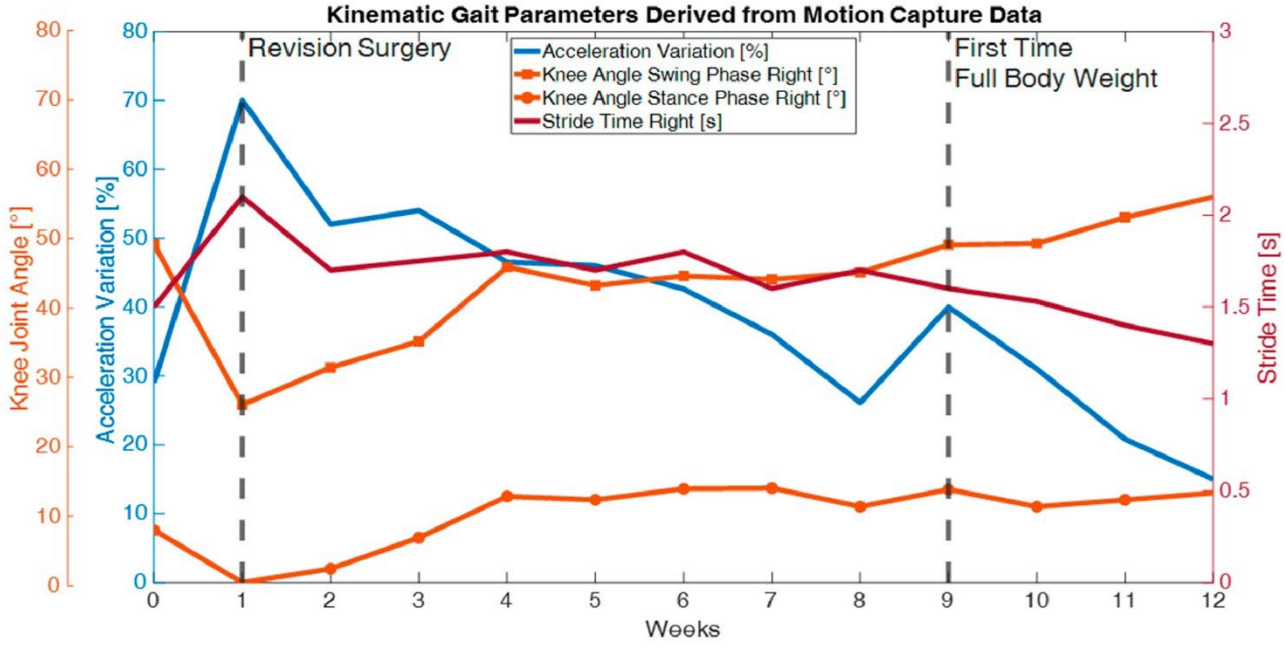

Figure 4. Temporal progression of kinematic parameters over a 12-week recovery period following a revision surgery.

5. Discussion

The data effectively captures a patient's recovery process after severe healing disturbances with implant failure requiring revision surgery in a young patient suffering from a lower leg fracture. Initial post-surgery asymmetry and reduced function gradually improved over time as seen in the temporal trends and gait cycle curves. There was noticeable asymmetry and reduced function initially, but these gradually improved over time as demonstrated by both the temporal trends and gait cycle curves. This corresponded to the clinical and radiological events in the medical follow-up visits.

Conventional rehabilitation monitoring relies on subjective clinical assessments and scheduled radiographic imaging, typically capturing information at fixed intervals—for instance, using X-rays to evaluate a tibial fracture at 6 weeks, 12 weeks, and 18 months. However, validation of X-ray analysis is insufficient until approximately 8 or 12 weeks after the operation, leaving a diagnostic window during which the acute healing status is not monitored. In contrast, integrating sensor insoles and inertial motion capture enables objective, continuous, and quantitative evaluation of patient mobility. Recent studies have demonstrated the efficacy of wearable inertial sensors in rehabilitation settings. For instance, a study focusing on Parkinson's disease patients utilized wearable sensors to identify early and subtle gait changes, which could serve as potential objective gait biomarkers for early diagnosis [20].

The study demonstrates for the first time several interesting parameters to monitor the course of bone healing. The primary goal is to use simple tools and parameters to accurately record changes in gait patterns during the healing process. The main advantage of the systems used is their independence from a special laboratory room. Both systems provide real-time feedback and function in both indoor and outdoor environments. Therefore, they offer great flexibility. This approach is supported by earlier work demonstrating that gait-related parameters, such as cadence and ground reaction forces (GRFs), are reliable indicators of musculoskeletal function and recovery [21,22]. The values obtained before the fractured leg reaches full weight-bearing status are particularly valuable. The factors of imbalance, ground reaction force, and acceleration variation, alone or in combination, may be helpful tools for monitoring the healing course using an additional, radiation-free tool. Therefore, they might be of interest in clinical practice and surgical aftercare. A large-scale study involving more subjects should validate the introduced parameters and establish precise reference values to identify a positive healing process or detect early signs of improper healing. Wearable technologies have already shown clinical utility in orthopedic rehabilitation and post-surgical monitoring [23–25]. Accordingly, the investigated parameters herein may be helpful additional parameters to evaluate the clinical course of events to estimate a healing disorder or—even more importantly—prevent the formation of a non-union and its accompanying high socio-economic burden [26–28]. We can simplify the setup by selecting specific parameters from the motion-capturing system. For instance, patients could sit on measuring insoles with one acceleration sensor on each thigh to monitor their movements. In the future, we anticipate a shift toward digital mobility outcomes, enabling patients to track their progress using data collected from mobile phones, smartwatches, and other digital devices. Ideally, they would also provide baseline measurements from before the fracture occurred. However, these initial results should serve as a foundational step in breaking down the healing process into its components, enabling precise monitoring of each patient. These systems provide instant feedback, which is essential for effective rehabilitation monitoring and compliance tracking. Unlike conventional methods, this approach operates independently of controlled environments, allowing for home-based and more real-time monitoring of continuous assessments. Additionally, this data analysis approach

is not limited to lower extremity fractures. It can also be applied to kinematic evaluations of upper extremities and fracture healing trends, broadening its clinical applications.

6. Limitations

Motion capture systems and sensor technologies provide valuable insights into patient recovery but also have limitations. Problems with accuracy and reliability can arise due to measurement errors, noise, or drift over time, which can impact data accuracy. During measurements, personnel trained to operate the system must be present to verify its correct functioning. This means that independent continuous measurement by patients is not yet possible. Another challenge is the cost and accessibility of these systems. The purchase of hardware, additional software, and license costs is often beyond the means of many healthcare providers, especially for smaller clinics or regions with limited financial resources. The hardware of the Xsens Awinda system is not particularly expensive. As with many other purchased solutions, the software license is costly. Nevertheless, the system as a whole is well below the cost of a camera-based motion-capturing system. One can make a similar comparison for the measuring soles. The cost of several pairs of soles (in different sizes, for example), including the software package, is within the price range of a standard force plate. Both systems have a long service life. We have been using both measuring systems for several years and for various types of measurements (gait analyses, gym measurements, open terrain measurements, etc.).

For long-term measurements involving multiple patients or general introduction into routine practice, the amount of data generated by motion capture and sensor-based systems necessitates the use of neural networks or artificial intelligence algorithms for efficient processing, interpretation, and analysis. Without automation, the workload increases, making real-time assessments impractical.

The findings are based on a single patient, restricting the generalizability of the results. Future studies should involve larger and more heterogeneous cohorts to validate the robustness of the observed parameters. The study observation period was limited to 12 weeks; extending follow-up to 6–12 months could yield additional insights into long-term rehabilitation trajectories. This study serves as a pilot and feasibility study to conduct a study with a larger cohort and validate the results.

7. Conclusions

The patient's kinetic and kinematic gait analysis reveals changes in biomechanical parameters during rehabilitation. During the first eight weeks of the partial weight-bearing phase, it is typical for the examined values to show greater asymmetry as the affected right side is still being spared. This asymmetry decreases with the transition to full weight-bearing from week 9 onwards, and normalization occurs more gradually over time. Adaptive compensation mechanisms can be observed during partial weight-bearing, which then decreases with the transition to full weight-bearing. Close observation of trends in the data can provide insight into whether the patient is adapting biomechanically to the increasing load or if there is deterioration, which would necessitate a change in rehabilitation measures. All in all, these are easy-to-use tools that do not require extensive prior knowledge and have a straightforward evaluation process, leading to quick findings.

Supplementary Materials: The following supporting information can be downloaded at https://www.mdpi.com/article/10.3390/s25133853/s25133853/s1: Figure S1: Moticon^{TM} sensor insole (A), distribution of pressure sensors and position of the coordinate system (B), and live display of pressure distribution while standing (C). Figure S2: Motion capturing system Xsens^{TM} setup (A), avatar in the Xsens^{TM} software (B), close-up of an IMU motion tracker (C), and a tracker with a strap (D). Figure S3: Comparison of the angles of the left and right knee joint during the measurements in week 2 and

week 9. Figure S4: Comparison of the angles of the left and right ground reaction force during the measurements in week 2 and week 9.

Author Contributions: Conceptualization, A.A.; methodology, A.A.; software, A.A.; validation, M.R. and M.O.; formal analysis, M.R.; investigation, A.A. and M.R.; resources, S.D.; data curation, A.A. and M.O.; writing—original draft preparation, A.A.; writing—review and editing, M.R., M.O. and S.D.; visualization, A.A.; supervision, S.D.; project administration, S.D. and M.R. All authors have read and agreed to the published version of the manuscript.

Funding: This research received no external funding.

Institutional Review Board Statement: The studies involving human participants were reviewed and approved; ethical approval was obtained from the IRB of Saarland Medical Board (Aerztekammer des Saarlandes, Germany, application number 30/21). Informed consent was obtained according to the Declaration of Helsinki. The study is part of Smart Implants 2.0—Weight-bearing and Gait Observation project for Early Monitoring of Fracture Healing and Individualized Therapy after Trauma, funded by the Werner Siemens Foundation. It is registered in the German Clinical Trials Register (DRKS-ID: DRKS00025108). The patients/participants provided their written informed consent to participate in this study. Written informed consent was obtained from the individual(s) to publish any potentially identifiable images or data in this article.

Informed Consent Statement: Informed consent was obtained from all subjects involved in the study.

Data Availability Statement: The original contributions presented in the study are included in the article; further inquiries can be directed to the corresponding author. Researchers who wish to request access to data should send an email indicating the research purpose. Every request must be reviewed by the responsible institutional review boards, considering the risk of patient reidentification and compliance with applicable data protection rules.

Conflicts of Interest: The authors declare no conflict of interest.

References

1. Prasanth, H.; Caban, M.; Keller, U.; Courtine, G.; Ijspeert, A.; Vallery, H.; von Zitzewitz, J. Weareble Sensor-Based Real-Time Gait Detection: A Systematic Review. *Sensors* **2021**, *21*, 2727. [CrossRef] [PubMed]
2. Warmerdam, E.; Orth, M.; Pohlemann, T.; Ganse, B. Gait Analysis to Monitor Fracture Healing of the Lower Leg. *Bioengineering* **2023**, *10*, 255. [CrossRef] [PubMed]
3. North, K.; Simpson, G.M.; Stuart, A.R.; Kubiak, E.N.; Petelenz, T.J.; Hitchcock, R.W.; Rothberg, D.L.; Cizik, A.M. Early postoperative step count and walking time have greater impact on lower limb fracture outcomes than load-bearing metrics. *Injury* **2023**, *54*, 110756. [CrossRef] [PubMed]
4. Pfeufer, D.; Becker, C.A.; Faust, L.; Keppler, A.M.; Stagg, M.; Kammerlander, C.; Böcker, W.; Neuerburg, C. Load-bearing detection with insole-force sensors provides new treatment insights in fragility fractures of the pelvis. *J. Clin. Med.* **2020**, *9*, 2551. [CrossRef]
5. Saathvik, A. Boompelli and Sambit Bhattacharya. Design of a telemetric gait analysis insole and 1-D convolutional neural network to track postoperative fracture rehabilitation. In Proceedings of the LifeTech 2021–2021 IEEE 3rd Global Conference on Life Sciences and Technologies, Kyoto, Japan, 9 March 2021; Institute of Electrical and Electronics Engineers Inc.: Piscataway, NJ, USA, 2021; pp. 484–488. [CrossRef]
6. Marmor, M.T.; Grimm, B.; Hanflik, A.M.; Richter, P.H.; Sivananthan, S.; Yarboro, S.R.; Braun, B.J. Use of Wearable Technology to Measure Activity in Orthopaedic Trauma Patients: A Systematic Review. *Indian J. Orthop.* **2022**, *56*, 1112–1122. [CrossRef]
7. Braun, B.J.; Veith, N.T.; Rollmann, M.; Orth, M.; Fritz, T.; Herath, S.C.; Holstein, J.H.; Pohlemann, T. Weight-bearing recommendations after operative fracture treatment—Fact or fiction? Gait results with and feasibility of a dynamic, continuous pedobarography insole. *Int. Orthop.* **2017**, *41*, 1507–1512. [CrossRef]
8. Braun, B.J.; Histing, T.; Herath, S.C.; Rollmann, M.F.R.; Reumann, M.; Menger, M.M.; Springer, F.; Andres, A.; Diebels, S.; Roland, M. Bewegungsanalyse und muskuloskeletale Simulation in der Pseudarthrosentherapie—Erfahrungen und erste klinische Ergebnisse. *Die Unfallchirurgie* **2022**, *125*, 619–627. [CrossRef]
9. Orth, M.; Ganse, B.; Andres, A.; Wickert, K.; Warmerdam, E.; Müller, M.; Diebels, S.; Roland, M.; Pohlemann, T. Simulation-based prediction of bone healing and treatment recommendations for lower leg fractures: Effects of motion, weight-bearing and fibular mechanics. *Front. Bioeng. Biotechnol.* **2023**, *11*, 7845. [CrossRef]

10. Warmerdam, E.; Wolff, C.; Orth, M.; Pohlemann, T.; Ganse, B. Long-term continuous instrumented insole-based gait analyses in daily life have advantages over longitudinal gait analyses in the lab to monitor healing of tibial fractures. *Front. Bioeng. Biotechnol.* **2024**, *12*, 1355254. [CrossRef]
11. Horenstein, R.E.; Goudeau, Y.R.; Lewis, C.L.; Shefelbine, S.J. Using magneto-inertial measurement units to pervasively measure hip joint motion during sports. *Sensors* **2020**, *20*, 4970. [CrossRef]
12. Horenstein, R.E.; Lewis, C.L.; Yan, S.; Halverstadt, A.; Shefelbine, S.J. Validation of magneto-inertial measuring units for measuring hip joint angles. *J. Biomech.* **2019**, *91*, 170–174. [CrossRef] [PubMed]
13. Ibrahim, N.I.; Ahmad, M.S.; Zulfarina, M.S.; Zaris, S.N.A.S.M.; Mohamed, I.N.; Mohamed, N.; Mokhtar, S.A.; Shuid, A.N. Activities of daily living and determinant factors among older adult subjects with lower body fracture after discharge from hospital: A prospective study. *Int. J. Environ. Res. Public Health* **2018**, *15*, 1002. [CrossRef] [PubMed]
14. Bovi, G.; Rabuffetti, M.; Mazzoleni, P.; Ferrarin, M. A multiple-task gait analysis approach: Kinematic, kinetic and EMG reference data for healthy young and adult subjects. *Gait Posture* **2011**, *33*, 6–13. [CrossRef] [PubMed]
15. Lauenroth, A.; Laudner, K.; Schulze, S.; Delank, K.S.; Fieseler, G.; Schwesig, R. Laufbandbasierte Gangreferenzdaten für gesunde Probanden: Abhängigkeit von funktionellen und morphologischen Parametern. *Man. Med.* **2018**, *56*, 182–187. [CrossRef]
16. Marimon, X.; Mengual, I.; López-de-Celis, C.; Portela, A.; Rodríguez-Sanz, J.; Herráez, I.A.; Pérez-Bellmunt, A. Kinematic Analysis of Human Gait in Healthy Young Adults Using IMU Sensors: Exploring Relevant Machine Learning Features for Clinical Applications. *Bioengineering* **2024**, *11*, 105. [CrossRef]
17. Medved, V.; Vastola, R.; Albano, D.; Pećina, M. Gait Analysis. In *Measurement and Analysis of Human Locomotion*; Springer International Publishing: Cham, Switzerland, 2022; pp. 219–255.
18. Hoffmann, T.; Falz, R.; Busse, M. Winkelveränderungen verschiedener Gelenke der unteren Extremitäten bei unterschiedlichen Geschwindigkeiten und Neigungswinkeln. *Klin. Sport. Sport. Med.* **2014**, *15*, 7–11.
19. Newman, S.D.S.; Mauffrey, C.P.C.; Krikler, S. Distal metadiaphyseal tibial fractures. *Injury* **2011**, *42*, 975–984. [CrossRef]
20. Zhang, W.; Ling, Y.; Chen, Z.; Ren, K.; Chen, S.; Huang, P.; Tan, Y. Wearable sensor-based quantitative gait analysis in Parkinson's disease patients with different motor subtypes. *npj Digit. Med.* **2024**, *7*, 169. [CrossRef]
21. Kaufman, K.R.; Hughes, C.; Morrey, B.F.; Morrey, M.; An, K.N. Gait characteristics of patients with knee osteoarthritis. *J. Biomech.* **2001**, *34*, 907–915. [CrossRef]
22. Perry, J.; Burnfield, J. *Gait Analysis: Normal and Pathological Function*; Slack Inc.: Thorofare, NJ, USA, 2010; pp. 85–534.
23. Amin, T.; Mobbs, R.J.; Mostafa, N.; Sy, L.W.; Choy, W.J. Wearable devices for patient monitoring in the early postoperative period: A literature review. *mHealth* **2021**, *7*, 50. [CrossRef]
24. Kobsar, D.; Masood, Z.; Khan, H.; Khalil, N.; Kiwan, M.Y.; Ridd, S.; Tobis, M. Wearable inertial sensors for gait analysis in adults with osteoarthritis—A scoping review. *Sensors* **2020**, *20*, 7143. [CrossRef] [PubMed]
25. Muro-de-la-Herran, A.; García-Zapirain, B.; Méndez-Zorrilla, A. Gait analysis methods: An overview of wearable and non-wearable systems, highlighting clinical applications. *Sensors* **2014**, *14*, 3362–3394. [CrossRef] [PubMed]
26. Antonova, E.; Le, T.K.; Burge, R.; Mershon, J. Tibia shaft fractures: Costly burden of nonunions. *BMC Musculoskelet. Disord.* **2013**, *14*, 42. [CrossRef] [PubMed]
27. Court-Brown, C.M.; Caesar, B. Epidemiology of adult fractures: A review. *Injury* **2006**, *37*, 691–697. [CrossRef]
28. Rupp, M.; Biehl, C.; Budak, M.; Thormann, U.; Heiss, C.; Alt, V. Diaphyseal long bone nonunions—Types, aetiology, economics, and treatment recommendations. *Int. Orthop.* **2018**, *42*, 247–258. [CrossRef]

16 Paper C

Title:

Advantages of digital twin technology in orthopedic trauma Surgery–Exploring different clinical use cases

Authors:

Annchristin Andres, Michael Roland, Kerstin Wickert, Stefan Diebels, Johannes Stöckl, Stefan Herrmann, Frank Reinauer, Leibinger Ralf, Atanas Pavlov, Lutz Schuppener, Daniel Schäfer, Tina Histing & Benedikt Johannes Braun

Original Publication:

Andres, A., Roland, M., Wickert, K., Diebels, S., Stöckl, J., Herrmann, S., Reinauer, F., Leibinger, R., Pavlov, A., Schuppener, L., Schäfer, D., Histing, T. & Braun, B. J. (2025). Advantages of digital twin technology in orthopedic trauma Surgery–Exploring different clinical use cases. *Scientific Reports*, *15*(1), 1-13. https://doi.org/10.1038/s41598-025-04792-w

scientific reports

Check for updates

OPEN

Advantages of digital twin technology in orthopedic trauma Surgery – Exploring different clinical use cases

Annchristin Andres[1]✉, Michael Roland[1], Kerstin Wickert[1], Stefan Diebels[1], Johannes Stöckl[2], Stefan Herrmann[2], Frank Reinauer[3], Ralf Leibinger[3], Atanas Pavlov[4], Lutz Schuppener[4], Daniel Schäfer[5], Tina Histing[5] & Benedikt J. Braun[5]

Digital twin technology offers significant benefits for addressing fracture non-unions in orthopedic trauma surgery, particularly in cases requiring revision surgery. In this study, we developed a clinically applicable digital twin workflow that integrates patient-specific imaging, motion capture, musculoskeletal modeling, and finite element simulation. We applied this workflow to five real patient cases involving different anatomical sites and treatment strategies, including implant modification, augmentative fixation, and corrective osteotomy. Each case was virtually reconstructed to evaluate mechanical conditions before and after revision surgery. The results demonstrated that digital twins can predict improvements in implant stress distribution and fracture strain states, offering valuable insights for optimizing surgical decisions. This work highlights the feasibility of digital twins and their clinical value in supporting individualized revision strategies, laying the foundation for their broader use in trauma care. .

Keywords Digital twin, Virtual reconstruction, Patient-specific model generation, Individualized Biomechanical simulation, Fracture healing, Non-unions, Surgical treatment.

Since its first appearance in 2003[1], digital twin (DT) technology has rapidly evolved as a field in medicine, enabling significant advances by transferring established concepts from engineering science and industry into clinical practice[2]. By generating virtual models that mirror the underlying physical entities, DTs currently enable the simulation of patient-specific issues within pre-defined application-related frameworks, thereby predicting health outcomes and enhancing diagnosis, treatment, and preventive care.

This wide spectrum encompasses diverse applications across several medical fields. In general healthcare and personalized medicine, DTs have been used in geriatric medicine[3], to identify optimal drug treatments[4], and for public health management[5,6]. DTs are also applied to cancer care[7], oncology workflows[8,9], and in radiology[10]. Additionally, DTs are used for investigating vertebrae and vertebroplasty procedures in cancer patients[11,12], for predicting the electrical field in cell culture experiments with human osteoblasts[13], and for osteoporosis research, particularly in the context of denosumab therapy[14,15].

Surgical planning applications have also emerged, particularly in oral and maxillofacial surgery. These include mandibular reconstruction using computer-aided design and computer-aided manufacturing (CAD/CAM) techniques alongside fibula flaps to create patient-specific reconstruction plates[16], or to prevent biologically inadequate reconstructions that lead to functional and aesthetic impairments[17], as well as cranial defect reconstructions with tailored resorbable implants[18]. DTs are also used in orthodontics, for example, in implant placement[19] and for simulating the human mandible after joint replacement[20,21]. Despite all progress, DTs are still underrepresented in orthopedic trauma surgery.

A PubMed search at the end of 2024 combining ("digital twin" OR "virtual twin") AND "fracture" AND ("tibia" OR "femur" OR "bone") yielded fewer than 20 articles, several of which were unrelated to medicine. This also included review articles and a viewpoint addressing arthroscopic knee surgery[22], virtual reality in bone

[1]Saarland University, Applied Mechanics, Saarbrücken, Germany. [2]csi entwicklungstechnik GmbH, Neckarsulm, Germany. [3]KLS Martin SE & Co. KG, Tuttlingen, Germany. [4]IL Innovationslabor GmbH, Berlin, Germany. [5]Faculty of Medicine, University Hospital Tuebingen on Behalf of the Eberhard-Karls- University Tuebingen, BG Hospital Tuebingen, Tuebingen, Germany. ✉email: annchristin.andres@uni-saarland.de

trauma procedures[23], digital technologies in orthopedics, with a focus on bone fracture[24], and the potential of integrating digital technologies into computer-assisted surgery[25].

Today, DTs in orthopedic trauma surgery are primarily based on 3D models of patient anatomy derived from clinical imaging to generate workflows for decision support, individualized product development, and scientific research.

The closest related work to this study is that of Aubert et al. (2021)[26], which presented a DT approach to optimize trauma surgery and postoperative management in tibial plateau fractures. While their study was a significant step forward in demonstrating the value of simulation for treatment planning, it focused on a narrow anatomical region, did not incorporate real patient-specific motion capture data, and offered limited integration into clinical surgical workflows. This study expands upon this by applying DTs across multiple anatomical sites and revision strategies, incorporating dynamic musculoskeletal simulations and real-world clinical imaging, and aiming for a more holistic decision-support system tailored for orthopedic trauma care.

If the literature search were extended to include terms such as "simulation" OR "finite element analysis" instead of DT, many more studies and articles would be found. Here, the review by Ghiasi and colleagues[27] provides a good first overview.

Although personalization and individualization of therapy through DTs are among the most promising trends in digital healthcare, there is still no consensus on standardizing or designing such systems for clinical use[28]. Human DTs are often loosely defined as "computer models of humans tailored to any patient," without specifying the necessary clinical, mechanical, or biological fidelity[29]. In orthopedic trauma, these challenges are compounded by the complexity of bone healing mechanics, variability in patient anatomy, and the practical limitations of clinical imaging. As Killen et al.[30] highlight, even well-established musculoskeletal modeling tools remain underutilized in practice due to barriers such as integration at the point of care, the need for specialized expertise, and limited clinical familiarity with simulation-based planning. Our work addresses some of these challenges by proposing a structured, patient-specific DT pipeline and demonstrating its feasibility in realistic clinical scenarios.

The goal of this study was to enhance treatment planning for non-union patients by utilizing a digital twin-based process chain. This approach integrates individualized computational models with patient-specific motion capture and clinical imaging data to create a data-driven DT. The resulting twin captures physical, biological, and treatment history data, enabling more informed and reliable surgical decision-making for revision procedures. The aim is to demonstrate how DTs can be utilized specifically in evaluating potential revision strategies and how they could provide decision support in the future.

Fracture revisions present a particularly complex problem for DT applications due to a combination of biological variability, incomplete healing histories, altered implant environments, and the often uncertain mechanical integrity of previous treatments. Unlike primary fractures, revision surgeries must address failed healing and suboptimal loading conditions, often without access to the original surgical data or implant CAD models. Furthermore, there is limited guidance on how to integrate patient-specific motion data, simulate realistic mechanical environments, or evaluate multiple revision strategies in silico. In this context, our work aims to develop and demonstrate a clinically oriented DT workflow capable of reconstructing both initial and revised treatment scenarios using real patient data, musculoskeletal modeling, and finite element analysis. By doing so, we seek to provide a reproducible, biomechanically validated framework for decision support in orthopedic fracture revision surgery. This study represents a step toward realizing predictive, patient-specific DT for preoperative planning in complex trauma care.

Results

Five cases were virtually processed using DT technology to evaluate different treatment strategies and loading scenarios, focusing on mechanical fracture healing conditions. The following sections present the main results, and the supplementary material provides more detailed information about the patients and the monitoring process. The primary objective in every case was to recreate the initial treatment situation based on current computed tomography (CT) data, analyzing the treatment's mechanical stability and the fracture's strain state. The revision strategy was then virtually modeled and, analogous to the initial treatment, mechanically analyzed and evaluated regarding improving healing chances.

Use case 1 - Variation of the thickness of an intramedullary nail

Non-union of the tibial shaft occurs when a fracture fails to heal properly. One treatment strategy involves changing the nail size to stabilize the bone, as shown in Fig. 1. Here, the surgeon replaced an 8 mm nail (initial treatment) with an 11 mm nail (current treatment) after reaming, which removes bone material to accommodate the larger nail. The treatment plan recommended pain-adapted, full weight-bearing without restrictions to promote healing. In the DT for this use case, the diameter of the original nail was virtually modified without altering its position. Biomechanical analysis revealed a significant reduction in implant von Mises stress, exceeding 50%, achieved by simply thickening the nail by 3 mm in diameter. This modification alleviated the fracture and highlighted the importance of structural changes in optimizing mechanical outcomes. The improvement was evident from the healing window, where the initial treatment had 7% of the volume of the fracture in the range of too much movement.

Use case 2 – Augmentative plate for a humeral fracture

Surgeons have proposed augmentative plating as an alternative to nailing, nail removal, and plate revision. In the following use cases, 2 and 3, the fractures were stabilized using an additional plate, improving the fracture situation. This technique is effective for non-union revision surgeries in both the lower and upper extremities.

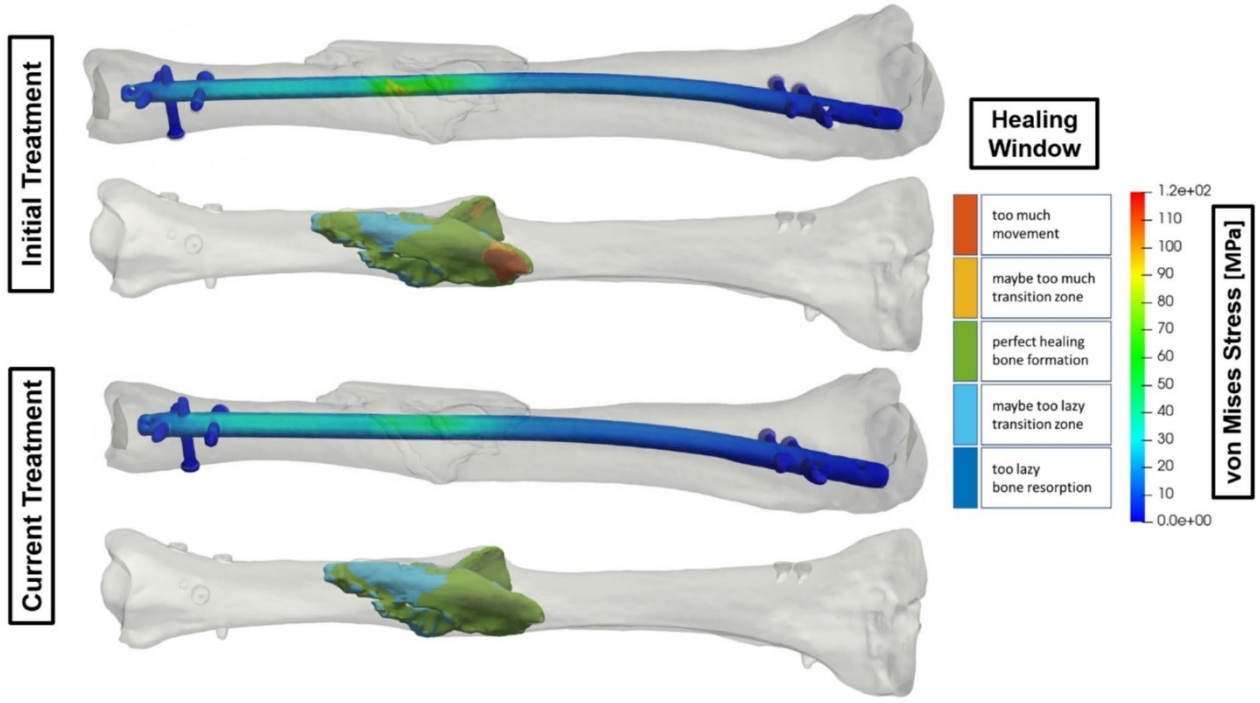

Fig. 1. Comparison of the strain state-based healing window in the fracture and the von Mises stress distribution for a diameter change of an intramedullary nail.

The results show a significant reduction in the von Mises stress in the central area of the implant examined using an augmentative plate combined with an intramedullary nail for a right humeral fracture (Fig. 2). In the initial treatment, the maximum von Mises stress of the implant reached 240 MPa, indicating a high mechanical loading. However, adding the augmentative plate reduced the stress maximum to 78 MPa, marking a significant improvement. This reduction by a factor of approximately 3 enhances the material's structural integrity and demonstrates the effectiveness of the treatment in reducing stress concentrations and improving mechanical performance. We used standard titanium alloy implants, which have an ultimate tensile strength slightly above the 860 to 925 MPa range, to obtain approval (e.g., DIN EN ISO 5832-3).

The 240 MPa, representing roughly 25% of the maximum load, explains why the implant remained intact, although prolonged loading could lead to fatigue and failure. While standard titanium alloys (e.g., Ti-6 Al-4 V) may have ultimate strengths above 860 MPa, their yield strengths often range between 240 and 550 MPa, depending on alloy and heat treatment, making the observed stress level clinically relevant. Therefore, the 78 MPa achieved in the new treatment is the better option. This also aligns with the healing window, reducing the elements in the range of too much movement to 0%.

Use case 3 – Augmentative plate for a femoral fracture

Figure 3 shows an augmentative plate for a femur fracture treated with an intramedullary nail. In the initial treatment, the von Mises stress maximum of 160 MPa on the nail is located at the center of the fracture, leading to instability and excessive fragment movement. Adding the augmentative plate significantly decreased the stress maximum to 30 MPa. The DT process chain includes virtually removing the additive plate and screws to recreate the original situation, address the instability from the initial treatment, and explore ways to improve the mechanical conditions for fracture healing. The current treatment, which incorporates a reinforcing plate, adds substantial strength and effectively reduces stress. As a result, fracture fragment movement reduces to the bone healing window without entering the transitional zone of bone resorption.

Use case 4 – Additional screw for a tibia fracture

Integrating additional screws, so-called strain reduction screws, in tibia fractures treated with intramedullary nails offers a refined approach to fracture management, as shown in Fig. 4. By enhancing the primary stabilization provided by the intramedullary nail, the supplementary screw improves the overall construct stability and provides targeted reinforcement at critical fracture sites. This strategy addresses various fracture patterns and patient-specific biomechanics, thereby contributing to faster healing and reduced complications. The torsion correction achieved by the additional screw increases the percentage of elements in the optimal healing window from 78 to 86%.

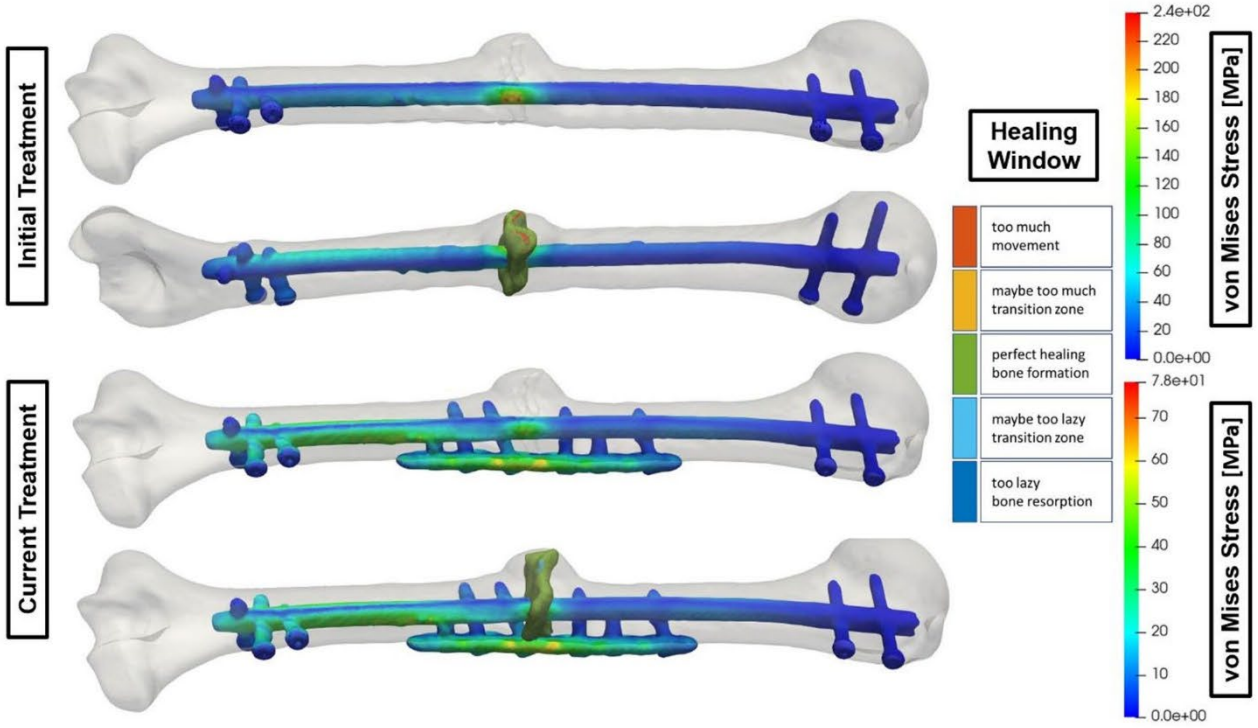

Fig. 2. Comparison of the fracture's strain state-based healing window and the treatment's von Mises stress distribution with and without an adaptive humerus plate.

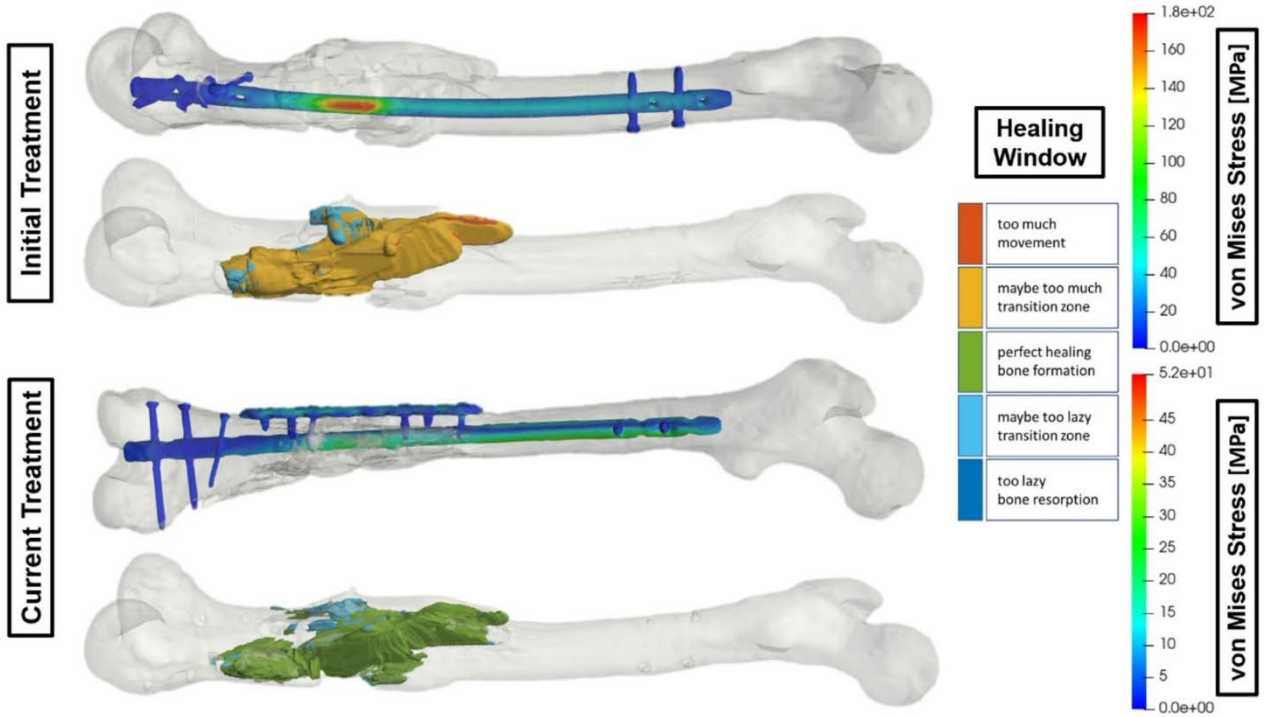

Fig. 3. Comparison of the strain state-based healing window of the fracture and the von Mises stress distribution of the treatment with and without an adaptive femur plate.

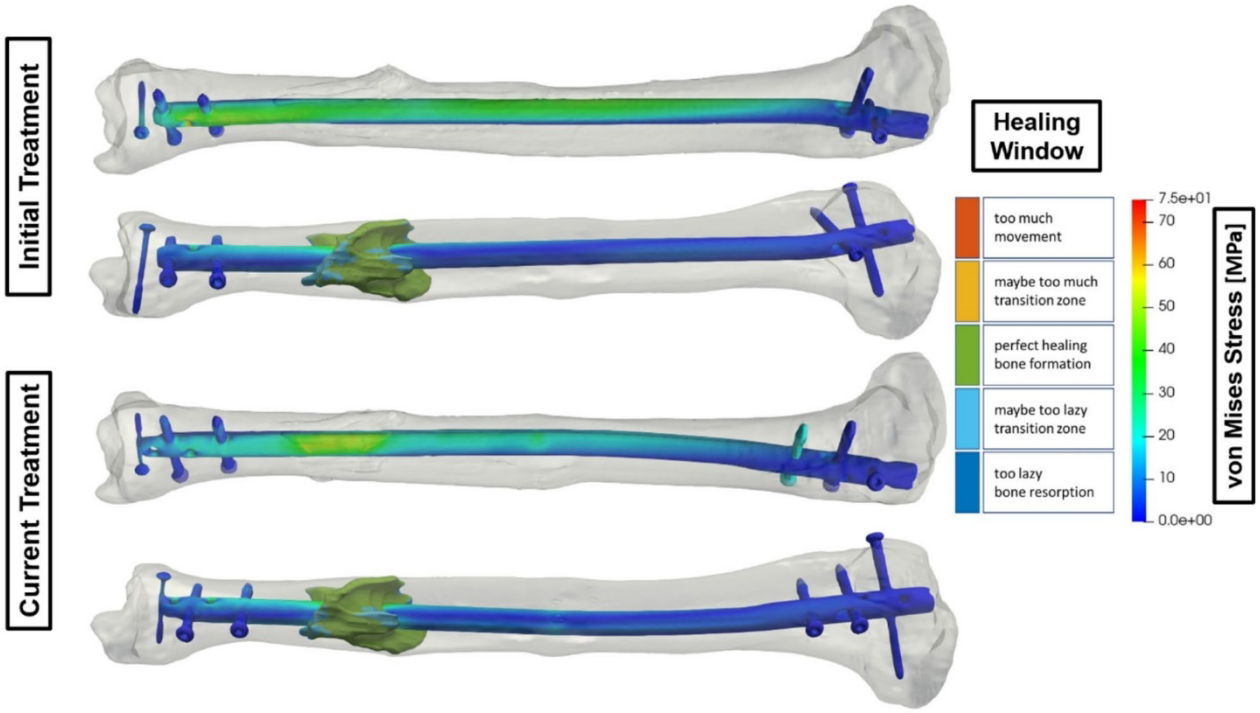

Fig. 4. Comparison of the strain state-based healing window of the fracture and the von Mises stress distribution of the treatment with and without an additional screw.

Use case 5 – Wrist movement after implant individualization

Use Case 5 represents a corrective osteotomy rather than a classical non-union case. In this scenario, the patient exhibited a malaligned wrist following prior treatment, impairing joint kinematics. The DT simulated pre- and postoperative wrist motion, aiding in the realignment strategy to restore normal biomechanics. Before the intervention, clinicians assessed the patient's range of motion using the described motion-capturing process. This preoperative analysis revealed restricted radial and ulnar deviation angles compared to the clinically established target ranges of 20–30 degrees for radial deviation and 30–40 degrees for ulnar deviation. The calculation determined the deviation angles as the angle between the anatomical axis of the radius and the vector representing the combined motion of the proximal carpal unit, defined as a rigid body including the scaphoid, lunate, and triquetrum. The virtual representation consisted of deformable and rigid components to simulate these conditions. The model treated the radius, ulna, and implant as deformable, while representing the scaphoid, lunate, and triquetrum as a single rigid unit.

Preoperatively, malalignment between the radius and ulna hindered attempts to achieve 40 degrees of ulnar deviation. This misalignment resulted in direct contact, seen in Fig. 5, between the carpal unit and the radius at higher deviation angles, thereby limiting the joint's functional range and preventing full rotational movement. Following the reconstructive surgery shown in Fig. 6, the realignment of the radius and optimization of implant positioning enabled the patient's wrist to move without impingement throughout the specified range. The procedure resulted in no structural interference when the wrist was positioned at 0 degrees. More importantly, when attempting 40 degrees of ulnar deviation, the configuration allowed full movement without any contact between the carpal bones and the ulna, indicating that the corrective measures had successfully restored normal joint mechanics. This outcome highlights the effectiveness of surgical intervention in improving joint mobility and restoring the functional range of motion in the patient's wrist. A process that can be largely tested and visualized in advance using DT technology.

Discussion

Integrating DT concepts into treatment strategies enables a dynamic and evolving representation of the patient's bone-implant system. The DT evolves in tandem with the patient's condition and treatment progress, continuously incorporating clinical imaging data, patient metadata, and biomechanical simulations. Mechanical simulations embedded within this DT framework offer a range of benefits, particularly in analyzing the micro-mechanics of fracture gaps and the associated healing process. They enhance our understanding of fracture mechanics, enabling researchers and clinicians to examine complex interactions between patient-specific anatomy, implants, and rehabilitation protocols with unprecedented detail. This holistic, data-driven approach enhances the accuracy of healing predictions and supports tailoring treatment strategies to individual patient needs. In this study, we analyzed five distinct clinical cases using DT technology to show different strategies for non-union treatment. Each case demonstrated a clear biomechanical benefit from the simulated intervention, ranging

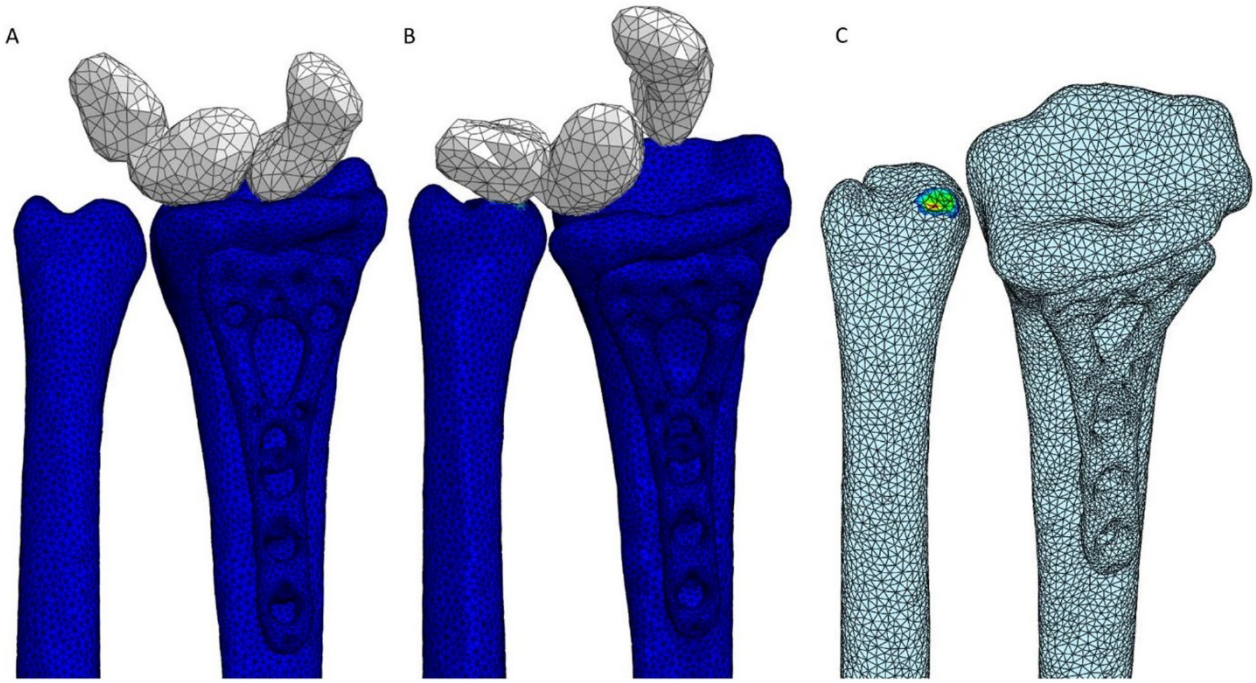

Fig. 5. Preoperative case, A: 0-degree ulnar deviation, B: 40-degree ulnar deviation, C: contact during the 40-degree ulnar deviation with fade-out rigid body part for better visualization.

from stress reduction in implants (Cases 2–3), improved strain states in fractures (Cases 1, 4), to functional restoration of joint mobility (Case 5). These results underscore the adaptability of DTs to individual treatment challenges and patient-specific variations. For instance, while nail diameter optimization in tibial fractures (Case 1) improved load transfer, the augmentative plating techniques (Cases 2–3) enhanced construct stability, and screw augmentation (Case 4) contributed to refined strain control. Notably, wrist mobility improvement in Case 5 exemplifies how DTs can simulate functional outcomes preoperatively.

Similarities across cases include the ability to evaluate mechanical performance under real patient-specific boundary conditions. Differences arise from anatomical locations, implant configurations, and motion dynamics. Our approach contrasts with Aubert et al.[26], which focused primarily on tibial plateau fractures and early-stage DT concepts; in contrast, our work applies a mature DT pipeline incorporating musculoskeletal dynamics and postoperative motion analysis.

While the first three cases demonstrate improvements in mechanical stability through implant reinforcement, such as increasing nail diameter or adding plates, these choices, though mechanically beneficial, may not universally translate into better clinical outcomes. Clinically, increased implant stiffness can lead to stress shielding, delayed healing, or unnecessary surgical burden. Therefore, stress reduction alone is insufficient for optimal treatment selection.

Within the DT environment, clinicians can efficiently test various implant configurations and rehabilitation scenarios, making informed decisions for specific fracture types and patient profiles in a safe and controlled environment. The ability to rapidly run these simulations reduces costs, improves turnaround time, and enhances the personalization of care, making DT-based simulations a compelling option for advancing orthopedic trauma surgery treatments. By modeling the fracture gap and simulating the biomechanical environment over time, DTs facilitate a more accurate estimation of the healing window. This helps guide interventions such as adjusting nail diameters, modifying plate constructs, or adding screws to improve stability, actions that can be informed by real-time feedback and continuous patient data integration. Similarly, by incorporating patient-specific movement data and boundary conditions, DTs shed light on the interaction between implants and native bone structure, helping determine when to intervene, how to optimize stress and strain distribution, and how to minimize complications. The adaptability of the DT to evolving clinical states underscores its potential to accurately represent the patient's biomechanical and biological milieu. A promising future application of DT lies in in silico clinical trials, where simulations may supplement traditional clinical data and, in select scenarios, help reduce reliance on early-stage human trials, particularly in rare or high-risk conditions[7]. DT of real patients can be used to create multiple problem-specific cohorts customized to address specific medical conditions, some of which may be impossible or unethical to replicate in physical clinical trials. Consequently, conditions that remain untestable in the physical world can now be explored virtually. In the context of osteosynthesis devices (e.g., plates and screws) utilized in orthopedic trauma surgery, in silico trials with DT present a valuable opportunity for the development of novel, innovative products for specialized applications. Because these specialized products serve small patient populations and have low production volumes, the high costs of regulatory certification often

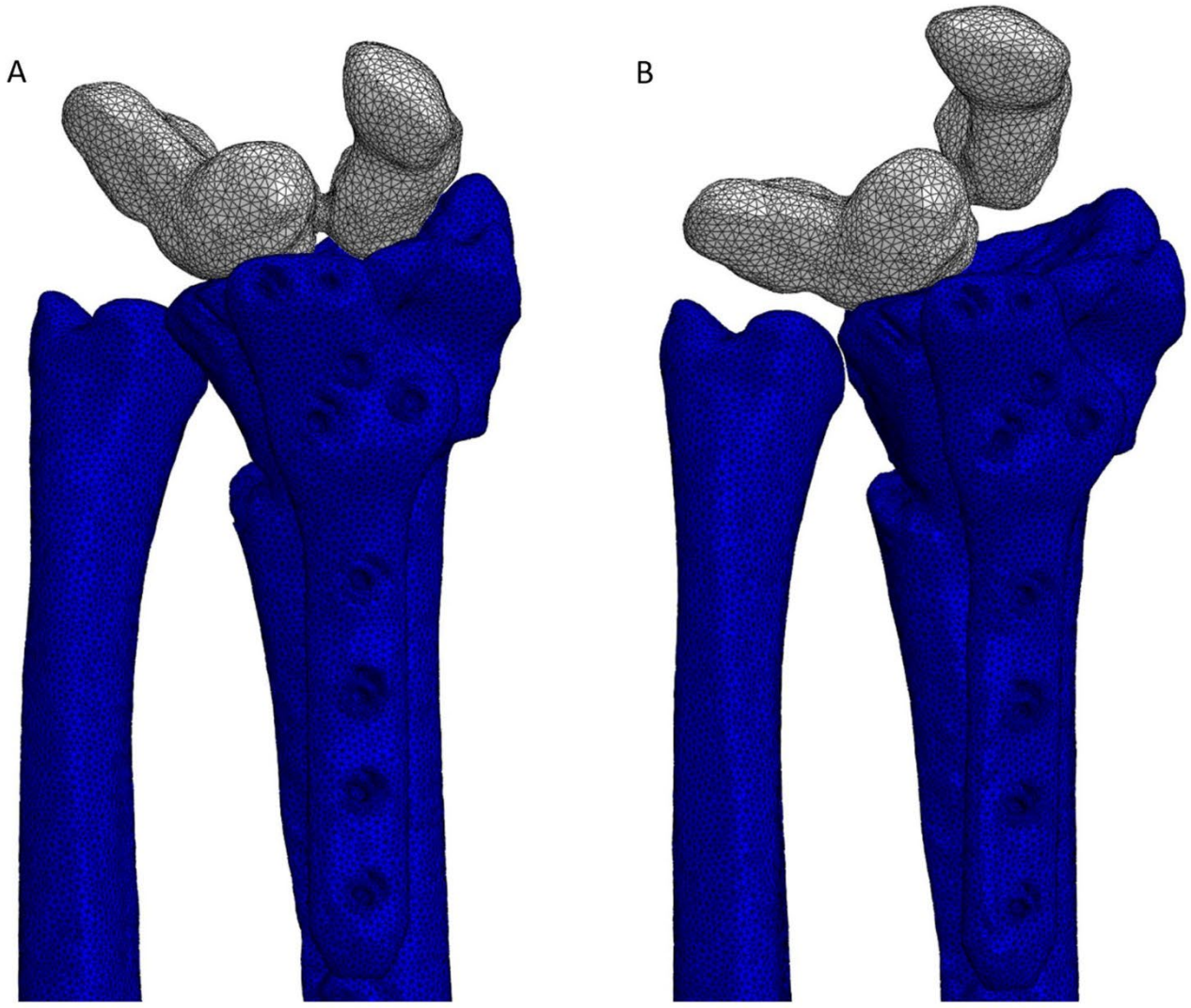

Fig. 6. Postoperative case, A: 0-degree ulnar deviation, B: 40-degree ulnar deviation.

make them commercially unfeasible. By leveraging DT for in silico trials, manufacturers can gather robust data on safety and efficacy without the high financial barriers associated with traditional clinical testing.

Despite the advantages offered by DTs, certain limitations persist. One key constraint is the reliance on manual segmentation processes due to the unavailability of original CAD data for implants in the scientific community. While segmented implant models can be derived from image data, the lack of direct CAD geometries hinders the precision and fidelity of implant representation. CAD-based models offer higher geometric accuracy, streamline simulations, and reduce manual modeling efforts.

Furthermore, the standard imaging protocols currently employed present several challenges. Calibration phantoms, which could ensure more reliable mapping of bone material properties, are not routinely used. As a result, bone properties must often be calibrated indirectly, which can potentially reduce the accuracy of subsequent simulations. In addition, CT scans, usually the imaging modality of choice, may have suboptimal quality and only capture the medically relevant segment of the extremity. This incomplete coverage frequently necessitates manual post-processing and extrapolation beyond the scanned region. Moreover, due to concerns about radiation exposure, the number of CT scans per patient is understandably limited. This benefits patients and their well-being, but it makes it difficult to evaluate simulations at different time points during the healing process. Continuous, longitudinal monitoring over several months to capture the healing process at fixed intervals requires multiple motion-capturing appointments, making it costly and time-consuming. These imaging and data availability constraints reduce the granularity and consistency of a DT, ultimately limiting its capacity to capture the complete patient-specific healing trajectory. A critical limitation of this approach, inherent to all patient-specific simulation-based analyses in orthopedics, is the lack of direct in vivo validation for stress and strain predictions. Unlike standard engineering applications, there is no practical or ethical way to measure internal mechanical states (e.g., interfragmentary strain, implant stresses) in live patients. As such, model predictions rely on boundary conditions derived from motion capture and musculoskeletal simulations,

which are themselves estimations. Although these simulations provide clinically useful insights, they must not be interpreted as absolute truths. Instead, they should be decision-support tools that assist, but never replace, experienced surgical judgment. We therefore recommend that all results from DT-based simulations be viewed with appropriate skepticism and always considered in conjunction with clinical findings and expert interpretation. In the paper by Wickert et al.[31] from our working group, we address the validation and verification of our simulations. Furthermore, we follow the concepts of what makes a good simulation published by Augat et al.[32,33]. Regarding a comparison with the clinical outcome, all five patients are fully healed after their revision surgery and have regained their full freedom of movement. The last follow-up appointments took place in 2022 for use case 2, in 2023 for use cases 1 and 3, and in 2024 for use cases 4 and 5.

The introduction of DTs in patient care, combined with mechanical simulations and precise biomechanical measurements, offers a patient-centric and data-rich paradigm that significantly enhances treatment outcomes. By analyzing the fracture gap in relation to the healing window through the DT, healthcare professionals gain insights that inform treatment decisions, facilitate patient involvement, and promote optimal healing trajectories. The DT's ability to simulate individual movement and patient-specific boundary conditions reinforces its role in refining surgical strategies and rehabilitation protocols. By enabling clinicians to explore various implant scenarios and track patient progress continuously pre-emptively, the DT paradigm exemplifies a synergistic relationship between cutting-edge computational tools, patient-specific modeling, and evidence-based medical care. This integrated approach improves the quality and efficiency of patient-centered interventions.

Future applications of DTs should integrate additional decision metrics, including bone-implant stiffness mismatch, expected surgical invasiveness, risk of soft tissue disruption, healing biology, and long-term implant performance. These factors could be modeled through extensions to the current framework, such as bone remodeling predictions, patient-specific healing simulations, or surgical time estimators. Ultimately, DTs are best viewed as multi-factorial planning tools that simulate what is mechanically optimal and what is surgically appropriate for the individual patient. Longitudinal DTs could also inform rehabilitation strategies and support in silico clinical trials to complement traditional studies, particularly for rare or complex orthopedic conditions.

Methods

The DT concept presented in this study builds upon an innovative digital process chain[34–36] developed and implemented by the authors and colleagues in the clinical environment at a level 1 trauma center in Germany. This concept incorporates elements from multiple levels of DT maturity, as illustrated in Fig. 7.

The DT concept used in this study integrates multiple maturity levels as defined in Fig. 7. Specifically, "Level 1 – Virtual Twin" is realized through patient-specific imaging, metadata, and CAD-based 3D models. "Level 2 – Connected Twin" is achieved by linking these models with patient-specific motion data from the musculoskeletal system. Additionally, the workflow incorporates aspects of a "Level 3 – Predictive Twin" by enabling semi-automated analysis of simulation outputs to support clinical decision-making. Future developments aim to advance toward Level 4 (Prescriptive Twin) by providing tailored real-time recommendations for patients during rehabilitation phases, and toward Level 5 (Autonomous Twin) by integrating artificial intelligence into the DT for continuous, adaptive treatment optimization.

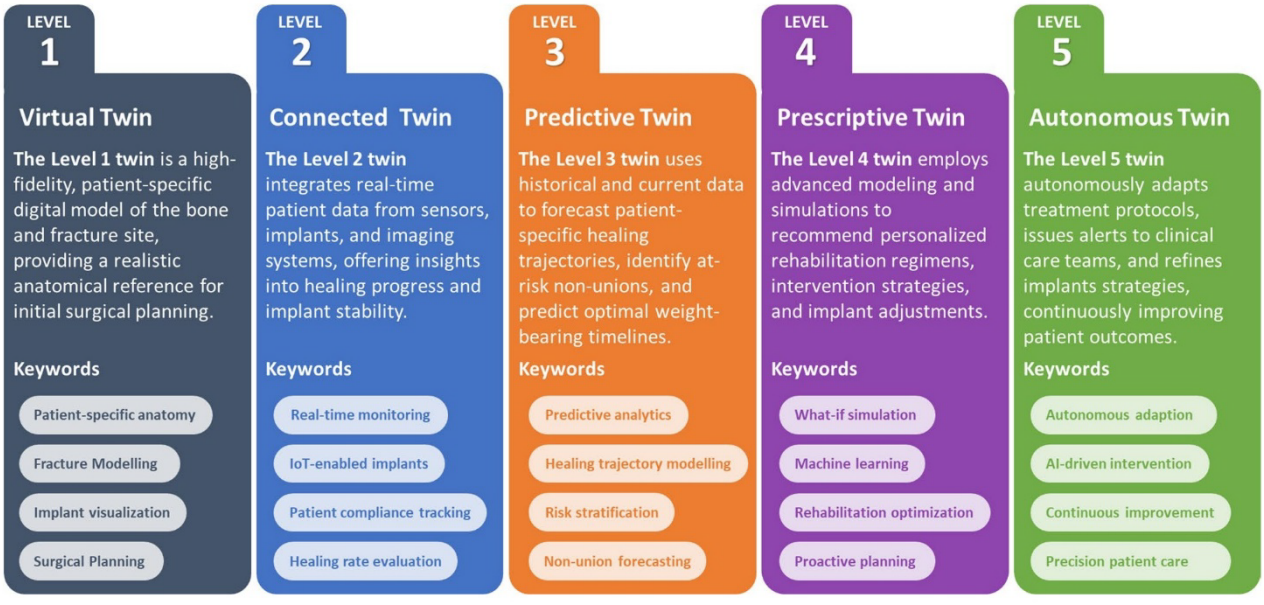

Fig. 7. The consortium introduces different levels of digital twin maturity.

Patient metadata

Comprehensive metadata is collected upon the patient's consultation at the clinic. This includes anthropometric information such as age, sex, body height, body weight, and body mass index, along with the AO classification of the fracture[37]. The patient's treatment history is documented, including previous surgeries, revision procedures, and prior rehabilitation efforts. Based on this information, the revision surgery is planned, explicit treatment goals are defined (e.g., enhancing biomechanical stability or restoring functional mobility), and subsequent rehabilitation strategies are outlined.

Workflow

The digital twin creation process followed a modular but consistent workflow across all five cases, consisting of (1) motion capture, (2) musculoskeletal simulation, (3) patient-specific image processing and segmentation, (4) virtual model generation, and (5) finite element simulation. While all cases shared this pipeline, differences arose primarily in the types of anatomical regions analyzed, the implant strategies under evaluation, and the integration of motion data. For Cases 1–4, a full-body motion capture system was used to monitor scenarios involving the lower and upper extremities under functional tasks such as walking or arm movement (see supplementary material). In Case 5, despite focusing on wrist motion, whole-body motion capture was used to ensure accurate arm segment orientation and to derive consistent kinematic constraints for the wrist joint. The setup captured segment-specific joint angles and positions, which were evaluated through an inverse dynamics pipeline within the AnyBody™ (AnyBody Technology A/S, Aalborg, Denmark) modeling system.

Patient motion capturing

During the initial consultation and subsequent follow-up appointments throughout the patient's recovery, a gait or motion analysis is performed under the supervision of the senior physician. The full-body motion-capturing system Xsens™ MVN Awinda (Xsens Technology B.V., Enschede, Netherlands) is used for this analysis. This system comprises 17 inertial measurement units (IMUs) placed in standardized anatomical positions across the patient's body to capture precise segmental and whole-body motion data. The process is described in detail by Braun et al.[36] and Andres et al.[38]. In addition to IMU-based data, specific anatomical parameters, such as segment lengths, are measured to enhance the accuracy of subsequent biomechanical simulations and analyses. The motion capture protocol was adapted to each case's injury location and clinical objective. Standard overground walking trials were recorded for lower-extremity cases (Cases 1, 3, and 4) to simulate weight-bearing loads during gait. For the humeral fracture in Case 2, shoulder and arm movements relevant to functional loading were captured. In Case 5, where the focus was on wrist malalignment, the patient performed isolated radial and ulnar deviations under clinical supervision.

Musculoskeletal simulation

Musculoskeletal simulations are performed using the AnyBody™ Modelling System. The AnyBody™ software system enables the generation of subject-specific biomechanical models for estimating muscle forces, joint loads, and ground reaction forces, thereby providing insights into the mechanical interactions between the musculoskeletal system and its environment. To ensure the accuracy of these simulations, key patient-specific anthropometric parameters, including height, weight, and segment lengths, are incorporated into the model configuration. The motion capture data of the patient serves as the kinematic input for the musculoskeletal simulations, providing time-resolved joint angles and segment orientations. By integrating these patient-specific parameters with recorded movement patterns, the resulting models reflect individual biomechanics, facilitating detailed assessments of musculoskeletal function under various conditions. This data then serves as boundary conditions in the biomechanical simulations, allowing a high degree of individualization[34].

Patient-specific image processing

Following the completion of patient-specific measurements and musculoskeletal simulations, the obtained CT scans undergo a segmentation process using the image processing software ScanIP™ (Synopsys, Mountain View, CA, United States). The anonymized digital imaging and communications in medicine (DICOM) image stacks are loaded into the software, where distinct anatomical and implant-related regions are identified based on threshold-based differences in greyscale values. Initially, automated segmentation routines are employed to create preliminary masks for bone, fracture, implant, and screws.

Subsequent manual refinements focus on areas requiring greater precision, particularly the proximal and distal bone regions and the screw trajectories. In addition, careful attention is given to accurately defining the fracture morphology and the corresponding callus area. Throughout this stage, consultation with the treating surgeon ensures a clinically appropriate segmentation and an accurate reconstruction of the patient-specific fracture configuration.

Virtual model generation

The next step in setting up the DT involves generating a virtual representation of the patient's treatment scenario. This reconstruction may represent a prior, current, or future surgical intervention. To achieve this, data from available CT scans, X-rays, and medical reports are thoroughly examined in conjunction with the clinical expertise of the treating surgeon. This data review ensures that the virtual model accurately reflects the anatomical and clinical realities.

A key aspect of virtual reconstruction is modifying and optimizing existing treatment strategies. For example, the model can be adjusted to change the thickness of an intramedullary nail, place or remove screws, add or remove plates, or predict wrist motion outcomes before and after a planned reconstruction surgery. Before these adjustments, the current implant situation is documented by measuring implant dimensions, assessing

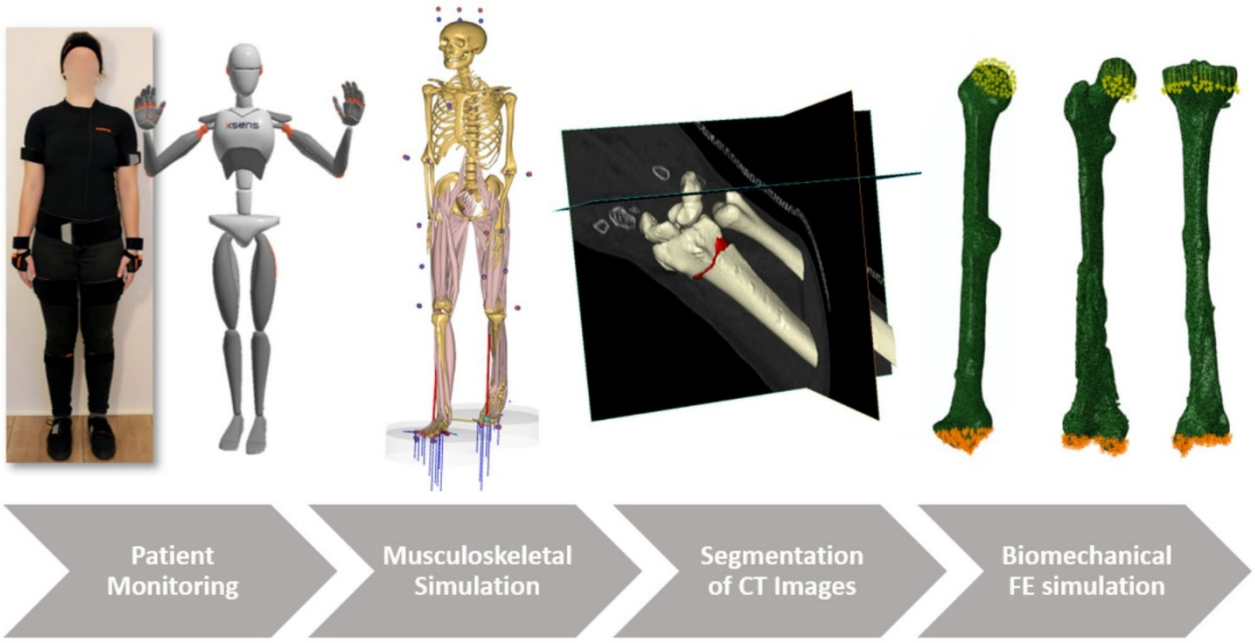

Fig. 8. Visualization of the workflow starting with the patient monitoring, then the inverse dynamic calculation of the joint forces, the generation of the 3D models, and the FE simulation with the applied boundary conditions.

the type and number of screws, plate hole configurations, and intramedullary nail sizes. This inventory serves as a baseline against which planned modifications are evaluated, ensuring that the proposed changes align with clinical goals and patient-specific needs. Further optional refinements, such as integrating motion measurement data obtained before surgical revisions, can be introduced.

Upon finalizing the virtual representation, attention turns to refining the fracture and callus areas. Manual adjustments supported by detailed imaging and surgical expertise ensure that these regions accurately represent the clinical situation. In some cases, incorporating relevant boundary conditions, such as recorded motion data, may be advantageous directly into the virtual representation, enhancing the model's predictive capacity regarding functional outcomes.

At this stage, two segmentation-based models are typically generated for each patient: one representing the current state and the other the previous or anticipated future treatment scenario. Using ScanIP™, finite element (FE) models are created for each virtual representation. Here, the image segmentation quality is first verified, after which meshing and material assignment are performed. Therefore, an adaptive meshing with quadratic tetrahedral elements of type C3D10, ten-node tetrahedra, is performed to represent the bone and implant structures. The bone material properties are derived from CT grey values following established approaches[34–36], while the mechanical characteristics of implants, nails, and screws are chosen based on clinically relevant design parameters. The fracture properties reflect the condition of the soft callus, as described by Claes and colleagues[39,40].

Subsequently, node sets are defined to integrate boundary and loading conditions for future simulations. Two cuboid regions at the distal and proximal ends of the bone typically serve as reference areas for applying loads or constraints. Once meshing, material assignments, and node-set configurations are complete, an input file is generated. This file contains all the necessary information to guide subsequent FE simulations.

To evaluate the clinical feasibility of the proposed workflow visualized in Fig. 8, the typical time requirements for each major step: CT image processing and segmentation (8–16 h), virtual model generation (2–4 h), meshing and simulation setup (1–2 h), and finite element simulation with result post-processing (1–10 h depending on model complexity). Musculoskeletal simulations based on motion capture data require approximately 1–2 h per patient. The end-to-end process from initial imaging to mechanical analysis results can be completed within 2–3 working days. While this timeframe is incompatible with emergency settings, it aligns well with revision surgeries and complex fracture cases involving planned interventions.

Biomechanical simulation

The input files from ScanIP™ are imported into the simulation environment Abaqus™ (Dassault Systèmes, Vélizy-Villacoublay, France). The finite element simulations were performed using the Abaqus Standard (implicit) solver and linear elastic material models. Dirichlet boundary conditions are typically applied at the bone's distal joint side, where displacements and rotations are constrained in all three spatial axes. The applied loading conditions correspond to static representations of peak joint loads, extracted from the dynamic musculoskeletal simulations at maximum loading during representative movement (e.g., mid-stance phase in gait). While full dynamic load

profiles were generated and are provided in the supplementary material, the finite element analyses used only the peak static load values to represent worst-case mechanical scenarios. Concurrently, loading conditions are imposed on the proximal bone segment, guided by musculoskeletal simulation outputs that define force vectors and load ratios. For example, as illustrated in Fig. 8, the femur is subjected to hip joint forces, while the tibia experiences knee joint forces representative of walking conditions. Similarly, relevant shoulder movements are modeled for upper arm fractures, and appropriate joint forces are applied at the shoulder.

Joint reaction forces and segmental loads were extracted from the musculoskeletal simulation at the time of maximum loading during the motion cycle, typically corresponding to mid-stance in walking or maximal muscle activation in upper-limb movement. The finite element simulations used these peak load vectors, including force directions and magnitudes, as boundary conditions. Specifically, loads were applied to the proximal joint surface of the bone models, while the distal ends were constrained. The stress and strain plots presented in the results represent the output of this peak-load simulation and reflect the condition most relevant for mechanical failure risk and decision-making.

Once the FE simulation concludes, a Python script automatically extracts essential data from the output database (ODB). This script initiates the conversion of simulation results into a visualization-friendly format using the Visualization Toolkit (VTK), capturing node labels and coordinates, element connectivity, and element sets for each mask from the segmentation and model generation steps.

Additionally, displacement vectors and stress and strain tensors are mapped to the defined masks, ensuring each structural component's mechanical response is accurately represented. This data extraction and mapping process enables a seamless transition from raw computational outcomes to clinically more interpretable results, suitable for further analysis.

Evaluation

To evaluate implant stability and component performance, von Mises stress distributions are analyzed, helping identify potential weaknesses in the chosen treatment configuration. However, the core focus of this study aims to understand fragment motion and how various treatments influence interfragmentary mechanics. The healing window thresholds are based on the mechanobiological criteria established by Claes et al.[39] and Shefelbine et al.[40]. This approach involves examining octahedral shear strain, which reflects distortional deformation, and volumetric strain, indicative of volumetric changes and hydrostatic pressure in the fracture gap.

The interplay of octahedral shear and volumetric strains has been linked to cellular responses and tissue differentiation, supported by the findings of Bishop and colleagues[41], Garcia and colleagues[42], and Doblaré and colleagues[43]. Each tetrahedral element in the FE model is individually analyzed to determine the local strain tensor. Subsequently, the octahedral shear and volumetric strains are calculated and evaluated within the specified limits established by the adopted mechanobiological modeling approach[39,40]. This analysis offers patient-specific and treatment-related insights into the mechanical environment surrounding the fracture, informing treatment strategies and guiding more effective, personalized orthopedic interventions.

Data availability

The original contributions presented in the study are included in the article; further inquiries can be directed to the corresponding author. Researchers who wish to request access to data should send an email indicating the research purpose. Every request must be reviewed by the responsible institutional review boards, considering the risk of patient reidentification and compliance with the applicable data protection rules.

Received: 4 March 2025; Accepted: 29 May 2025
Published online: 06 June 2025

References

1. Grieves, M. Digital twin: manufacturing excellence through virtual factory replication. *White Paper*. **1**, 1–7 (2014).
2. Sun, T., He, X. & Li, Z. Digital twin in healthcare: recent updates and challenges. *Digit. Health*. **9**, 1–13. https://doi.org/10.1177/20552076221149651 (2023).
3. Liu, Y. et al. A novel Cloud-Based framework for the elderly healthcare services using digital twin. *IEEE Access*. **7**, 49088–49101. https://doi.org/10.1109/ACCESS.2019.2909828 (2019).
4. Björnsson, B. et al. Digital twins to personalize medicine. *Genome Med.* **12**, 4. https://doi.org/10.1186/s13073-019-0701-3 (2019).
5. Boulos, M. & Zhang, P. Digital twins: from personalised medicine to precision public health. *J. Personalized Med.* **11**, 745. https://doi.org/10.3390/jpm11080745 (2021).
6. Croatti, A., Gabellini, M., Montagna, S. & Ricci, A. On the integration of agents and digital twins in healthcare. *J. Med. Syst.* **44**, 161. https://doi.org/10.1007/s10916-020-01623-5 (2020).
7. Kaul, R. et al. The role of AI for developing digital twins in healthcare: the case of cancer care. *Wiley Interdisciplinary Reviews: Data Min. Knowl. Discovery*. **13**, e1480. https://doi.org/10.1002/widm.1480 (2022).
8. Wu, C. et al. Integrating mechanism-based modeling with biomedical imaging to build practical digital twins for clinical oncology. *Biophys. Reviews*. **3** (2), 021304. https://doi.org/10.1063/5.0086789 (2022).
9. Thiong'o, G. & Rutka, J. Digital twin technology: the future of predicting neurological complications of pediatric cancers and their treatment. *Front. Oncol.* **11**, 781499. https://doi.org/10.3389/fonc.2021.781499 (2022).
10. Pesapane, F., Rotili, A., Penco, S., Nicosia, L. & Cassano, E. Digital twins in radiology. *J. Clin. Med.* **11**, 6553. https://doi.org/10.3390/jcm11216553 (2022).
11. Ahmadian, H. et al. Toward an artificial intelligence-assisted framework for reconstructing the digital twin of vertebra and predicting its fracture response. *Int. J. Numer. Methods Biomed. Eng.* **38**, e3601. https://doi.org/10.1002/cnm.3601 (2021).
12. Ahmadian, H. et al. A digital twin for simulating the vertebroplasty procedure and its impact on mechanical stability of vertebra in cancer patients. *J. Numer. Methods Biomedical Eng.* **38**, e3600. https://doi.org/10.1002/cnm.3600 (2021).
13. Bielfeldt, M. et al. Discrimination between the effects of pulsed electrical stimulation and electrochemically conditioned medium on human osteoblasts. *J. Biol. Eng.* **17**, 71. https://doi.org/10.1186/s13036-023-00393-1 (2023).

14. Siris, E. et al. Estimation of Long-Term Efficacy of Denosumab Treatment in Postmenopausal Women with Osteoporosis: A FRAX- and Virtual Twin-Based Post Hoc Analysis from the FREEDOM and FREEDOM Extension Trials. JBMR Plus, 4(4): e10348, (2020). https://doi.org/10.1002/jbm4.10348
15. Ferrari, S. et al. Favorable skeletal benefit/risk of long-term denosumab therapy: A virtual-twin analysis of fractures prevented relative to skeletal safety events observed. *Bone* **134**, 115287. https://doi.org/10.1016/j.bone.2020.115287 (2020).
16. Schepers, R. H. et al. Accuracy of fibula reconstruction using patient-specific CAD/CAM reconstruction plates and dental implants: A new modality for functional reconstruction of mandibular defects. *J. Craniomaxillofac. Surg.* **43** (5), 649–657. https://doi.org/10.1016/j.jcms.2015.03.015 (2015).
17. Wilde, F., Cornelius, C-P. & Schramm, A. Computer-Assisted mandibular reconstruction using a Patient-Specific reconstruction plate fabricated with Computer-Aided design and manufacturing techniques. *Craniomaxillofacial Trauma. Reconstruction.* **7** (2), 158–166. https://doi.org/10.1055/s-0034-1371356 (2014).
18. Essig, H. et al. Patient-specific biodegradable implant in pediatric craniofacial surgery. *J. Craniomaxillofac. Surg.* **45** (2), 216–222. https://doi.org/10.1016/j.jcms.2016.11.015 (2017).
19. Ahn, S. et al. Toward digital twin development for implant placement planning using a parametric Reduced-Order model. *Bioengineering* **11**, 84. https://doi.org/10.3390/bioengineering11010084 (2024).
20. Pinheiro, M., Willaert, R., Khan, A., Krairi, A. & van Paepegem, W. Biomechanical evaluation of the human mandible after temporomandibular joint replacement under different biting conditions. *Sci. Rep.* **11**, 14034. https://doi.org/10.1038/s41598-021-93564-3 (2021).
21. Demir, O., Uslan, I., Buyuk, M. & Salamci, M. U. Development and validation of a digital twin of the human lower jaw under impact loading by using non-linear finite element analyses. *J. Mech. Behav. Biomed. Mater.* **148**, 106207. https://doi.org/10.1016/j.jmbbm.2023.106207 (2023).
22. Bjelland, Ø. et al. Toward a digital twin for arthroscopic knee surgery: A systematic review. *IEEE Access.* **10**, 45029–45052. https://doi.org/10.1109/ACCESS.2022.3170108 (2022).
23. Ugwoke, C. K., Albano, D., Umek, N., Dumić-Čule, I. & Snoj, Ž. Application of virtual reality systems in bone trauma procedures. *Medicina* **59**, 562. https://doi.org/10.3390/medicina59030562 (2023).
24. Chen, Y., Zhang, K., Hao, Y. & Hu, Y. Research status and application prospects of digital technology in orthopaedics. *Orthop. Surg.* **4**, 131–138. https://doi.org/10.1111/j.1757-7861.2012.00184.x (2012).
25. Qin, J. & Wu, J. Realizing the potential of Computer-Assisted surgery by embedding digital twin technology. *JMIR Med. Inf.* **10** (11), e35138. 2022/11/e35138 (2022).
26. Aubert, K. et al. Development of digital twins to optimize trauma surgery and postoperative management. A case study focusing on tibial plateau fracture. *Front. Bioeng. Biotechnol.* **9**, 722275. https://doi.org/10.3389/fbioe.2021.722275 (2021).
27. Ghiasi, M. S., Chen, J., Vaziri, A., Rodriguez, E. K. & Nazarian, A. Bone fracture healing in Mechanobiological modeling: A review of principles and methods. *Bone Rep.* **6**, 87–100. https://doi.org/10.1016/j.bonr.2017.03.002 (2017).
28. Lauer-Schmaltz, M. W., Cash, P., Hansen, J. P. & Maier, A. Designing human digital twins for Behaviour-Changing therapy and rehabilitation: A systematic review. *Proc. Des. Soc.* **2**, 1303–1312. https://doi.org/10.1017/pds.2022.132 (2022).
29. Barricelli, B. R., Casiraghi, E., Gliozzo, J., Petrini, A. & Valtolina, S. Human digital twin for fitness management. *IEEE Access.* **8**, 26637–26664. https://doi.org/10.1109/ACCESS.2020.2971576 (2020).
30. Killen, B. A., Falisse, A., de Groote, F. & Jonkers, I. Silico-Enhanced treatment and rehabilitation planning for patients with musculoskeletal disorders: can musculoskeletal modelling and dynamic simulations really impact current clinical practice?? *Appl. Sci.* **10** (20), 7255. https://doi.org/10.3390/app10207255 (2020).
31. Wickert, K. et al. Experimental and virtual testing of bone-implant systems equipped with the AO fracture monitor with regard to interfragmentary movement. *Front. Bioeng. Biotechnol.* **12**, 1–20. https://doi.org/10.3389/fbioe.2024.1370837 (2024).
32. Augat, P. et al. Biomechanical models: key considerations in study design. *OTA Int.* **4** (2), E099. https://doi.org/10.1097/OI9.0000000000000099 (2021a).
33. Augat, P., Hollensteiner, M. & von Rüden, C. The role of mechanical stimulation in the enhancement of bone healing. *Injury* **52**, S78–S83. https://doi.org/10.1016/j.injury.2020.10.009 (2021b).
34. Orth, M. et al. Simulation-based prediction of bone healing and treatment recommendations for lower leg fractures: effects of motion, weight-bearing and fibular mechanics. *Front. Bioeng. Biotechnol.* **11**, 1067845. https://doi.org/10.3389/fbioe.2023.1067845 (2023).
35. Braun, B. J. et al. *Bewegungsanalyse Und Muskuloskeletale Simulation in Der Pseudarthrosentherapie - Erfahrungen Und Erste Klinische Ergebnisse* (Unfallchirurgie, 2022). https://doi.org/10.1007/s00113-022-01208-6
36. Braun, B. J. et al. Individualized determination of the mechanical fracture environment after tibial exchange Nailing – A Simulation-Based feasibility study. *Front. Surg.* **8**, 749209. https://doi.org/10.3389/fsurg.2021.749209 (2021).
37. Müller, M. E., Koch, P., Nazarian, S. & Schatzker, J. *The Comprehensive Classification of Fractures of long Bones* (Springer, 1990). https://doi.org/10.1007/978-3-642-61261-9_7
38. Andres, A. et al. Individual postoperative and preoperative workflow for patients with fractures of the lower extremities. *Clin. Biomech. Elsevier Ltd*. https://doi.org/10.1016/j.clinbiomech.2025.106503 (2025).
39. Claes, L. E. & Heigele, C. A. Magnitudes of local stress and strain along bony surfaces predict the course and type of fracture healing. *J. Biomech.* **32** (3), 255–266. https://doi.org/10.1016/S0021-9290(98)00153-5 (1999).
40. Shefelbine, S. J., Augat, P., Claes, L. & Simon, U. Trabecular bone fracture healing simulation with finite element analysis and fuzzy logic. *J. Biomech.* **38** (12), 2440–2450. https://doi.org/10.1016/j.jbiomech.2004.10.019 (2005).
41. Bishop, J. A., Palanca, A. A., Bellino, M. J. & Lowenberg, D. W. Assessment of compromised fracture healing. *J. Am. Acad. Orthop. Surg.* **20** (5), 273–282. https://doi.org/10.5435/JAAOS-20-05-273 (2012).
42. Garcia, J. M., Kuiper, J. H. & Doblare, M. R. J. A numerical model to study the mechanical influences on bone fracture healing. *Acta Bioeng. Biomech.* **4**, 394–395 (2003).
43. Doblaré, M., García, J. M. & Gómez, M. J. Modelling bone tissue fracture and healing: A review. *Eng. Fract. Mech.* **71** (13–14), 1809–1840. https://doi.org/10.1016/j.engfracmech.2003.08.003 (2004).

Acknowledgements

This study was mainly funded by the German Federal Ministry for Science and Education (BMBF) under the grant "VirtuS" (FKZ: 13GW0572).

Author contributions

A.A. conceptualized the study, performed the movement analysis, and prepared the manuscript. M.R. initiated the concept and research and wrote and reviewed the manuscript. K.W. assisted in the movement analysis. S.D. and T.H. supervised all aspects and secured the funding. J.S., S.H., F.R., L.R., A.P., L.S., and D.S. contributed to the research design and provided scientific guidance for the various aspects of the research. B.B. did the clinical treatment and decision process, initiated the concept and research, and wrote and reviewed the manuscript. All authors have read and approved the submitted and final version of the manuscript.

Funding
Open Access funding enabled and organized by Projekt DEAL.

Declarations

Competing interests
The authors declare no competing interests.

Ethics Statement
Ethical approval for this study was indeed obtained, and all participants provided written informed consent. All study procedures involving human participants were conducted in accordance with the Declaration of Helsinki and approved by the Ethics Committee of the University of Tuebingen (protocol codes 317 and 318/2022BO2). Patients were recruited from the outpatient trauma surgery clinic, and all participants provided written informed consent prior to inclusion in the study.

Additional information
Supplementary Information The online version contains supplementary material available at https://doi.org/10.1038/s41598-025-04792-w.

Correspondence and requests for materials should be addressed to A.A.

17 Paper D

Title:

Simulation of a Custom-Made Temporomandibular Joint – An Academic View on an Industrial Workflow

Authors:

Annchristin Andres, Kerstin Wickert, Elena Gneiting, Franziska Binmoeller, Stefan Diebels & Michael Roland

Original Publication:

Andres, A., Wickert, K., Gneiting, E., Binmoeller, F., Diebels, S. & Roland, M. (2025). Simulation of a Custom-Made Temporomandibular Joint – An Academic View on an Industrial Workflow. Bioengineering, 12(5), 545. https://doi.org/10.3390/bioengineering12050545

bioengineering

MDPI

Article

Simulation of a Custom-Made Temporomandibular Joint—An Academic View on an Industrial Workflow

Annchristin Andres [1,†], Kerstin Wickert [1,†], Elena Gneiting [2], Franziska Binmoeller [2], Stefan Diebels [1] and Michael Roland [1,*]

[1] Applied Mechanics, Saarland University, Campus A4 2, 1. OG, 66123 Saarbrücken, Germany; annchristin.andres@uni-saarland.de (A.A.); kerstin.wickert@uni-saarland.de (K.W.); s.diebels@mx.uni-saarland.de (S.D.)
[2] KLS Martin SE & Co. KG, 78532 Tuttlingen, Germany; elena.gneiting@klsmartin.com (E.G.); franziska.binmoeller@klsmartin.com (F.B.)
* Correspondence: michael.roland@uni-saarland.de; Tel.: +49-681-302-3789; Fax: +49-681-302-3992
† These authors contributed equally to this work.

Abstract: Temporomandibular joint replacement is a critical intervention for severe temporomandibular joint disorders, enhancing pain levels, jaw function and overall quality of life. In this study, we compare two finite element method-based simulation workflows from both academic and industrial perspectives, focusing on a patient-specific case involving a custom-made temporomandibular joint prosthesis. Using computed tomography data and computer-aided design data, we generated different 3D models and performed mechanical testing, including wear and static compression tests. Our results indicate that the academic workflow, which is retrospective, purely image-based and applied post-operatively, produced peak stress values within 9–20% of those obtained from the industrial workflow. The industrial workflow is prospective, pre-operative, computer-aided design-based and guided by stringent regulatory standards and approval protocols. Observed differences between workflows were attributed primarily to distinct modelling assumptions, simplifications and constraints inherent in each method. To explicitly quantify these differences, multiple additional models were generated within the academic workflow using partial data from the industrial process, revealing specific sources of variation in stress distribution and implant performance. The findings underscore the potential of patient-specific simulations not only to refine temporomandibular joint prosthesis design and enhance patient outcomes, but also to highlight the interplay between academic research methodologies and industrial standards in the development of medical devices.

Keywords: temporomandibular joint replacement; finite element analysis; biomechanics; custom-made prothesis; experimental prothesis testing; patient-specific model generation

Academic Editors: Chiara Giulia Fontanella and Karthik K. Tappa

Received: 23 January 2025
Revised: 25 April 2025
Accepted: 13 May 2025
Published: 20 May 2025

Citation: Andres, A.; Wickert, K.; Gneiting, E.; Binmoeller, F.; Diebels, S.; Roland, M. Simulation of a Custom-Made Temporomandibular Joint—An Academic View on an Industrial Workflow. *Bioengineering* **2025**, *12*, 545. https://doi.org/10.3390/bioengineering12050545

1. Introduction

Temporomandibular joint replacement (TMJR) represents a critical surgical intervention for patients with severe temporomandibular joint (TMJ) disorders, offering significant improvements in pain levels, jaw function and quality of life [1]. This procedure has become a standard of care for end-stage TMJ disease, particularly when conservative treatments fail to provide relief. The TMJ concepts system, along with other prosthetic systems, has shown promising results in restoring form and function, reducing pain and improving dietary consistency [2,3]. Studies have also found that total alloplastic TMJ prostheses are an efficient, safe and stable long-term solution, with significant improvements in mouth

opening, pain relief and satisfaction with the surgery [4]. In addition, studies in humans and animals have shown that disturbances in normal masticatory function can lead to morphological and functional changes in the craniomaxillofacial system [5,6]. Despite all these advancements, the long-term implications of TMJR on masticatory function and overall biomechanics remain not fully understood [7,8]. Therefore, a clearer understanding of the biomechanical effects of TMJR is essential both to identify design shortcomings and to optimize the prostheses as well as the patient care.

The outcome of TMJ reconstruction is highly dependent on the kinematic performance, especially in the treatment of patients with internal derangement cases and in restoring form and function following the removal of failed TMJ implants [9]. In this context, understanding the biomechanics of the TMJR is important for improving the design and ensuring long-term success [10]. A kinematic study comparing the TMJ movements of healthy subjects with those of patients undergoing unilateral TMJ arthrotomy with metal fossa-eminence partial joint replacement showed significant differences in joint kinematics, underlining the need for biomechanical testing in design and development [11].

Finite element (FE) modelling has been widely used to evaluate the biomechanical behavior of TMJ prostheses [12,13]. Simulation-based studies have also shown that relevant shear forces can occur during mastication, which underpins the need for accurate musculoskeletal modelling in surgical planning [14]. It has also been shown that the development of customized temporomandibular fossa prostheses based on musculoskeletal simulations can significantly improve the outcome of total joint replacement procedures [15]. Simulation techniques, such as computed tomography (CT) scan data modelling, have been instrumental in the development and evaluation of custom prostheses for TMJ reconstruction [8]. These methods provide valuable insights into the performance and longevity of prosthetic joint replacements.

Joint simulators, like the VIVOTM joint simulator [16,17], provide a platform for evaluating the mechanics of joint replacements, including TMJ [18]. Computational modelling has also been used to study the fixation of fossa components in TMJR surgery, demonstrating the importance of personalized 3D-printed joint prostheses for optimal outcomes [19]. The biomechanics of the intact and implanted mandible during different biting tasks can reveal significant differences in joint movements and load distribution, which is helpful in identifying design limitations and improving possibilities.

In this study, we compare two different workflows for a selected real patient identified as a relevant clinical use case. The first workflow is the process of the manufacturer of the patient-specific TMJ prosthesis. This workflow is based on the pre-operative clinical image data, the surgical planning and the individualized design of the prosthesis together with the treating clinician. This procedure includes the mechanical tests and simulations required by the regulatory framework for the use of patient-specific TMJ prosthesis. This prospective workflow takes place entirely before the patient's surgery.

In contrast, the academic workflow is based exclusively on post-operative clinical image data and takes place retrospectively to the patient's surgery. In this context, the term "academic workflow" specifically refers to a simulation process relying solely on image segmentation and post-operative CT data, rather than proprietary pre-operative computer-aided design CAD data. As 3D-CAD data from manufacturers are not normally available in the academic environment or are only accessible with high barriers [20], academic simulation models are normally obtained exclusively from segmentation processes. To better assess the differences between the two concepts, one industry-driven and prospective and the other downstream and retrospective, we generated additional models based on the academic approach that link the segmented models with the manufacturer's CAD data.

We show that the differences between the simulation results are small within the different assumptions and simplifications made. The study thus provides important insights regarding the possibilities of patient data-based simulations for TMJ prostheses, which hold substantial interest for the scientific community of this field. The main goal of this study was to show academic groups working purely retrospectively on image data, as the authors themselves normally do, a comparison with industry data-based simulations to enable them to better evaluate their own results.

The structure of the paper is organized as follows: Section 2 describes the patient data and methods used in both workflows to generate the computational models. Section 3 presents experimental results, including wear and static compression tests, as well as the simulation outcomes from both workflows. Section 4 discusses these results, focusing on the comparison between the industrial and academic approaches. Finally, Section 5 summarizes the key findings and conclusions drawn from the study.

2. Materials and Methods

2.1. Patient Case Data

A 35-year-old female patient presented with a fracture of the condylar process due to trauma. Initial treatment involved standard fracture management with mini plates. However, post-operative complications included an infection necessitating the removal of the condylar fragment. The patient exhibited reduced dentition, attributed to poor oral hygiene rather than trauma. Pre-operative planning was carried out using CT imaging, while post-operative assessments were conducted utilizing different imaging modalities, including CT, digital volume tomography (DVT) and orthopantomography (OPT). A custom-made TMJ prosthesis, consisting of a titanium alloy (Ti-6Al-4V) condyle and fossa component with ultra-high molecular weight polyethylene (UHMWPE) as joint surface, was inserted. Figure 1 provides an overview of the treatment and the personalized TMJ prosthesis.

The Ti-6Al-4V material used for the prosthesis offers a favorable surface for osseointegration, combined with high mechanical strength and ductility [21]. Due to the issues associated with a pure UHMWPE fossa, such as increased backside wear, poor surface for bone fixation, the increased chance for "cold flow" and a higher risk of osteolysis [19], we did not select a fossa made entirely of UHMWPE. Instead, UHMWPE was utilized as a sliding layer between two titanium alloy components, specifically as the joint surface on a Ti-6Al-4V base for the fossa component. The UHMWPE part is pressed onto a Ti-6Al-4V base body. This design combines the mechanical benefits of Ti-6Al-4V with the low-friction properties of UHMWPE at the articulating surface. Additionally, UHMWPE is recognized as a suitable material for articulating surfaces in joint implants according to DIN EN ISO 21534:2009. The condylar head's design closely resembles the natural condyle, potentially leading to more natural movement for the patient. Custom-made prostheses outperform stock devices by providing a better fit, reducing operating time since no modifications are needed during surgery, and potentially decreasing wear and increasing implant longevity [19].

2.2. Industrial Workflow

The prosthesis manufacturer's workflow described below is certified and officially approved by the authorities. After that, the workflow is frozen and has no room for changes, experiments or tests.

2.3. Segmentation and 3D Geometric Model Generation

The pre-operative CT scan was segmented using Mimics Medical 23.0 (Materialise, Löwen, Belgium). The CT data comprised 711 slices, each with a pixel size of 0.43 mm,

a slice increment of 0.3 mm and a slice thickness of 0.5 mm. Masks were created for the mandible and teeth to generate stereolithography (STL) files for the finite element simulation. Additional masks for the facial nerve, cranium and soft tissue were generated to assist in the pre-operative planning process. These additional masks ensured safe distances from critical anatomical structures during the surgical procedure but were not included in the FE model used for biomechanical analysis. A standardized thresholding process, as suggested by Mimics, was applied, followed by visual control and manual post-processing as needed. The segmented data were then used to generate a 3D model, which was exported as an STL file. Case planning and the design of the TMJ prosthesis, including the placement of screws, were conducted using Geomagic Freeform Plus 2021.0.56 (3D Systems, Rock Hill, SC, USA). The mandible and teeth were merged into a single part, and the final design was exported as STL files for further processing and manufacturing.

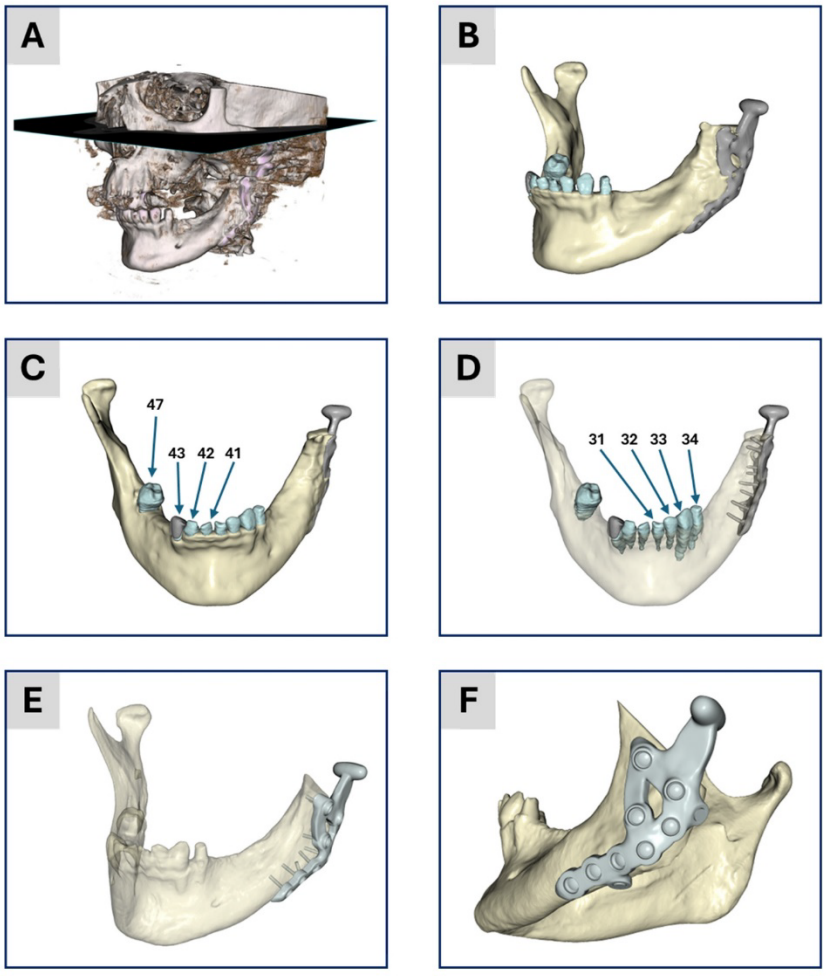

Figure 1. Illustration of the segmentation and model generation process. (**A**) Threshold-based image of the 3D tomogram giving an overview of the patient situation. (**B**–**D**) The results from the academic workflow and (**E**,**F**) the results from the industrial workflow. (**B**) Lateral view of the segmentation result. (**C**) Anterior view of the geometric 3D model after segmentation. (**D**) Same illustration as (**C**) with transparent bone to show the segmentation of the teeth and the position of the screws. The numbers correspond to the numbering of teeth according to the FDI world dental federation notation. (**E**) Segmentation results together with the CAD data of the treatment from the surgical planning. (**F**) Overview of the CAD data for visualization of the treatment. Items (**A**–**D**) were generated based on data from ScanIP, and items (**E**,**F**) were generated using data from Mimics; see the Segmentation and 3D Geometric Model Generation section of the two workflows below for further details.

2.4. Material Assignment and Meshing

The following material properties were used in the modelling: the part representing the mandible and the teeth were modelled as isotropic and linear elastic material [22] with a Young's modulus of 10 GPa and a Poisson's ratio of 0.3. The TMJ prosthesis and the screws are also modelled as isotropic linear elastic material with the values for Ti-6Al-4V given in [23] and in Table 1. The mesh generation resulted in a FE model with quadratic ten-node tetrahedral elements. The mesh information is given in Table 2.

Table 1. This table is essentially taken from Pinheiro et al. [12] and has only been adapted here to our application and its underlying data.

Mask	Young's Modulus E (MPa)	Poisson's Ratio	CT Values (HU)	CT Density ρ (kg/m^3)	Young's Moduli Law
Mandibular, Trabecular Bone	180–380	0.300	−1000–500	$0 \leq \rho < 1000$	$E = 0.0004\ \rho^{2.01}$
Mandibular, Cortical Bone	11,300–22,900	0.300	501–1500	$1001 \leq \rho < 2000$	$E = 0.005\ \rho^{2.01}$
Dentin	24,535	0.300	≤2000	-	-
Enamel	39,605	0.300	>2000	-	-
Ti–6Al–4V	113,800	0.342	-	-	-
Bone	10,000	0.3	-	-	-

Table 2. Number of nodes and mesh cells of all models from both workflows.

		Number of Nodes	Number of Mesh Cells										
					Teeth								
Workflow	Model		Mandibular	TMJ Prosthesis	No. 31	No. 32	No. 33	No. 34	No. 41	No. 42	No. 43	No. 47	Treatment of No. 43
Academic	Model No. 1	1,055,863	535,018	75,635	7295	6147	10,902	7024	5641	7763	5391	17,721	3485
	Model No. 2	1,069,302	544,807	76,398	6679	6152	10,908	6962	5886	7616	4986	17,377	3351
	Model No. 3	1,056,745	536,552	74,826	6701	5956	10,941	7192	5710	7742	5347	17,688	3560
	Model No. 4	157,867	72,602	19,148	-	-	-	-	-	-	-	-	-
Industrial	-	975,770	164,306	435,695	-	-	-	-	-	-	-	-	-

2.5. Boundary Conditions

To ensure a high level of comparability between the two workflows, the boundary conditions used in the industrial workflow were also applied in the academic workflow. To apply the Dirichlet boundary conditions for the fixation of the models, two regions of interest (ROIs) were marked: one for the TMJ prosthesis and one for the opposite side of the mandible. These ROIs were exported as node sets during the meshing process. Another ROI was defined as tooth number 47, the first molar, to apply the bite force. In addition, ROIs were also marked to apply the boundary conditions given by the different muscles, cf. Figure 2.

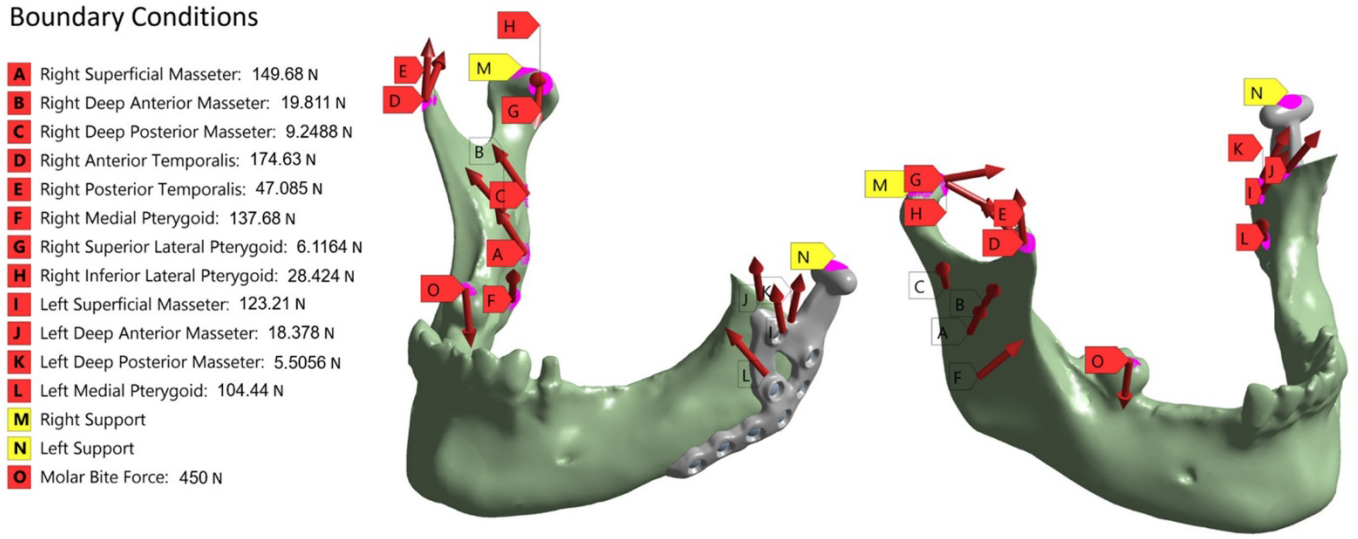

Figure 2. Illustration of the set-up of the boundary conditions based on the musculoskeletal simulation. In addition, the two supports for the fixed Dirichlet boundary conditions are shown in purple as well as the area for applying the molar bite force. The left-hand column contains all the values that were applied for the individual muscle forces.

Therefore, a standardized musculoskeletal simulation was performed using the AnyBody standard symmetric mandible model [24,25] within the AnyBody modelling system (AnyBody Technology A/S, Aalborg, Denmark). In this framework, muscle forces are computed using inverse dynamics combined with static optimization, which determines the net forces necessary to perform a given task. A biting task was simulated by applying a 450 N force at the first molar on the right side. This force was lower than the maximum bite forces reported by Ferrario et al. [26] and closely matched the loading conditions used by Pinheiro et al. [12], corresponding to 50% of the bite force values documented by Woodford et al. [27]. The resulting muscle forces (Figure 2) exceeded the values reported by Waltimo et al. [28], yet remained within the range documented in [12] and were accepted for use in the authorization process.

The simulation calculates both the magnitude and direction of each muscle force based on the geometry and kinematics of the underlying model.

Subsequently, the computed muscle forces were directly transferred to the patient-specific FE model. The force directions and magnitudes were used unaltered, and the muscle attachment points were mapped from the AnyBody model onto the patient-specific model. Muscles attached to the resected bone parts were removed to reflect the actual surgical conditions, ensuring the accuracy of the biomechanical environment post-resection.

To simulate the post-operative stabilization, the condyles were fixed. The boundary conditions are given in Figure 2. The illustration shows the positioning and the applied forces of the individual muscles. In addition, the fixed support of the condyles and the applied molar bite force are shown.

2.6. FEA Simulations

A standardized workflow was performed to generate the simulation model. This industry process ensured consistency and reproducibility across simulations and cases. To accurately simulate the biomechanical interactions, contact was established using the following constraints: (1) screws and prosthesis: bonded with a multi-point constraint and (2) screws and mandible: bonded with a multi-point constraint. The modelled bonded contact for the screw interface replicates the fixed connection between screw and bone

material for an ingrown condition as well as between screw and plate for a locked thread connection. This condition is known to effectively replicate the global deformation behavior and the load transfer through the fixation construct when local stresses in the threads and the interface are not considered [29,30]. These constraints accurately reflected the clinical conditions and ensured the reliability of the simulation results. The contact between prosthesis and mandible was considered as part of the approval process of the software in the verification step, but as there was no penetration of the bone, it was decided not to consider this contact in the frozen workflow.

2.7. Mechanical Testing

The TMJ prosthesis by KLS Martin (KLS Martin SE & Co. KG, Tuttlingen, Germany) was realized as a custom-made device made of Ti-6Al-4V and UHMWPE. The average wear of the prosthesis was tested on the robotic system HORST600 (fruitcare robotics GmbH, Konstanz, Germany). The wear test was conducted with reference to the standard ISO 14243-1. The prosthesis components were moved against each other in a cyclic movement consisting of 5 Mio cycles with a constant load representing a normal chewing force of 20 N [31,32]. This movement consisted of a combination of a 12° rotation and a translational movement of 8.5 mm anterior/posterior and 0.7 mm medial/lateral of the condyle. The wear was measured gravimetrically, and the net mass loss and average wear rate were calculated in accordance with ISO 14243-2.

For the static compression tests, the worst-case design was tested on the standard testing device Z020 (ZwickRoell GmbH & Co. KG, Ulm, Germany) with five testing samples. The native bone was replaced with a patient-specific mandible model made of polyamide (PA), produced via additive manufacturing on EOS Formiga P110 (EOS GmbH, Krailling, Germany). The TMJ prosthesis, including the titanium condyle component, was fixed to this PA mandible model in a closed jaw position (0° opening) and loaded until failure. PA was chosen as the bone substitute material because it allowed for accurate replication of the patient's mandible geometry and consistent fixation of the implant [33,34]. We acknowledge that the use of PA may affect contact stiffness compared to natural bone or titanium. Nonetheless, it provided a practical and reproducible means to evaluate the prosthesis under standardized testing conditions [35,36]. The load was applied 30 percent on the contralateral and 70 percent on the ipsilateral side of the defect, as has been done in similar test setups [37]. After testing, the samples were scanned with the 3D scanner ATOS Core (Carl Zeiss Industrielle Messtechnik GmbH, Oberkochen, Germany) to compare the state of the samples before and after testing to check for deformation.

2.8. Academic Workflow

Segmentation and 3D Geometric Model Generation

The individual digital imaging and communications in medicine (DICOM) image stack of the patient's post-operative CT scan was used to create a geometric model. The tomogram consists of 434 images with a constant voxel, i.e., volumetric pixel, size of 0.3 mm in all three spatial directions. The image stack was segmented into different masks: (1) the mandible, (2) TMJ prosthesis, (3)/(4) the two mandibular central incisors, numbers 41 and 31 in the FDI world dental federation notation (ISO 3950), (5)/(6) the two mandibular lateral incisors, numbers 42 and 32, (7)/(8) the two mandibular canines, numbers 43 and 33, (9) the lower left mandibular first premolar, number 34, (10) the lower right mandibular second molar, number 47 and (11) a past treatment of tooth number 43, i.e., mask (7). The segmentation process was realized in the software ScanIP (ScanIP V24-06 - Academic, Synopsys, Mountain View, CA, USA) and started with an adaptive thresholding procedure for every mask. After that, for each mask, the morphological filters "island

removal", "cavity fill" and "fill gaps" with a priority order were applied resulting in a first segmentation. Then for each mask, the results were visually controlled and manually post-processed to provide a high-quality segmentation without detectable problems, cf. Figure 1A–D for the segmentation result.

Since the industrial workflow uses computer-aided design (CAD) data of the treatment rather than a segmented model of the TMJ prosthesis, we decided to create four models within the academic workflow to gradually transition from a purely segmented model toward the industrial workflow and to highlight differences in the results. These four models are:

Model No. 1: A standard version based solely on the segmented data (bone, teeth and prosthesis).

Model No. 2: A segmented bone-teeth model in which the prosthesis was replaced by the CAD-data from the prosthesis design representing the actual treatment.

Model No. 3: A segmented bone-teeth model in which the prosthesis was replaced by the CAD-based prosthesis design (the same as Model No. 2) but including two additional "dummy screws" (described below) from the surgical pre-operative planning, i.e., the model used in the industrial workflow.

Model No. 4: A further adaptation (described under subsection FEA simulations) that incorporates contact boundary conditions and a more simplified model, closely reflecting the industrial approach.

Here, the term "dummy screw" refers to two screws that were planned to be used during the pre-operative consultation with the clinician but could not be placed intraoperatively due to surgical constraints. Since the industrial workflow (based on pre-operative data) includes these screws, whereas the academic workflow (based on post-operative data) generally does not, both variants were simulated for consistency and comparability. This approach enables a thorough comparison of all models via biomechanical FE analysis.

For Models No. 2, No. 3 and No. 4, the CAD data of the two prosthesis designs were imported into ScanIP and manually aligned with the segmentation using the "position and orientation" tool. Subsequently, the surface deviation between the CAD-based prosthesis and the segmented prosthesis was computed via ScanIP's surface deviation function, which uses sampling points and the closest-point method. This procedure facilitates assessment of the segmentation quality.

2.9. Material Assignment and Meshing

The assignment of material properties proceeded as follows. The mandible was modelled as an isotropic, non-homogeneous, linear elastic material. In this context, "non-homogeneous" indicates that the Young's modulus was computed for each mesh cell based on the corresponding Hounsfield units (HU) from the CT data, with each mesh cell treated as homogeneous at that local scale. All other materials were defined as isotropic, homogeneous and linear elastic. The complete set of material parameters and HU-based mappings can be found in Table 1.

Because no calibration phantom was used, the CT scans were calibrated via linear interpolation between two known data points, as described by Zannoni et al. [38]. Following the approach of Gray et al. [39], the mean radiographic densities of water and air served as reference points. Subsequently, the calibrated CT data were mapped linearly to CT density in accordance with the values presented in Table 1. The Young's modulus for each mesh cell was then calculated by applying the power–law relationship also provided in Table 1.

For the masks representing the teeth, we used the mean values reported in Pinheiro et al. [12] for dentin and enamel, referencing Murphy et al. [40] and Zhou et al. [41]. The distinction between dentin and enamel was established according to the respective HU in

the CT data. For the treatment area of tooth number 43, we assigned the material parameters of enamel, since this region does not influence the FEA outcome and is treated equivalently to healthy tooth structure. The TMJ prostheses were assigned material properties from Pinheiro et al. [12] and Korioth et al. [42]. All material assignments were performed in ScanIP, where the Young's modulus and Poisson's ratio were stored for each mesh cell in the computational grid.

Regarding the meshing strategy, we selected quadratic, ten-node tetrahedral finite elements (C3D10) with straight edges for all masks. Volume meshing was carried out in ScanIP using a coarseness factor of "−10" for all masks. The resultant mesh details are summarized in Table 2. Following the meshing step, all data were exported as input files for the Abaqus CAE/2022 simulation environment (Dassault Systèmes, Vélizy-Villacoublay, France).

The four finite element (FE) models developed and employed in the academic workflow are illustrated in Figure 3. Model 1 was generated solely from segmentation data and served as baseline geometry. Model 4 was specifically developed for contact simulations to better replicate prosthesis–screw–bone interactions. Models 2 and 3 integrated segmented mandibular and dental anatomy with the CAD-based prosthesis: Model 2 corresponds to the finalized clinical treatment scenario, while Model 3 reflects the pre-treatment planning stage, including two additional dummy screws for simulation purposes.

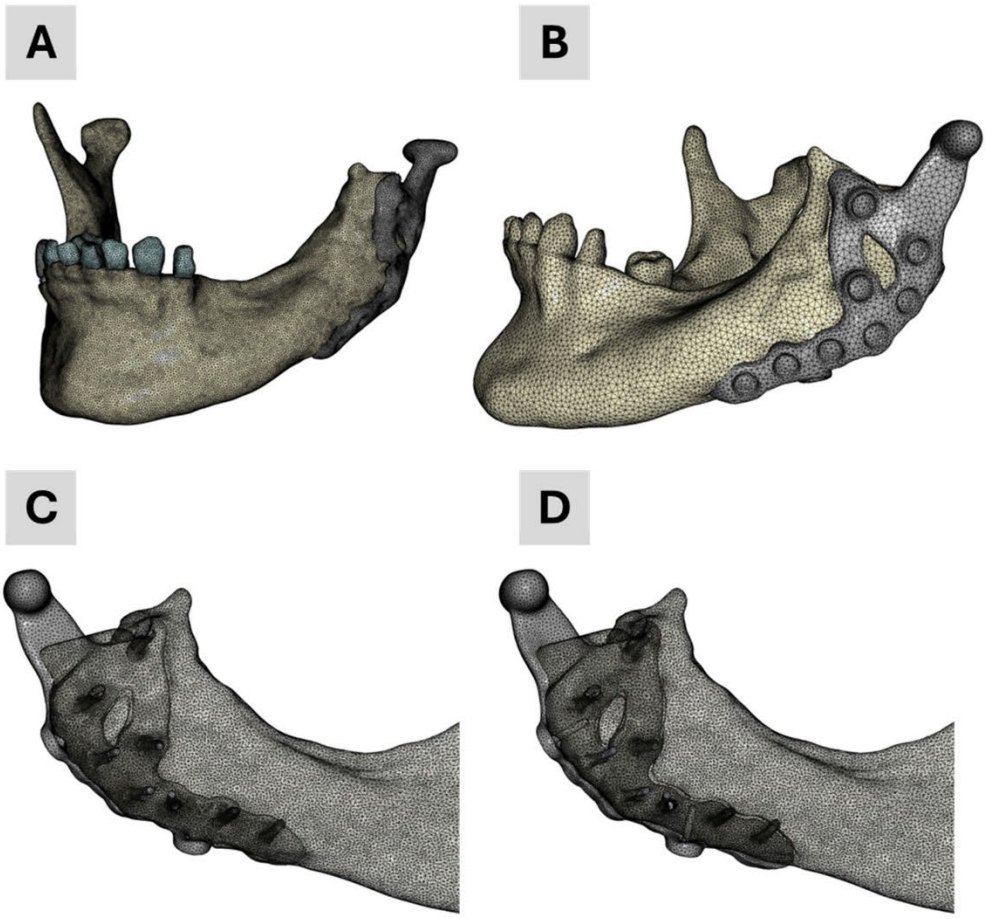

Figure 3. Finite element meshes of the four models used in the academic workflow: (**A**) Model 1—segmentation only; (**B**) Model 4—used for contact simulations; (**C**) Model 2—final treatment model combining segmentation and CAD prosthesis; (**D**) Model 3—planning stage model with two additional dummy screws.

2.10. FEA Simulations

To biomechanically simulate the patient's current treatment, we adopted a simulation workflow previously employed for patient-specific analyses and virtual testing of bone-implant systems [43–45]. In the present work, we partially transferred this established workflow to the patient-specific evaluation of a TMJ prosthesis.

All simulations were performed in Abaqus on a standard workstation (Intel® Core™ i9-9920X CPU @ 3.50 GHz, 128 GB RAM, 64-bit Windows 10 Pro). The simulations were run sequentially in a queue managed by a custom Python script (Abaqus Python 3.7). Result files in the Abaqus output database (odb) format were post-processed with Python-based in-house software. Consistent with the previously cited workflows, contact interactions were initially omitted. This approach is typical in academic workflows, which often rely on segmented datasets that produce large, highly refined meshes. Such fine meshes substantially increase computational time, particularly when the prosthesis is also generated by segmentation. This approach can introduce geometric inaccuracies compared to a CAD-based representation.

Nevertheless, recognizing the importance of contact conditions on the biomechanical performance of TMJ prostheses, we conducted two additional simulations mirroring the industrial workflow: one with contact and one without. To reduce computational expense, we created a simplified mesh by merging the mandible and all teeth into a single mask and assigning a uniform elastic modulus of 10 GPa. This simplified model, introduced above as Model No. 4, was derived from the CAD representation of the prosthesis, including the two dummy screws.

In the contact simulation, "surface-to-surface contact" was specified in Abaqus, with a friction coefficient of 0.3 [46] for tangential behavior and "hard contact" for normal behavior. The contact surfaces were automatically generated in ScanIP and exported via the Abaqus input file. Figure 4 depicts the results from these two simulations, illustrating the potential influence of contact interactions on the overall biomechanical analysis.

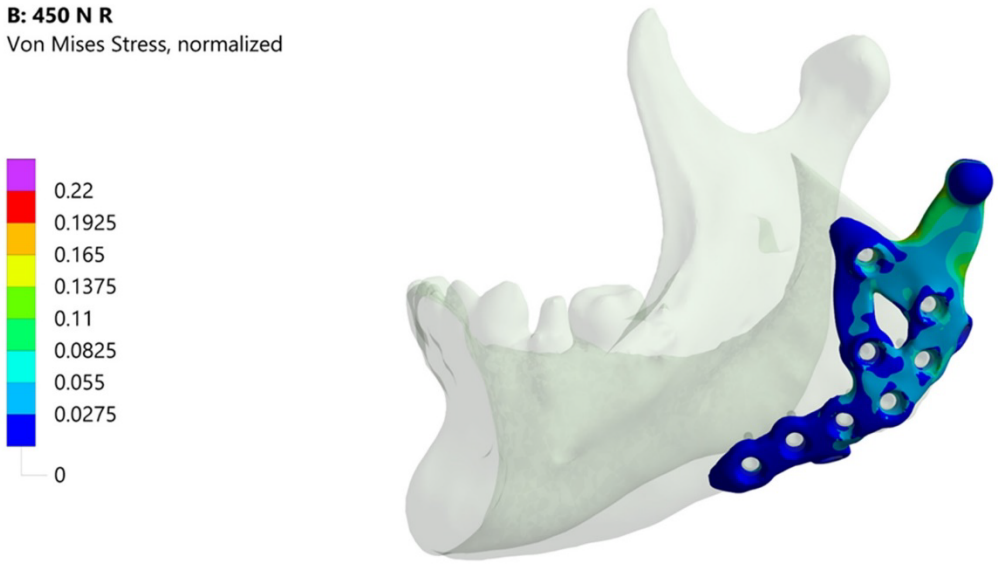

Figure 4. *Cont.*

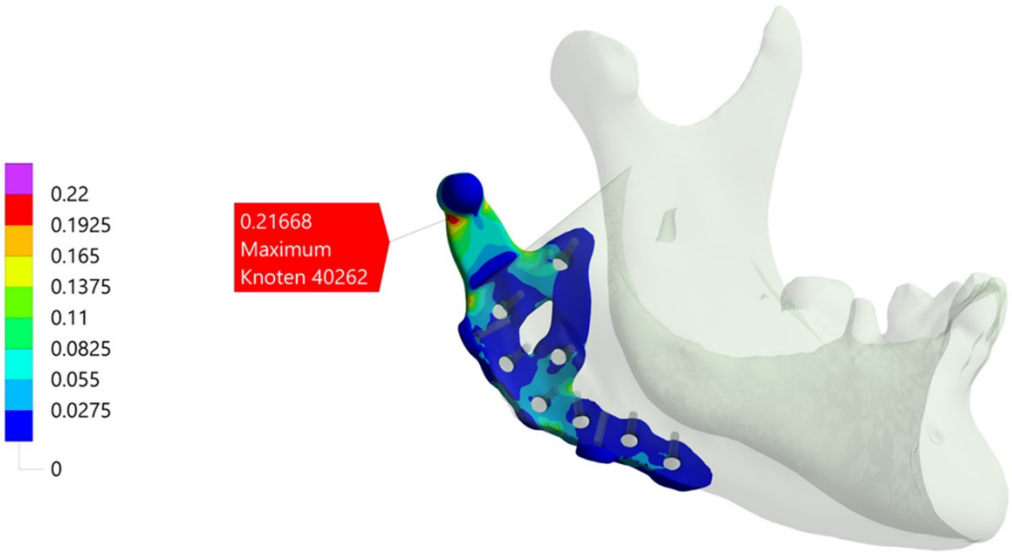

Figure 4. Illustration of the simulation result of the industrial workflow. The images show the normalized von Mises stress distribution of the prosthesis for the given molar bite force.

3. Results

3.1. Mechanical Testing

Figure 5 shows the average wear rate recorded during testing. The graph shows a peak for both components after the first 500,000 cycles, followed by a decrease. These results align with general findings that indicate a "running-in" phase, followed by a "steady-state" phase [47]. Calculating the volume loss based on the number of cycles results in a wear of 0.624 $mm^3/10^6$ cycles for the fossa components and 0.0688 $mm^3/10^6$ cycles for the condyle component. The results for the fossa component are similar to the volume losses found in comparable devices, such as the fossa component of the Groningen prosthesis (0.65 mm^3/year) [48,49]. However, the results for the condyle component are less comparable due to a lack of data on the wear of metal components in total joint replacements. Therefore, the results are compared to metal-on-metal pairings in hip prostheses, which showed wear between 0.24 $mm^3/10^6$ cycles and 1.84 $mm^3/10^6$ cycles [50]. In both cases, the custom-made TMJ prosthesis demonstrated wear rates below those of other total joint replacements.

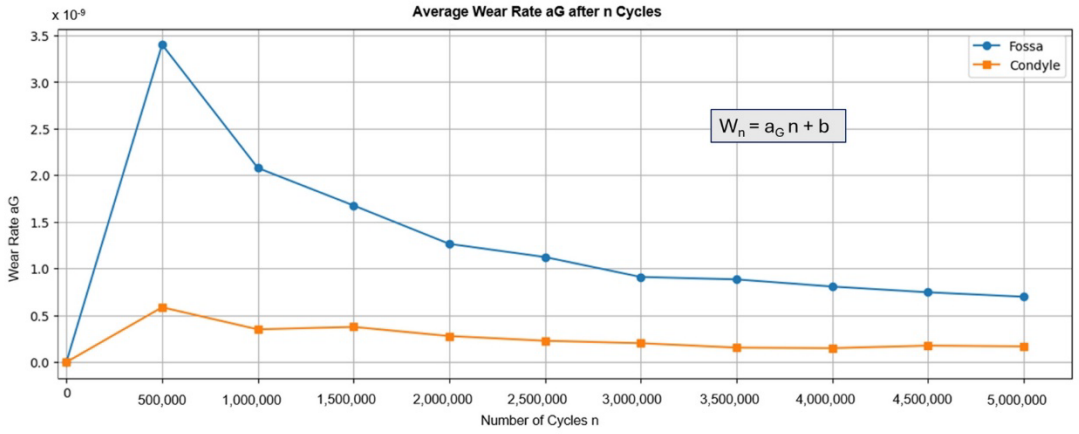

Figure 5. Graph displaying the average wear rate of the fossa and condyle components during wear testing in steps of 500,000 cycles. The wear rate was calculated according to ISO 14243-2, chapter 4.6.5. Here, W_n is the net loss in mass after n cycles and b is a constant.

In the static compression test, no differences were observed between scans before and after testing, indicating no deformation in the implants, with only minimal deformation observed in the fossa. The maximum loads reached 1540 N on average. Failure occurred in the tested samples due to screws being pulled out of the polyamide jaw at the maximum loading of the test setup, not due to damage to the implant itself. Figure 6A illustrates the typical load case, Figure 6B,C show a before/after comparison for the worst case of the Fossa component (B) and the Condyle component (C). For both components, the deviation of the surface area stays below 0.3 mm. The Fossa component (B) has a slight indentation at the point where the condyle was pressed into it. The condyle component does not show any deformation from the compression test. Overall, the results demonstrate the robustness and wear resistance of the custom-made TMJ prosthesis compared to other devices.

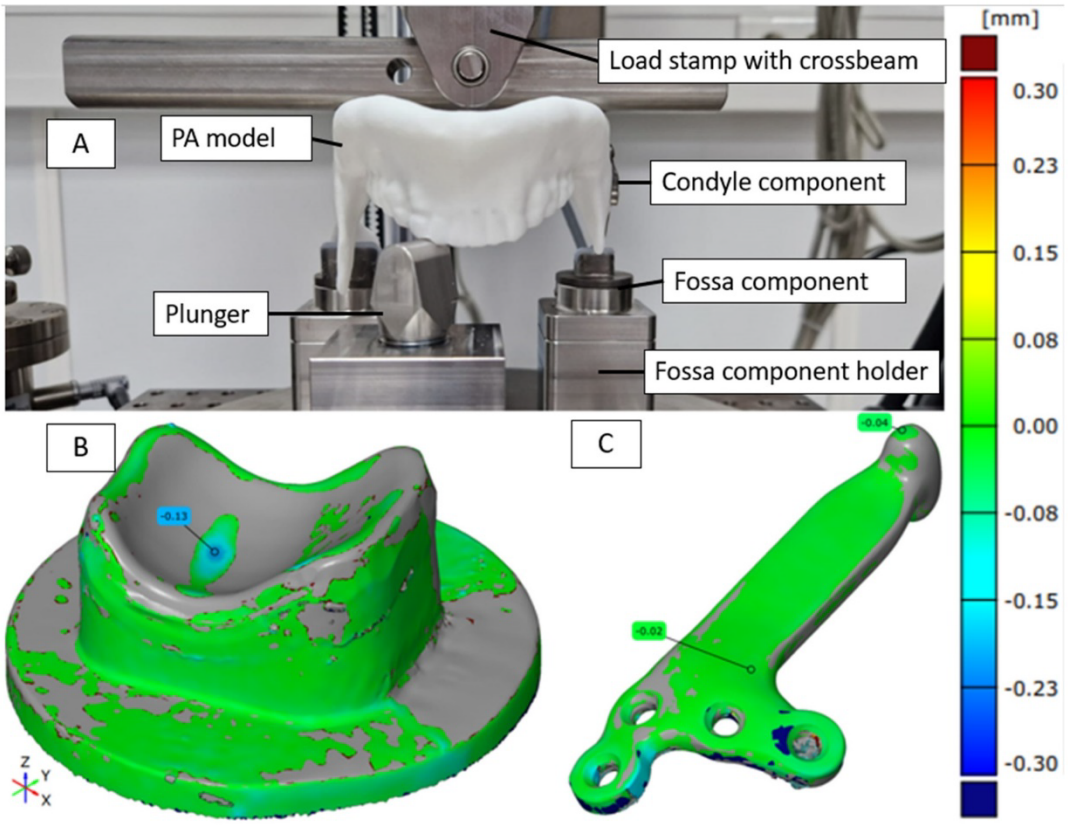

Figure 6. Illustration of the static compression test of the TMJ prosthesis by KLS Martin. (**A**) The test setup used for the compression test. (**B**,**C**) An example of a comparison of the surface of a fossa (**B**) and condyle (**C**) component before and after loading.

3.2. Segmentation and 3D Geometric Model Generation

Figure 1 presents the segmentation results from both workflows. Figure 1A shows a threshold-based representation of the 3D tomogram to provide an overview of the patient situation after surgery. Figure 1B–D display the results of the academic workflow, whereas Figure 1E,F show the industrial workflow. In Figure 1B, a lateral view of the segmentation is depicted, while Figure 1C,D show an anterior view of the 3D model. Figure 1D is partially transparent to highlight the segmented teeth and screws. Figure 1E depicts the segmentation result from the industrial workflow alongside the generated CAD data of the planned treatment. Finally, Figure 1F provides an overview of this planned treatment.

A direct comparison of the segmented mandible bones was omitted because different software systems and masks were used. For a valid comparison, the segmented masks in the academic workflow would have to be converted into STL surfaces to align with the STL data

from the industrial segmentation. However, especially for small structures such as teeth, artifacts and minor errors occur during file conversion, affecting the results. Consequently, no comparison was conducted for the segmented bones. Instead, as described below, the focus was on comparing the TMJ prosthesis.

Figure 7 displays the segmentation results for the TMJ prosthesis. Figure 7A,B show the prosthesis based on the CAD data from the surgical planning provided by the industrial partner. Figure 7C illustrates the corresponding segmentation outcome in the academic workflow, which captures the prosthesis geometry reasonably well, despite minor artifacts. Figure 7D shows the same model after applying recursive Gaussian smoothing with an isotropic value of 1.5 pixels. Although smoothing reduces artifacts, it introduces new challenges for the segmented screws. Because the screws in this application are relatively small (in this study, the voxel size is 0.3 mm^3, and thus each screw consists of only a few voxels), even adding or removing one or two voxels becomes visibly significant in the 3D model. Consequently, recursive Gaussian smoothing was not applied to preserve the screws. Figure 7E shows the screws on the back side of Figure 7C. This configuration was used for Model No. 1 in the academic workflow, with each screw visually inspected and manually refined when needed. Another difference between the CAD-based surgical planning and the segmented TMJ prosthesis is as explained above the presence of two so-called "dummy screws" in the planning (Figure 7B) and their absence in Figure 6E.

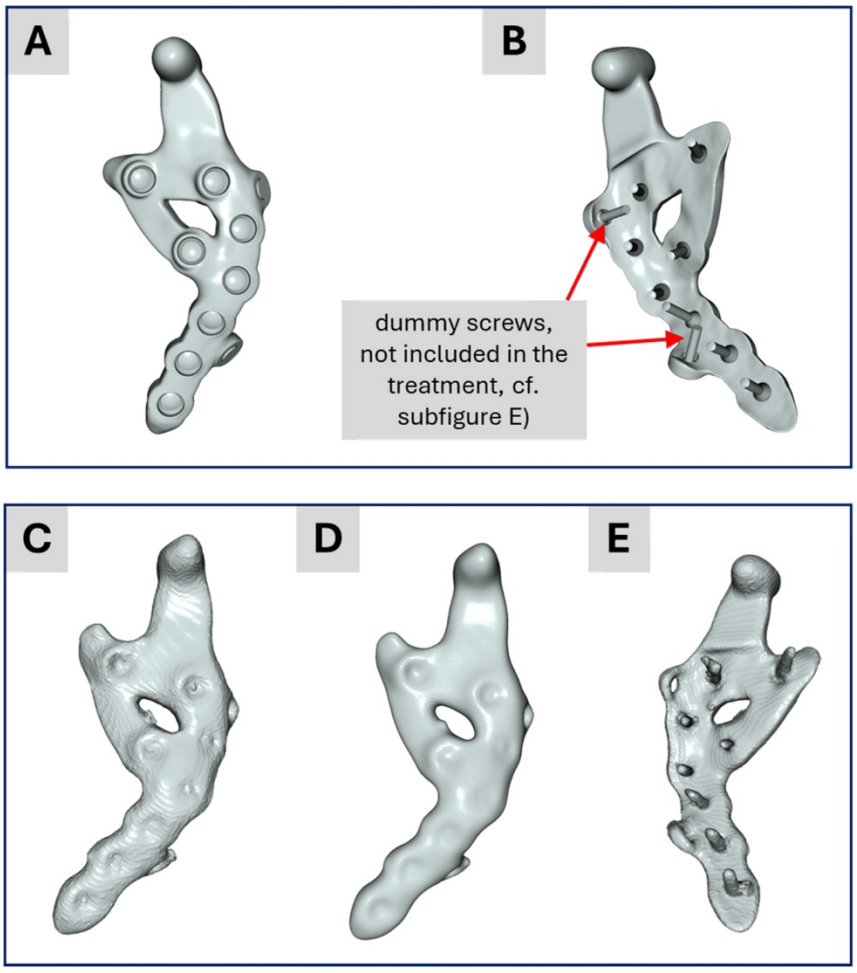

Figure 7. (**A**,**B**) Illustration of the CAD data representing the custom-made implant. (**C**) Result of the academic segmentation process for the implant. (**D**) Implant from (**C**) after applying a recursive Gaussian smoothing. (**E**) Backside of the segmented implant from (**C**).

Figure 8 presents the distance map (in millimeters) between the CAD data of the TMJ prosthesis and its segmented counterpart, visualized on the CAD model. The distances are mostly below 1 mm, with the greatest deviations around the two dummy screws, which are only present in the CAD data but not in the current treatment. These small discrepancies indicate that the segmentation results are largely accurate, consistent with the similarity observed in the subsequent simulation outcomes.

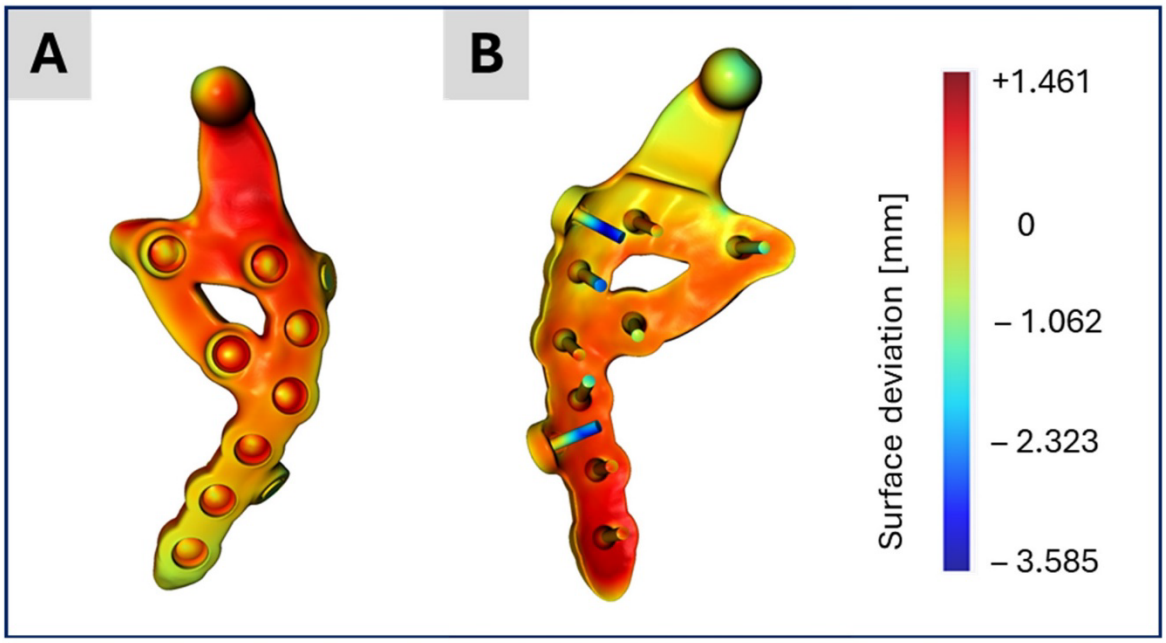

Figure 8. Illustration of the surface deviation in millimeter of the CAD-based TMJ prosthesis after their placement on the segmented TMJ prosthesis in the CT image stack. The highest differences are at the two dummy screws which are of course missing in the segmented TMJ prosthesis. (**A**) shows the lateral view on the prosthesis and (**B**) the backside and the screws.

3.3. Biomechanical FE Simulations

The industrial partners in this study normalize their simulation results against an in-house material limit, specified in MPa and calculated as von Mises stress. This material limit incorporates requirements for the selected material, the manufacturing process and a safety factor. Because these details are proprietary, all academic workflow results are normalized relative to the industrial workflow's maximum stress value, without disclosing the latter.

Figure 9 shows the academic workflow's simulation results. Figure 9A illustrates the outcome for the fully segmented model, exhibiting a normalized maximum von Mises stress of approximately 1.20, about 20 percent above the industrial workflow reference. This maximum is also roughly 10 percent higher than those seen in the two other academic simulations, highlighting differences between a segmented representation of the treatment and its CAD-based version.

Figure 9B,C both show maxima of around 1.11 and 1.09, respectively. The slight variation mainly arises from differences in mesh generation and the manual alignment of the prosthesis. These results also indicate that the two dummy screws present only in the planning phase have no relevant impact on the performance of this custom-made TMJ prosthesis. All three academic models display their maximum stress at the same prosthesis location for the analysed molar bite force.

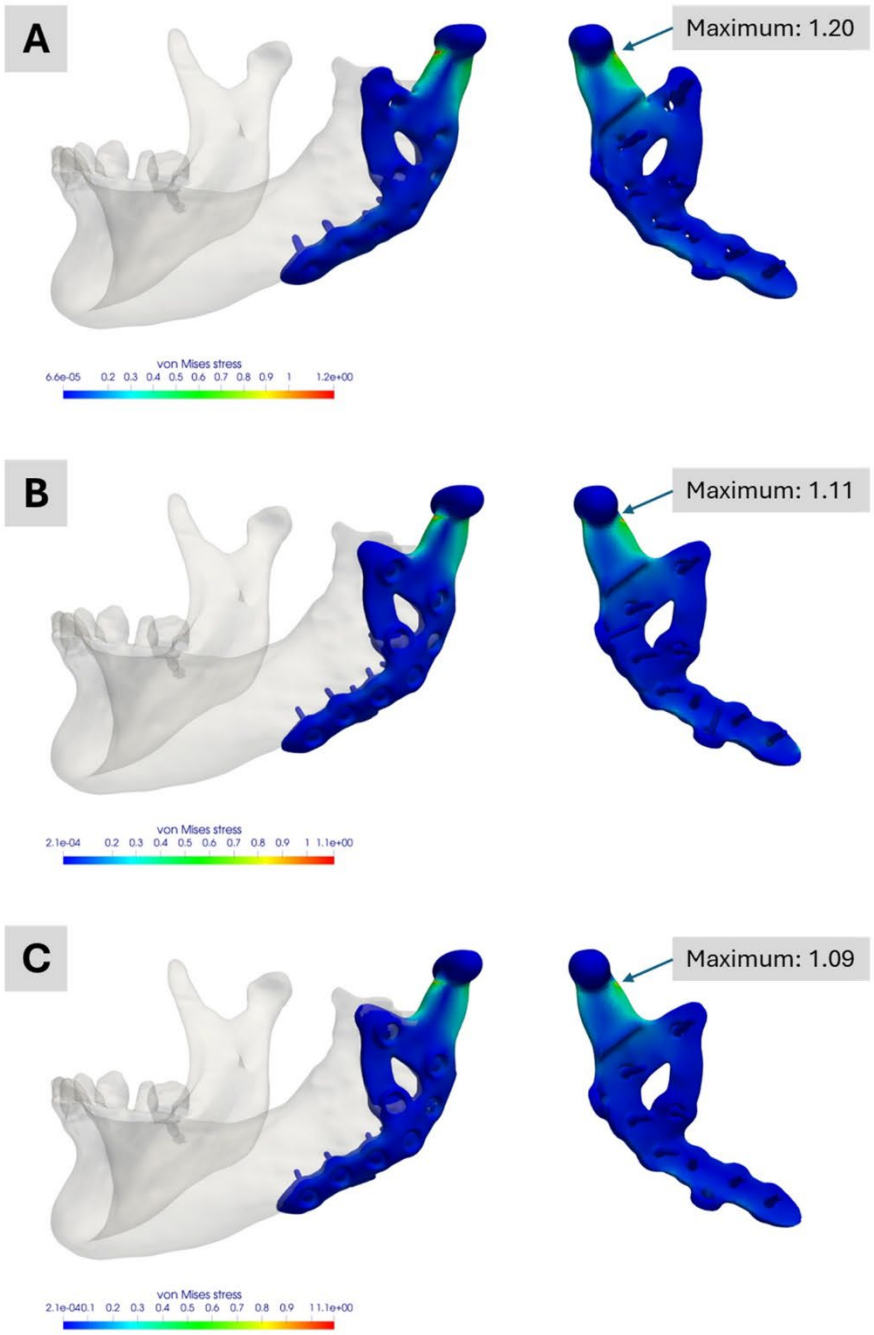

Figure 9. Simulation results of the Models No. 1, No. 2 and No. 3 in the academic workflow. (**A**) Model No. 1 based on the segmentation results. (**B**) Model No. 2 combining segmentation and CAD data of the prosthesis for real treatment. (**C**) Model No. 3 combining segmentation and CAD data of the prosthesis with the two additional screws. All images show the von Mises stress distribution of the prosthesis for the considered molar bite force.

Figure 4 presents the industrial workflow's simulation results. Under the specified boundary conditions, about one-fifth of the material limit is reached. Notably, the maximum stress region differs from that observed in the academic workflow simulations, partly due to how boundary conditions are applied. In the industrial workflow, they are derived from a corresponding model, whereas in the academic workflow, muscle attachment sites must be manually defined in ScanIP or Abaqus. Additionally, minor differences in the coordinate systems of the various software platforms may contribute to these deviations.

Figure 10 compares simulations with and without contact conditions between the prosthesis and the mandible for the simplified version Model No. 4. When contact conditions are excluded (Figure 10A), slightly higher peak stresses are observed. Including contact (Figure 10B) reduces the peak stress by nearly 9 percent. Although this difference is small in the current application, it may be significant in other scenarios. Decisions regarding whether to include contact conditions should thus be made on a case-by-case basis.

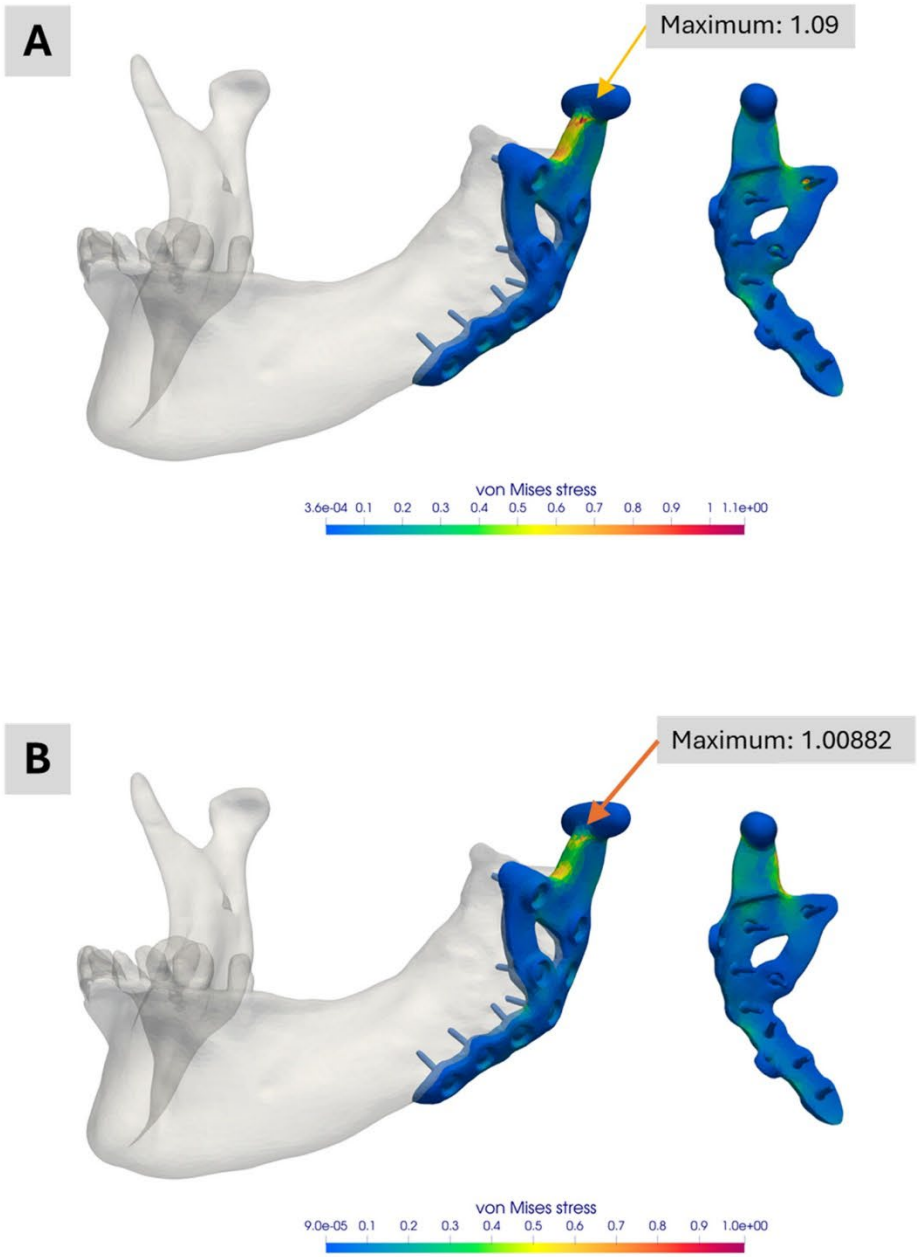

Figure 10. Illustration of the simulation result comparing the influence of contact conditions between prosthesis and mandibular. (**A**) Normalized von Mises stress distribution for the simplified version of Model 3 without contact conditions. (**B**) Normalized von Mises stress distribution for the same model with contact conditions. In the case of contact conditions, the peak stress is almost 9 percent lower.

4. Discussion

This study demonstrates that two simulation workflows, each relying on different preconditions and assumptions, can nevertheless yield comparable results. The observed

differences can be explained by the different assumptions made in each workflow, highlighting opportunities for future investigations.

A key factor affecting the academic workflow's outcomes, as noted by Pinheiro et al. [12], is the absence of a dedicated material mapping law for the mandible in literature. We therefore adopted the material mapping introduced by Pinheiro and colleagues. Although their choice is well-reasoned, addressing this limitation would require extensive experimental work, which lies beyond the scope of the current study. This issue is closely linked to the industrial workflow's use of a single set of material parameters; indeed, differences in the level of detail for bone stiffness likely contribute to the observed variations.

Another closely related aspect is the segmentation process itself, which is subject to error. As Irshad et al. [51] showed, repeated segmentation may yield inconsistent results, and outcomes can also depend on the software employed. Moreover, boundary conditions could potentially be enhanced by using alternative meshing techniques, such as iso-topological meshes [52], which were not part of either workflow here but may offer advantages in future studies.

Further consideration is the handling of contact between the prosthesis and screws, and between the prosthesis and bone. In the academic workflow, no contact was defined, as such a distinction is not feasible when both prosthesis and screws are purely segmented. By contrast, in the industrial workflow, contact conditions are included, leading to a more realistic stress distribution.

The manual alignment of the 3D prostheses also affects the results. Minor deviations arise both within the academic workflow (across different models) and between the academic and industrial workflows. In addition, small discrepancies exist between the planned prosthesis positioning and its actual intraoperative placement, particularly for the screws and their insertion angles. These deviations from the ideal 3D CAD model are unavoidable in surgery but were found to have only a minimal impact on the simulation outcome, as illustrated by the simulations in the academic workflow. They also confirm that excluding the two unused "dummy screws" has little influence on the peak stress.

In addition to these technical considerations, our findings have important implications for patient care and the future design of TMJ prostheses. First, the simulation-based approach presented here can enhance clinical outcomes by enabling more personalized treatment strategies. By providing a detailed, patient-specific biomechanical analysis, such methods have the potential to optimize implant design for individual anatomical variations, potentially reducing surgical time and minimizing post-operative complications.

Moreover, the retrospective simulation method offers a valuable tool for future design improvements. It allows researchers and clinicians to evaluate the performance of prosthesis designs using post-operative data, thereby identifying design limitations and areas for enhancement that may not be apparent during pre-operative planning. This retrospective analysis also enables academic groups to develop and test alternative designs independently, without relying on proprietary CAD data from manufacturers. While this independence can spur innovation by fostering novel design approaches, it also carries certain risks. For instance, designs developed solely through academic simulation may not fully consider manufacturing constraints or regulatory requirements and therefore must be rigorously validated before clinical adoption.

While our study is based on a single clinical case, we view this work as a proof-of-concept that establishes the feasibility of comparing simulation workflows in TMJ replacement. The patient included in this report was specifically selected because she underwent a unilateral TMJ replacement with comprehensive pre- and post-operative imaging data. Moreover, she was one of the first patients to receive a customized TMJ prosthesis, limiting our ability to increase the number of cases at this stage. The limited number of cases

restricts the generalizability of our findings, and we acknowledge that further validation with a larger cohort is required to statistically substantiate these preliminary results. In the future, we plan to conduct a simulation-based study involving a larger patient cohort, allowing for statistical analysis and improved generalizability. Nevertheless, the insights gained from this single-case comparison offer valuable guidance for refining simulation models and identifying key design parameters that could influence prosthesis performance.

5. Conclusions

This study demonstrates that academic and industrial simulation workflows for TMJ prostheses, despite differing in data sources, assumptions and timing, can yield comparable biomechanical outcomes. The academic workflow, relying solely on retrospective, image-based modelling, was able to reproduce key features of the industrial, pre-operative CAD-driven process. Differences observed between workflows were primarily due to variations in material assumptions, segmentation detail and modelling of contact conditions.

In terms of clinical significance, our findings suggest that simulation-based approaches have the potential to enhance patient care by enabling personalized treatment strategies for TMJ replacement. A detailed, patient-specific biomechanical analysis can help optimize implant design to match individual anatomical and functional requirements, potentially reducing surgery time and minimizing post-operative complications. Moreover, the retrospective simulation method offers a means to refine prosthesis designs based on real-world clinical outcomes, complementing the manufacturer-based pre-operative planning process. However, it is important to recognize that while academic-driven simulation models provide an independent avenue for innovation, they also carry risks if designs are developed without fully integrating manufacturing constraints or regulatory requirements. Therefore, rigorous validation and collaboration with industry partners remain essential for the successful clinical translation of these findings.

Overall, our results underscore the potential of simulation-based methodologies to drive future improvements in TMJ prosthesis design and ultimately enhance clinical outcomes. Future studies with a larger patient cohort will be critical to further explore these parameters and validate the clinical applicability of our simulation approaches. Nevertheless, our results suggest that simulation-based approaches have the potential to enhance clinical outcomes by enabling more personalized treatment strategies and improving the design of custom-made TMJ prostheses.

Author Contributions: A.A.: writing-original draft, writing-review and editing, conceptualization, data curation, simulation and methodology (academic workflow); K.W.: writing-original draft, writing-review and editing, conceptualization, data curation, simulation and methodology (academic workflow); E.G.: writing-original draft, writing-review and editing, conceptualization, data curation, simulation and methodology (industrial workflow); F.B.: writing-original draft, writing-review and editing, conceptualization, data curation, methodology and mechanical experiments (industrial workflow); S.D.: funding acquisition and writing–review and editing; M.R.: writing-original draft, writing-review and editing, general concept, conceptualization, visualization and project administration. All authors have read and agreed to the published version of the manuscript.

Funding: This study was partly financed by Saarland University through on-board budget and partly by KLS Martin SE & Co. KG from in-house funding for research and development. Furthermore, the study was also partly funded by the German Federal Ministry of Education and Research under the grant FKZ:13GW0572.

Informed Consent Statement: Written informed consent was obtained for anonymized patient information to be used and published. This retrospective study did not have any influence on patient treatment and was performed after treatment was completed.

Data Availability Statement: The original contributions presented in the study are included in the article, further inquiries can be directed to the corresponding author. Researchers who wish to request access to data should send an email, with a clear indication of the research purpose. Every request must be reviewed by the responsible institutional review boards, considering the risk of patient reidentification and the compliance with the applicable data protection rules.

Acknowledgments: The authors thank Philippe Korn and the MHH (Medizinische Hochschule Hannover) for providing the used patient data, his feedback and expert knowledge on the case.

Conflicts of Interest: The authors E.G. and F.B. are employees of KLS Martin SE & Co. KG, and therefore, they have received/will receive benefits for personal or professional use from KLS Martin SE & Co. KG related directly or indirectly to the subject of this manuscript. A.A., K.W., S.D. and M.R. declare that the research was conducted in the absence of any commercial or financial relationships that could be construed as a potential conflict of interest.

References

1. Sidebottom, A.J.; Gruber, E. One-year prospective outcome analysis and complications following total replacement of the temporomandibular joint with the TMJ Concepts system. *Br. J. Oral Maxillofac. Surg.* **2013**, *51*, 620–624. [CrossRef] [PubMed]
2. Guarda-Nardini, L.; Manfredini, D.; Ferronato, G. Total temporomandibular joint replacement: A clinical case with a proposal for post-surgical rehabilitation. *J. Craniomaxillofac. Surg.* **2008**, *36*, 403–409. [CrossRef] [PubMed]
3. Yadav, P.; Roychoudhury, A.; Kumar, R.D.; Bhutia, O.; Bhutia, T.; Aggarwal, B. Total Alloplastic Temporomandibular Joint Replacement. *J. Maxillofac. Oral Surg.* **2021**, *20*, 515–526. [CrossRef]
4. Briceño, F.; Ayala, R.; Delgado, K.; Piñango, S. Evaluation of temporomandibular joint total replacement with alloplastic prosthesis: Observational study of 27 patients. *Craniomaxillofac. Trauma Reconstr.* **2013**, *6*, 171–178. [CrossRef]
5. Kiliaridis, S.; Engström, C.; Thilander, B. The relationship between masticatory function and craniofacial morphology. I. A cephalometric longitudinal analysis in the growing rat fed a soft diet. *Eur. J. Orthod.* **1985**, *7*, 273–283. [CrossRef]
6. Tanaka, E.; Detamore, M.S.; Mercuri, L.G. Degenerative disorders of the temporomandibular joint: Etiology, diagnosis, and treatment. *J. Dent. Res.* **2008**, *87*, 296–307. [CrossRef]
7. Mercuri, L.G. Alloplastic temporomandibular joint reconstruction. *Oral Surg. Oral Med. Oral Pathol. Oral Radiol. Endod.* **1998**, *85*, 631–637. [CrossRef]
8. Rodrigues, Y.L.; Mathew, M.T.; Mercuri, L.G.; da Silva, J.S.P.; Henriques, B.; Souza, J.C.M. Biomechanical simulation of temporomandibular joint replacement (TMJR) devices: A scoping review of the finite element method. *Int. J. Oral Maxillofac. Surg.* **2018**, *47*, 1032–1042. [CrossRef]
9. Mercuri, L.G. Considering Total Temporomandibular Joint Replacement. *Cranio* **1999**, *17*, 44–48. [CrossRef]
10. Ingawale, S.M.; Goswani, T. Design and Finite Element Analysis of Patient-Specific Total Temporomandibular Joint Implants. *Materials* **2022**, *15*, 4342. [CrossRef]
11. Yoon, H.-J.; Baltali, E.; Zhao, K.D.; Rebellato, J.; Kademani, D.; An, K.-N.; Keller, E.E. Kinematic Study of the Temporomandibular Joint in Normal Subjects and Patients Following Unilateral Temporomandibular Joint Arthrotomy with Metal Fossa-Eminence Partial Joint Replacement. *J. Oral Maxillofac. Surg.* **2007**, *65*, 1569–1576. [CrossRef] [PubMed]
12. Pinheiro, M.; Willaert, R.; Khan, A.; Krairi, A.; van Paepegem, W. Biomechanical evaluation of the human mandible after temporomandibular joint replacement under different biting conditions. *Sci. Rep.* **2021**, *11*, 14034. [CrossRef] [PubMed]
13. Bhargava, D.; Neelakandan, R.S.; Dalsingh, V.; Sharma, Y.; Pandey, A.; Pandey, A.; Beena, S.; Koneru, G. A three dimensional (3D) musculoskeletal finite element analysis of DARSN temporomandibular joint (TMJ) prosthesis for total unilateral alloplastic joint replacement. *J. Stomatol. Oral Maxillofac. Surg.* **2019**, *120*, 517–522. [CrossRef] [PubMed]
14. Ackland, D.C.; Moskaljuk, A.; Hart, C.; Lee, P.V.S.; Dimitroulis, G. Prosthesis Loading After Temporomandibular Joint Replacement Surgery: A Musculoskeletal Modeling Study. *J. Biomech. Eng.* **2015**, *137*, 041001. [CrossRef]
15. Ryu, J.; Cho, J.; Kim, H.M. Bilateral Temporomandibular Joint Replacement Using Computer-Assisted Surgical Simulation and Three-Dimensional Printing. *J. Craniofac. Surg.* **2016**, *27*, e450–e452. [CrossRef]
16. Henke, P.; Ruehrmund, L.; Bader, R.; Kebbach, M. Exploration of the Advanced VIVOTM Joint Simulator: An In-Depth Analysis of Opportunities and Limitations Demonstrated by the Artificial Knee Joint. *Bioengineering* **2024**, *11*, 178. [CrossRef]
17. Cuevas-Andrade, J.L.; Beltrán-Fernández, J.A.; Hermida-Ochoa, J.C.; Rebattú y González, M.G.; Hernández-Gómez, L.H.; Uribe-Cortés, T.B.; Trujillo-Pérez, C.A.; Moreno-Garibaldi, P. Dynamic and Experimental Testing of a Biomechanical System: Cadaveric Temporomandibular Specimen and a Multiaxial Joint. In *Engineering Design Applications V.*; Öchsner, A., Altenbach, H., Eds.; Springer: Cham, Switzerland, 2023; pp. 251–280. [CrossRef]

18. Mazzocco, A.G.; Jardini, A.L.; Nunes, E.L.; Filho, R.M. Custom-made Temporomandibular Joint Mechanical Simulation: Different Fixation Pattern. In Proceedings of the Computer Aided Chemical Engineering, 30th European Symposium on Computer Aided Process Engineering, Milano, Italy, 31 August–2 September 2020; Pierucci, S., Manenti, F., Bozzano, G.L., Manca, D., Eds.; Elsevier: Amsterdam, The Netherlands, 2020; pp. 535–540. [CrossRef]
19. Mercuri, L.G. Custom TMJ TJR Devices. In *Temporomandibular Joint Total Joint Replacement—TMJ TJR*; Mercuri, L.G., Ed.; Springer: Cham, Switzerland, 2016. [CrossRef]
20. Andriole, K.P.; Morin, R.L. Transforming medical imaging: The first SCAR TRIP conference a position paper from the SCAR TRIP subcommittee of the SCAR research and development committee. *J. Digit. Imaging.* **2006**, *19*, 6–16. [CrossRef]
21. Lemons, J.E. Biomaterials and Orthopedic Considerations for Endoprostheses. *Oral Maxillofac. Surg. Clin. N. Am.* **2015**, *12*, 43–55. [CrossRef]
22. Shibata, Y.; Tanimoto, Y.; Maruyama, N.; Nagakura, M. A review of improved fixation methods for dental implants. Part II: Biomechanical integrity at bone–implant interface. *J. Prosthodont. Res.* **2015**, *59*, 84–95. [CrossRef]
23. Sam Froes, F.H.; Qian, M. *Titanium in Medical and Dental Applications*, 1st ed.; Elsevier: Amsterdam, The Netherlands, 2018.
24. de Zee, M.; Dalstra, M.; Cattaneo, P.M.; Rasmussen, J.; Svensson, P.; Melsen, B. Validation of a musculo-skeletal model of the mandible and its application to mandibular distraction osteogenesis. *J. Biomech.* **2007**, *40*, 1192–1201. [CrossRef]
25. Koolstra, J.H.; van Eijden, T.M.G.J. Combined finite-element and rigid-body analysis of human jaw joint dynamics. *J. Biomech.* **2005**, *38*, 2431–2439. [CrossRef] [PubMed]
26. Ferrario, V.F.; Sforza, C.; Zanotti, G.; Tartaglia, G.M. Maximal bite forces in healthy young adults as predicted by surface electromyography. *J. Dent.* **2004**, *32*, 451–457. [CrossRef] [PubMed]
27. Woodford, S.C.; Robinson, D.L.; Abduo, J.; Lee, P.V.S.; Ackland, D.C. Muscle and joint mechanics during maximum force biting following total temporomandibular joint replacement surgery. *Biomech. Model Mechanobiol.* **2024**, *23*, 809–823. [CrossRef]
28. Waltimo, A.; Nyström, M.; Könönen, M. Bite force and dentofacial morphology in men with severe dental attrition. *Scand. J. Dent. Res.* **1994**, *102*, 92–96. [CrossRef]
29. Inzana, J.A.; Varga, P.; Windolf, M. Implicit modeling of screw threads for efficient finite element analysis of complex bone-implant systems. *J. Biomech.* **2016**, *49*, 1836–1844. [CrossRef]
30. MacLeod, A.R.; Pankaj, P.; Simpson, A.H. Does screw-bone interface modelling matter in finite element analyses? *J. Biomech.* **2012**, *45*, 1712–1716. [CrossRef]
31. Gallo, L.M. Analyse der Biomechanik des Kiefergelenks. *Die MKG-Chir.* **2016**, *9*, 155–166. [CrossRef]
32. Iwasaki, L.R.; Gonzalez, Y.M.; Liu, Y.; Liu, H.; Markova, M.; Gallo, L.M.; Nickel, J.C. TMJ energy densities in healthy men and women. *Osteoarthr. Cartil.* **2017**, *25*, 846–849. [CrossRef]
33. Maintz, M.; Msallem, B.; de Wild, M.; Seiler, D.; Herrmann, S.; Feiler, S.; Sharma, N.; Dalcanale, F.; Cattin, P.; Thieringer, F.M. Parameter optimization in a finite element mandibular fracture fixation model using the design of experiments approach. *J. Mech. Behav. Biomed. Mater.* **2023**, *144*, 105948. [CrossRef]
34. Shash, Y.H. Mandibular biomechanics rehabilitated with different prosthetic restorations under normal and impact loading scenarios. *BMC Oral Health.* **2024**, *24*, 946. [CrossRef]
35. Mesnard, M.; Ramos, A. Experimental and numerical predictions of Biomet® alloplastic implant in a cadaveric mandibular ramus. *J. Craniomaxillofac. Surg.* **2016**, *44*, 608–615. [CrossRef] [PubMed]
36. Dowgierd, K.; Kawlewska, E.; Joszko, K.; Kropiwnicki, J.; Wolanski, W. Biomechanical Evaluation of Temporomandibular Joint Reconstruction Using Individual TMJ Prosthesis Combined with a Fibular Free Flap in a Pediatric Patient. *Bioengineering* **2023**, *10*, 541. [CrossRef] [PubMed]
37. Gateno, J.; Cookston, C.; Hsu, S.; Stal, D.; Durrant, S.; Gold, J.; Ismaily, S.; Alexander, J.; Noble, P.; Xia, J. Biomechanical Evaluation of a New MatrixMandible Plating System on Cadaver Mandibles. *J. Oral Maxillofac. Surg.* **2013**, *71*, 1900–1914. [CrossRef]
38. Zannoni, C.; Mantovani, R.; Viceconti, M. Material properties assignment to finite element models of bone structures: A new method. *Med. Eng. Phys.* **1998**, *20*, 735–740. [CrossRef]
39. Gray, H.A.; Taddei, F.; Zavatsky, A.B.; Cristofolini, L.; Gill, H.S. Experimental Validation of a Finite Element Model of a Human Cadaveric Tibia. *J. Biomech. Eng.* **2008**, *130*, 031016. [CrossRef]
40. Murphy, W.; Black, J.; Hastings, G. *Handbook of Biomaterial Properties*; Springer: Berlin/Heidelberg, Germany, 2016. [CrossRef]
41. Zhou, Z.-R.; Yu, H.-Y.; Zheng, J.; Qian, L.-M.; Yan, Y. *Dental Biotribology*; Springer: Berlin/Heidelberg, Germany, 2013. [CrossRef]
42. Korioth, T.W.; Hannam, A.G. Deformation of the human mandible during simulated tooth clenching. *J. Dent. Res.* **1994**, *73*, 56–66. [CrossRef]
43. Braun, B.J.; Orth, M.; Diebels, S.; Wickert, K.; Andres, A.; Gawlitza, J.; Bücker, A.; Pohlemann, T.; Roland, M. Individualized Determination of the Mechanical Fracture Environment After Tibial Exchange Nailing-A Simulation-Based Feasibility Study. *Front. Surg.* **2021**, *8*, 749209. [CrossRef]

44. Orth, M.; Ganse, B.; Andres, A.; Wickert, K.; Warmerdam, E.; Müller, M.; Diebels, S.; Roland, M.; Pohlemann, T. Simulation-based prediction of bone healing and treatment recommendations for lower leg fractures: Effects of motion, weight-bearing and fibular mechanics. *Front. Bioeng. Biotechnol.* **2023**, *11*, 1067845. [CrossRef]
45. Wickert, K.; Roland, M.; Andres, A.; Diebels, S.; Ganse, B.; Kerner, D.; Frenzel, F.; Tschernig, T.; Ernst, M.; Windolf, M.; et al. Experimental and virtual testing of bone-implant systems equipped with the AO Fracture Monitor with regard to interfragmentary movement. *Front. Bioeng. Biotechnol.* **2024**, *12*, 1370837. [CrossRef]
46. Eberle, S.; Göttlinger, M.; Augat, P. An investigation to determine if a single validated density-elasticity relationship can be used for subject specific finite element analyses of human long bones. *Med. Eng. Phys.* **2013**, *35*, 875–883. [CrossRef]
47. Heisel, C.; Streich, N.; Krachler, M.; Jakubowitz, E.; Kretzer, J.P. Characterization of the running-in period in total hip resurfacing arthroplasty: An in vivo and in vitro metal ion analysis. *J. Bone Jt. Surg. Am.* **2008**, *90*, 125–133. [CrossRef] [PubMed]
48. van Loon, J.P. *The Groningen Temporomandibular Joint Prosthesis*; Groningen Rijksuniversiteit: Groningen, The Netherlands, 1999.
49. van Loon, J.P.; de Bont, L.G.; Stegenga, B.; Spijkervet, F.K.; Verkerke, G.J. Groningen temporomandibular joint prosthesis. Development and first clinical application. *Int. J. Oral Maxillofac. Surg.* **2002**, *31*, 44–52. [CrossRef]
50. Vassiliou, K.; Elfick, A.P.D.; Scholes, S.C.; Unsworth, A. The effect of 'running-in' on the tribology and surface morphology of metal-on-metal Birmingham hip resurfacing device in simulator studies. *Proc. Inst. Mech. Eng. Part H J. Eng. Med.* **2006**, *220*, 269–277. [CrossRef]
51. Irshad, T.B.; Pascoletti, G.; Bianconi, F.; Zanetti, E.M. Mandibular bone segmentation from CT scans: Quantitative and qualitative comparison among software. *Dent. Mater.* **2024**, *40*, e11–e22. [CrossRef]
52. Pascoletti, G.; Aldieri, A.; Terzini, M.; Bhattacharya, P.; Calì, M.; Zanetti, E.M. Stochastic PCA-Based Bone Models from Inverse Transform Sampling: Proof of Concept for Mandibles and Proximal Femurs. *Appl. Sci.* **2021**, *11*, 5204. [CrossRef]